WHEN STREAMS SIGH: HYDROLOGICAL AND BIOPHYSICAL CONTROLS ON OXYGEN AND CARBON DIOXIDE DYNAMICS IN LOTIC ECOSYSTEMS

A Dissertation

Presented to the Faculty of the Graduate School

of Cornell University

In Partial Fulfillment of the Requirements for the Degree of

Doctor of Philosophy

by

Nicole Breanne Hill

August 2016

WHEN STREAMS SIGH: HYDROLOGICAL AND BIOPHYSICAL CONTROLS ON OXYGEN AND CARBON DIOXIDE DYNAMICS IN LOTIC ECOSYSTEMS

Nicole Breanne Hill, Ph. D.

Cornell University 2016

Atmospheric carbon dioxide (CO_2) contributions from rivers and streams, known as CO_2 evasion, are estimated to be an order of magnitude greater than CO_2 outgassed from volcanoes. CO_2 evasion is a function of the CO_2 gas transfer rate coefficient and the CO_2 concentration gradient at the surface water – atmosphere interface. Methods to measures surface water – atmosphere gas exchange (i.e. reaeration) rates typically require the use of tracer gases, which are labor intensive, expensive, and are not representative of reaeration rates for all streamflow regimes. This dissertation presents a method to estimate the CO_2 reaeration rate coefficient from the diel dissolved oxygen (DO) curve. The partial pressure of free CO_2 (pCO_2) was monitored in Fall Creek, a stream in New York's Finger Lakes region, from May 2015 – May 2016 to identify hydrological and biophysical controls on CO_2 fluxes, evaluate the spatiotemporal variability of CO_2 emissions, and estimate the relative proportion of in-stream CO_2 derived from internal metabolic processes (autochthonous) compared to CO_2 inputs from terrestrial sources (allochthonous).

Fall Creek is a net heterotrophic system and requires external organic carbon inputs to sustain this status. The proportion of allochthonous CO_2 to autochthonous CO_2 in Fall Creek is approximately 1:2.6 in its headwaters and increases to 1:1.7 downstream. CO_2 emissions vary on diurnal and seasonal time scales with the highest evasion rates (~6.8

g C m^{-2} d^{-1}) occurring at nighttime during the summer. These emissions were strongly dependent on the CO_2 gas transfer velocity, which was twice as high downstream on the turbulent main channel as it was upstream in the calmer headwaters. Autochthonous CO_2 is produced during aquatic respiration, which has a strong Arrhenius temperature dependence. Respiration rates in Fall Creek's headwaters were less sensitive (activation energy, E_a = 0.61 eV) to temperature changes than the downstream location (E_a = 0.67 eV) where CO_2 emissions were greater. The highest CO_2 emissions were estimated for Fall Creek during low flow conditions due to elevated CO_2 reaeration rates (~23 d^{-1}), increased respiration from higher temperatures, and more substantial CO_2 contributions (~45% total in-stream CO_2) from groundwater. Future climate predictions indicate warmer summers with more erratic storm events for the Northeast, which may lead to prolonged periods of low stream flows during summer droughts and amplified CO_2 evasion.

BIOGRAPHICAL SKETCH

Nicole Breanne Hill (Potter) was born on Valentine's Day 1988 to Gina and Jay Potter in Springfield, MA. She has one younger brother, Jonathan. Nicole attended Ludlow High School where she ran cross country and track and field. It was during her many long distance runs, through the rolling hills of the Pioneer Valley, that she found her love and appreciation for nature along with an interest in environmental processes.

Inspired by her father's career as an engineer, Nicole earned her B.S. in Civil Engineering from UMass Amherst graduating *cum laude* with distinction from Commonwealth Honors College in 2010. For her undergraduate capstone research, she worked under the mentorship of Dr. John Tobiason to evaluate the filtration performance of the Springfield Water and Sewer Commission's West Parish Direct Filtration Plant (SWSC WPDFP) and recommend updated coagulation and backwash procedures to the SWSC board. Following graduation, Nicole completed a summer internship in the Simulated Lunar Operations (SLOPE) facility for the Space Experiments Lab within the Fluid Physics and Transport Branch at NASA Glenn Research Center in Cleveland, OH.

While at UMass, Nicole tutored thermodynamics and fluid mechanics for the Engineering Diversity Programs discovering a passion for both physics and teaching. She met her husband, a philosophy student and musician, on Halloween 2008 in Amherst. After many stimulating physics-philosophy discussions, they decided to advance their educations and enrolled at SUNY Binghamton together. Nicole studied geophysics for three semesters and grew certain that she wanted to apply her skills in engineering and physics to environmental processes and earn her doctorate. On Earth Day 2011, Nicole married Jordan Hill in Binghamton, NY.

In 2012, Nicole began her graduate studies at Cornell University as a trainee in the Cross Scale Biogeochemistry and Climate (CSBC) IGERT program supported by NSF. Advised by Dr. Susan Riha, Nicole's research focused on investigating environmental controls on aquatic nitrogen and carbon cycles by combining discrete stream measurements and continuous data logging in the Finger Lakes region of NY with laboratory microcosm experiments, qPCR, and biophysical modeling. In addition to her dissertation research, Nicole was committed to teaching and mentoring on campus. She helped design an environmental physics course with Susan Riha and Mark Wysocki, for which she was the teaching assistant (TA) for three semesters. She was a Center for Teaching Excellence graduate fellow, TA trainer and program designer for Engineering Learning Initiatives, program assistant for the Engineering Diversity Program's CURIE Academy, and reinstated Cornell's Enviro-Mentors program.

From Ithaca, Nicole will be returning home to the Pioneer Valley and will pursue her passion for teaching as tenure-track environmental science faculty at Greenfield Community College in MA. There, she will begin by teaching courses in environmental science, physical geology, climate science, and astronomy.

For Jordan

ACKNOWLEDGMENTS

First and foremost, I thank my advisor, Dr. Susan Riha, Charles L. Pack Professor in the Department of Earth and Atmospheric Sciences at Cornell. She was a wonderful mentor in every way and provided me with brilliant intellect, wisdom, and encouragement academically, professionally, and personally. I also thank my special committee members, Drs. Bill Philpot and Todd Walter, Professors of Civil and Environmental Engineering and Biological and Environmental Engineering at Cornell, respectively, for their advice and support. I am grateful to Drs. Brian Rahm (New York State Water Resources Institute) and Steve Shaw (SUNY ESF) for their mentorship throughout my first research project at Cornell. I am also grateful to Dr. John Tobiason (UMass Amherst) for the positive introduction to research I received as an undergraduate.

I was fortunate to receive funding from the National Science Foundation Integrated Graduate Education and Research Traineeship (NSF IGERT) in Cross Scale Biogeochemistry and Climate (CSBC), two CSBC small grants supported by the IGERT and the Atkinson Center for a Sustainable Future at Cornell, two conference travel grants from the Cornell Graduate School, travel assistance for fieldwork at the Savannah River Site in South Carolina from the Cornell Graduate School and further support was provided by the Department of Energy-Savannah River Operations Office through the U.S. Forest Service Savannah River under Interagency Agreement DE-AI09-00SR22188, funding as a Cornell teaching assistant provided by the Department of Earth and Atmospheric Sciences, Cornell's Engineering Learning Initiatives (ELI), and

Cornell's Center for Teaching Excellence (CTE). I further acknowledge Linda Tompkins from ELI and Derina Samuel from CTE for their mentorship in teaching and professional development opportunities. I also thank my advisor, Susan Riha, and Mark Wysocki for their guidance and expertise in teaching and providing me with the invaluable opportunity of being involved in designing an innovative environmental physics course as a graduate student.

I thank my field assistants, Cynthia Chan (Cornell '16) and Adam Schecter (Cornell '17) for their energy and enthusiasm. I also thank my lab mate, Liz Carter, for her positive outlook and never failing to boost my moral. I thank my family—mom, dad, and Jonathan for their love, understanding, and patience. I thank Simmy and Sebastian, my orange tabby cats, for their fuzzy cuddliness and keeping me sane throughout the writing processes. Finally, I thank Jordan, my love, for always believing in me and for the first birthday painting you gave me that read, "Shoot for the moon. Even if you miss you'll land amongst the stars." Thank you for helping with fieldwork, for endless emotional support, and for being my best friend and light at the end of a long day.

TABLE OF CONTENTS

LIST OF FIGURES

LIST OF TABLES

LIST OF ABBREVIATIONS

Avg.	average
BOD	biological oxygen demand
CMB	conductivity mass balance
CO_2	carbon dioxide
DO	dissolved oxygen
DOC	dissolved organic carbon
ER	ecosystem respiration
EVM	extreme value method
GPP	gross primary productivity
MME	mean multiplicative error
NDIR	non-dispersive infrared
NDM	net daily metabolism
NEWA	Network for Environment and Weather Applications
NHLD	Northern Highland Lake District
NOAA	National Oceanic and Atmospheric Administration
NPP	net primary productivity
NRCC	Northeast Regional Climate Center
NSM	nighttime slope method
OM	organic matter
PTFE	polytetrafluoroethylene
PQ	photosynthetic quotient
RQ	respiratory quotient
SD	standard deviation
USGS	United States Geological Survey
WFP	water filtration plant
WS	weather station
WWTP	wastewater treatment plant

LIST OF SYMBOLS

A	surface area
A_{DComo}	catchment drainage area for Como site
$A_{DFreese}$	catchment drainage area for Freese site
A_{Dgauge}	catchment drainage area at stream gauge
a	exponential constant
b	exponential constant
C_{DO}	dissolved oxygen concentration
C_{DOs}	dissolved oxygen saturation concentration
$C_{CO2,alloc}$	concentration of carbon dioxide from allochthonous sources
CF_{AN}	correction factor for carbon dioxide measured after noon
CF_{BN}	correction factor for carbon dioxide measured before noon
C_{k1}	English units constant for empirical reaeration rate coefficient equations
C_{k2}	metric units constant empirical reaeration rate coefficient equations
C_{k3}	constant for empirical reaeration rate coefficient equations
C_L	quantity describing turbulence that relates film thickness to viscosity
D	dissolved oxygen deficit
D_m	molecular diffusivity of oxygen
$D_{max,}$	maximum dissolved oxygen deficit
D_{min}	minimum dissolved oxygen deficit
E	energy dissipation in a fluid
E_a	activation energy
f	photoperiod
Fr	Froude number
$\mathcal{F}_{CO2}$	surface water – atmosphere carbon dioxide flux
g	acceleration due to gravity
H	average channel depth
H_{Como}	average channel depth at Como site
H_{Freese}	average channel depth at Freese site
H_{gauge}	stream gauge height
k_B	Boltzmann constant
k_{CO2}	carbon dioxide reaeration rate coefficient
K_H	Henry's law solubility coefficient for carbon dioxide in freshwater
K_{LCO2}	gas transfer velocity of carbon dioxide
K_{Lg}	gas transfer velocity of a gas
K_{LO2}	gas transfer velocity of oxygen
K_{Lt}	gas transfer velocity of a tracer gas
k_m	measured reaeration

k_{O2}	oxygen reaeration rate coefficient
$k_{O2,20\cdot C}$	oxygen reaeration rate coefficient at 20°C
k_p	predicted reaeration
L	film thickness
m_C	mass of carbon
M_{DO}	dissolved oxygen mass
m_{O2}	mass of oxygen
N	number of reaeration measurements
n	property of the water surface (0.5 – 1)
O_2	oxygen
P	photosynthesis
P_{O2}	photosynthesis rate in terms of oxygen
$P_{O2,avg}$	average daily photosynthesis rate in terms of oxygen
$P_{O2,max}$	maximum daily photosynthesis rate in terms of oxygen
P_{CO2}	photosynthesis rate in terms of carbon dioxide
$P_{CO2,avg}$	average daily photosynthesis rate in terms of carbon dioxide
$P_{CO2,max}$	maximum daily photosynthesis rate in terms of carbon dioxide
$P_{CO2,minD}$	photosynthesis rate at minimum daytime carbon dioxide concentration
pCO_2	partial pressure of carbon dioxide
pCO_{2atm}	partial pressure of carbon dioxide in the atmosphere
$pCO_{2,avg}$	average partial pressure of carbon dioxide in water
pCO_{2m}	measured partial pressure of carbon dioxide in water
$pCO_{2,max}$	maximum nighttime partial pressure of carbon dioxide in water
$pCO_{2,min}$	minimum nighttime partial pressure of carbon dioxide in water
pCO_{2n}	partial pressure of carbon dioxide in water at solar noon
pCO_{2w}	partial pressure of carbon dioxide in water
Q	volumetric stream discharge
Q_{10}	temperature coefficient for kinetic rate changes at 10°C increments
Q_{BF}	baseflow component of volumetric stream discharge
Q_{Como}	volumetric stream discharge at Como site
Q_{Freese}	volumetric stream discharge at Freese site
Q_{gauge}	volumetric stream discharge at stream gauge
r	radius of an oxygen molecule in water
R	respiration
R_{CO2}	respiration rate in terms of carbon dioxide
R_a	autotrophic respiration
R_o	respiration rate at reference temperature
R_{O2}	respiration rate in terms of oxygen
S	channel slope
s	surface renewal rate
Sc	Schmidt number
SC	specific conductance
SC_{BF}	specific conductance baseflow end-member

SC_{RO}	specific conductance runoff end-member
Sc_{CO2}	Schmidt number for carbon dioxide
Sc_g	Schmidt number for a gas
Sc_{O2}	Schmidt number for oxygen
Sc_t	Schmidt number for tracer gas
t	time
t_m	time of measurement
t_{minD}	time of minimum oxygen saturation deficit
$t_{minD,C}$	time of daytime minimum carbon dioxide concentration
t_n	solar noon
T	stream temperature
T_{avg}	average daily stream temperature
T_o	reference stream temperature
U	stream velocity
V	volume
W	average channel width
W_{Como}	average channel width at Como site
W_{Freese}	average channel width at Freese site
x	distance parallel to water surface
z	distance perpendicular to water surface
δ	sampling interval
μ	dynamic viscosity of water
ν	kinematic viscosity of water
θ	temperature coefficient
θ_a	temperature coefficient for reaeration
θ_P	temperature coefficient for photosynthesis
θ_R	temperature coefficient for respiration
ρ	density of water
τ	one diel cycle

CHAPTER 1

INTRODUCTION

1.1 The Metabolic Mass Balance of Streams

Complex biophysical and biogeochemical processes govern fluxes of nutrients within an ecosystem. On a macro-scale, ecosystems have been described as super-organisms where rivers can be thought of as blood vessels delivering matter and energy throughout a watershed and streams acting as the liver with their benthos processing nutrients and purifying water (Palmer and Febria, 2012; Demars *et al*., 2015). Analogous to drawing a blood sample, the general health of a watershed can be interpreted from the physical and chemical properties (i.e. quality) of its waters. The concentration of dissolved oxygen (DO) is a vital water quality indicator. It has been recognized for over a century that a plentiful supply of DO is required to maintain healthy aquatic ecosystems (e.g. Streeter and Phelps, 1925). Heterotrophic organisms become stressed under poorly oxygenated conditions since they consume oxygen and organic carbon to produce energy while respiring carbon dioxide. Primary producers, on the other hand, use solar energy to fix inorganic carbon and generate chemical energy, store organic matter, and release oxygen. Net primary productivity (NPP) describes the portion of energy stored as biomass within an autotrophic organism. However, some energy is lost through autotrophic respiration (R_a). Gross primary productivity (GPP) is the sum of the energy stored (NPP) and respired (R_a) by autotrophs. The net daily metabolism (NDM) can be described by the difference between GPP and total ecosystem respiration (ER). ER includes both heterotrophic and

autotrophic respiration since it is difficult to isolate R_a from R_h (Bott, 2007). Streams are classified as net heterotrophic when GPP/ER is less than one and as net autotrophic when GPP/ER is greater than one. Most aquatic ecosystems are considered to be net heterotrophic and require allochthonous carbon inputs to sustain this status (Cole and Caraco, 2001).

Odum (1956) pioneered the open-channel diel oxygen method to calculate NDM from DO measurements taken in flowing waters. The observed daily oxygen curve is the product of oxygen gained from photosynthesis throughout a photoperiod, oxygen consumed during respiration, and the diffusion of oxygen at the air-water interface, which is driven by the reaeration rate and the oxygen saturation gradient. Therefore, the following mass balance, proposed by O'Conner and Di Toro (1970), between photosynthesis (P), respiration (R), and diffusion can describe the change in DO concentration observed throughout the course of a day:

$$\frac{\partial C_{DO}}{\partial t} = -U\,\frac{\partial C_{DO}}{\partial x} + k_{O2}(C_{DOs} - C_{DO}) + P(x, t) - R(x) \qquad (1.1)$$

where C_{DO} is the concentration of dissolved oxygen (mg L^{-1}), t is time (d), U is the stream velocity (m d^{-1}), x is distance (m), k_{O2} is the reaeration rate coefficient for oxygen (d^{-1}), and C_{DOs} is the concentration of dissolved oxygen at saturation (mg L^{-1}). This partial differential can be simplified under the common assumption that a given stream reach has generally uniform spatial distribution of plants, heterotrophic communities, and dissolved gases:

$$\frac{dC_{DO}}{dt} = k_{O2}(C_{DOs} - C_{DO}) + P(t) - R \qquad (1.2)$$

This relation is depicted in Figure 1.1 for idealized conditions of constant temperature, constant reaeration, and full sun. In the upper graph (a.), the green shaded area under the daily photosynthesis curve is the GPP and the grey area is the ER. Odum noted that the measured in-stream dissolved oxygen concentration could also be impacted by groundwater accrual. However, the groundwater term is usually taken to be negligible and discarded from the mass balance. Hall and Tank (2005) point out that groundwater seepage could impact the in-stream DO concentration since groundwater tends to be depleted in oxygen compared to surface waters. This would cause a dilution effect leading to an underestimation of GPP and an overestimation of ER.

Theoretically, Odum's open-channel approach can be applied to dissolved carbon dioxide and yield the same NDM results as the DO procedure but with a reversed sign (Odum, 1956; Guasch *et al*., 1998; Bott, 2007). The lower graph (b.) in Figure 1.1 depicts the resultant CO_2 curve from the metabolic rates shown in the upper plot under the assumption that there are no CO_2 inputs from groundwater and that the gas transfer velocity of CO_2 behaves similar to that of O_2. A mismatch between NDM calculated from DO and CO_2 would indicate allochthonous dissolved gas inputs from groundwater, runoff, or precipitation. Therefore, comparing metabolic rates resulting from both DO and CO_2 could give useful insights regarding the sources of CO_2 to aquatic systems. Even so, the vast majority of aquatic metabolism studies derive GPP and ER from the diel oxygen curve with only a handful having investigated diel carbon dioxide (e.g. Odum, 1957; Wright and Mills, 1967; Guasch *et al*., 1998; Lynch *et al*., 2010).

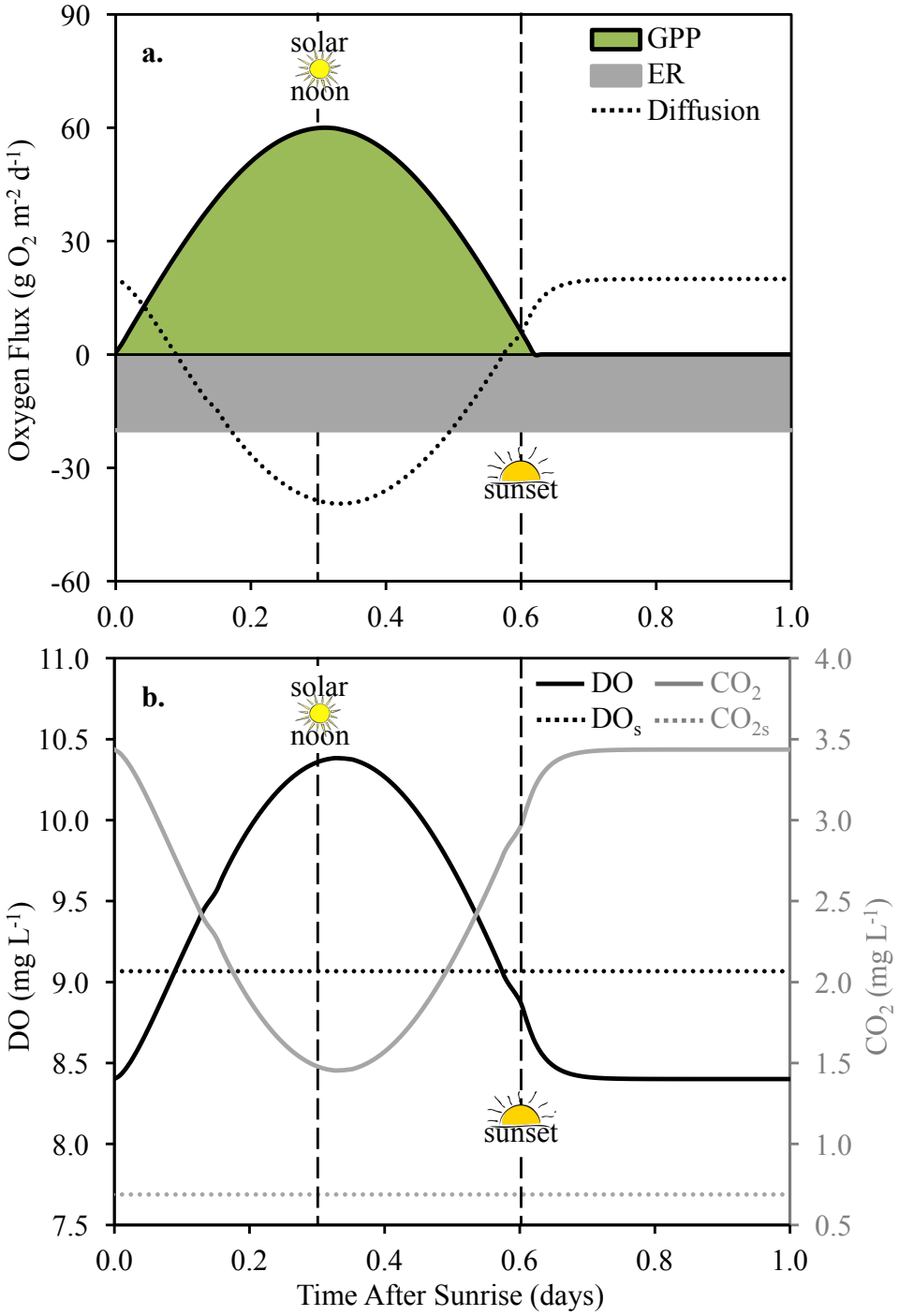

Figure 1.1. Idealized daily rates of photosynthesis (GPP), respiration (ER), and diffusion **(a.)** with resultant dissolved O_2 and CO_2 concentrations and saturated (DO_s and CO_{2s}) concentrations at 20°C **(b.)**.

1.2 Respiration and the Release of Carbon Dioxide from Inland Waters

In addition to the GPP/ER ratio, another indicator of net heterotrophy may be the partial pressure of CO_2 (pCO_2) in aquatic systems (Raymond *et al*., 2000; Sobek *et al*., 2005). In order for waters to be supersaturated in pCO_2, internal ER either must exceed NPP causing net heterotrophy, and/or the water body must be receiving terrestrially derived sources of CO_2. Inland waters tend to be supersaturated in pCO_2 with respect to the atmosphere (e.g. Cole *et al*., 1994, Sobek *et al*., 2005; Raymond *et al*., 2012; Prasad *et al*., 2013; Peter *et al*., 2014), which has a global average concentration of approximately 400 ppm_v. For reference, the concentration of oxygen in the atmosphere is close to 210,000 ppm_v. Evasion of CO_2 from surface waters to the atmosphere depends on the gas transfer velocity, solubility of CO_2 (a function of temperature, pressure, and salinity), and the partial pressure of CO_2 in the water. The sources of and the controls on terrestrial-aquatic CO_2 dynamics remain understudied as it was only within the last decade that inland waters, especially small rivers and streams, have become widely recognized as significant components of the global carbon cycle. Inland waters have been identified as key transporters (Cole *et al*, 2007; Battin *et al*., 2009), processers (Battin *et al*., 2009; Hotchkiss *et al*., 2015), and emitters (Butman and Raymond, 2011; Crawford *et al*., 2013; Raymond *et al*., 2013; Hotchkiss *et al*., 2015; Kokic *et al*., 2015) of carbon dioxide in terrestrial-aquatic ecosystems. Due to their high degree of connectivity (benthic surface area to water volume ratio) with the surrounding landscape and steep channel slopes, headwater streams have been identified as hotspots for CO_2 evasion on the global scale (Butman and Raymond, 2011; Raymond *et al*., 2013; Hotchkiss *et al*., 2015).

The sources of CO_2 to inland waters must be elucidated before the controls on CO_2 evasion can be better understood. In-stream pCO_2 is the product of both internal and upland metabolic processes, so it provides insight to the linkages between terrestrial and aquatic environments (Jones and Mulholland, 1998; Richey *et al*., 2002). Dissolved CO_2 produced from soil and root respiration or weathering can be transported to rivers and streams by overland and groundwater flows (Finlay, 2003; Jones *et al*., 2003). It has been proposed that for lakes, pCO_2 supersaturation will be driven by both internal and external processes while for rivers and streams, the terrestrially-derived CO_2 sources will dominate (Sobek *et al*., 2005). Hotchkiss *et al*. (2015) investigated the proportions of CO_2 produced from internal versus external processes for NDM studies in rivers and streams across the United States. They found that 28% of CO_2 emitted by rivers and streams was sourced from internal metabolic processes. This percentage decreased as a function of decreasing stream size with terrestrial CO_2 exports serving as the dominant CO_2 source to the smallest streams. The mass balance of carbon dioxide and oxygen in stream ecosystems will be analyzed to quantify the relative proportion of autochthonous (internal) to allochthonous (external) CO_2 production in the chapters that follow.

1.3 Motivation and Overview

The overall goal of this dissertation is to characterize the hydrological and biophysical controls on carbon dioxide dynamics in Fall Creek, a stream in the New York Finger Lakes region. While few researchers have utilized CO_2 measurements to quantify metabolic rates in aquatic ecosystems, even fewer have compared NDM using

both DO and CO_2 data. Chapter 2 will focus on the relationship between temperature, reaeration, and oxygen consumption during nighttime respiration for baseflow conditions. Reaeration will be studied under all flow regimes in chapter 3. Additionally, the spatiotemporal variability of and environmental controls on carbon dioxide evasion will be examined. Coupled O_2-CO_2 dynamics will be analyzed in chapter 4 through the development and parameterization of an O_2-CO_2 simulation model, which estimates allochthonous CO_2 inputs by resurrecting Odum's groundwater accrual term as a component in the metabolic mass balance. Finally, NDM will be calculated and the efficiencies for the conversion of oxygen to carbon dioxide during respiration (e.g. respiratory quotient, RQ) and carbon dioxide to oxygen during photosynthesis (e.g. photosynthetic quotient, PQ) will be discussed.

CHAPTER 2

APPLICATION OF THE NIGHTTIME SLOPE METHOD TO CHARACTERIZE OXYGEN CONSUMPTION DURING RESPIRATION AND REAERATION FOR BASEFLOW CONDITIONS

2.1 Introduction

Temperature is an indisputable control on ecosystem metabolism and, therefore, oxygen and carbon dioxide fluxes. However, there is much debate over the nature of the temperature dependence on metabolic processes and whether researchers are appropriately "correcting" for its effects (Demars *et al*., 2015; González-Pinzón *et al*., 2016). Aquatic ecosystems may be more sensitive to changes in temperature than terrestrial ecosystems (Yvon-Durocher *et al*., 2012). In order to improve climate and carbon cycle models and better understand carbon-climate feedbacks, it is important to characterize the response of aquatic ecosystem respiration rates on increasing temperatures associated with climate change (Mahecha *et al*., 2010; Jankowski *et al*., 2014).

Nighttime is convenient for studying oxygen consumption during respiration without the interference of oxygen production from photosynthesis. Equation 1.2 can then be simplified to:

$$\frac{dC_{DO}}{dt} = k_{O2}(C_{DOs} - C_{DO}) - R = k_{O2}\,D - R \qquad (2.1)$$

where C_{DO} is the concentration of dissolved oxygen (mg L^{-1}), t is time (d), k_{O2} is the reaeration rate coefficient for oxygen (d^{-1}), C_{DOs} is the concentration of dissolved oxygen at saturation (mg L^{-1}), and D is the dissolved oxygen deficit (mg L^{-1}). Applying

this model in its original form would require holding respiration rates calculated at night constant during the daytime to close the oxygen mass balance (Odum, 1956; Chapra and Di Toro, 1991; Wang *et al*., 2003). However, it is becoming common practice to adjust daytime respiration by assuming a van't Hoff Q_{10}, Arrhenius activation energy E_a (eV), or temperature coefficient (θ) derived from Arrhenius kinetics. All of these can be described by the activation energy, which is mathematically the most accurate (Gillooly *et al*., 2001; Demars *et al*., 2015):

$$E_a = \ln(Q_{10})\, k_B T_o T \tag{2.2}$$

$$\theta = \exp\left[E_a \left(k_B T_o T\right)^{-1}\right] \tag{2.3}$$

where k_B is the Boltzmann constant (8.62×10^{-5} eV K^{-1}), T is the temperature (K), and T_o is the reference temperature (15^oC = 288.15 K). The problem with equations 2.2-2.3 is that there is not one universal E_a for respiration, which has been shown to be dependent on ecosystem community composition varying from 0.26-0.38 eV for terrestrial ecosystems and from 0.57-0.98 eV for aquatic ecosystems (Yvon-Durocher *et al*., 2012). E_a can be calculated from a linearized Arrhenius function (Perkins *et al*., 2012):

$$\ln(R) = -E_a\left(\frac{1}{k_B T} - \frac{1}{k_B T_o}\right) + \ln(R_o) \tag{2.4}$$

where R is the measured rate of respiration (mg L^{-1} m^{-2}) and R_o is the respiration at the reference temperature. The expression $\left(\frac{1}{k_B T} - \frac{1}{k_B T_o}\right)$ is referred to as the standardized temperature, which centers the model intercept around zero providing a biologically meaningful intercept of $\ln(R_o)$ and slope of E_a (Perkins *et al*., 2012).

In lieu of bottle or chamber measurements, R can be calculated from equation 2.1 using *in situ* nighttime dissolved oxygen (C_{DO}) measurements, which will be discussed in section 2.3.1. For shallow freshwater systems, the solubility of oxygen in water (C_{DOs}) is a function of temperature (T in ^{o}C) and can be calculated from the following (Weiss, 1970):

$$C_{DOs} = 1.4276 \exp\left[\begin{array}{c} -173.4292 + 249.6339\left(\frac{100}{T}\right) \\ +143.3483 \ln\left(\frac{T}{100}\right) - 21.8492\left(\frac{T}{100}\right) \end{array}\right] \quad (2.5)$$

This leaves one unknown variable in equation 2.1—reaeration.

2.1.1 Reaeration

Reaeration, the exchange of atmospheric gases with surface water, is an important driver of mass flux at the air-water interface. When the DO in a water column falls below saturation it is recharged by the atmosphere. Oxygen gas is lost to the atmosphere when DO is above saturation (i.e. supersaturated), which is typically the case during the daytime. Reaeration can be modeled by Fick's first law of diffusion:

$$\frac{dM_{DO}}{Adt} = -D_m\left(\frac{dC_{DO}}{dz}\right) \quad (2.6)$$

where M_{DO} is the mass of dissolved oxygen, D_m is the molecular diffusivity of DO (m^2 d^{-1}), A is the area through which the oxygen passes, and z is the distance in the direction normal to the surface. Through the adoption of a two-film model (Lewis and Whitman, 1924), Fick's law will take the familiar form shown previously in the mass balance equations (Demars and Manson, 2013; Nguyen *et al*. 2015):

$$\frac{dC_{DO}}{dt} = \frac{K_{LO2}A}{V}(C_{DOs} - C_{DO}) \quad (2.7)$$

where K_{LO2} is the gas transfer velocity of oxygen (m d^{-1}) and A/V is the air-water interface surface area per unit volume of air and water. In streams with a relatively smooth surface area, $K_{LO2}/H \sim k_{O2}$ where H is the average channel depth (m). It is critical to note that a smooth surface area is assumed in the mass balance model (equations 1.1-1.2, 2.1).

Since atmospheric exchange is an essential component in the metabolic mass balance of streams, it is imperative to have accurate reaeration rate coefficients or gas transfer velocity measurements with the resolution of daily timescales. Unfortunately, the gas transfer velocity is difficult to measure directly. Most field-based efforts utilize a tracer gas, which is injected at an upstream location and measured some distance downstream on a reach that is not gaining significant volumes of water from tributaries or groundwater seepage. Any downstream mass losses of the tracer gas are assumed to have been degassed to the atmosphere. There are a number of problems with this method to quantify gas exchange. First, the mixing length for a reach must be appropriately defined. There are theoretical equations (e.g. Wallis and Manson, 2004) to predict mixing length, but optimal lateral and vertical mixing cannot be guaranteed in practice (Young and Huryn, 1999). Second, for gases with low solubilities, up to 99% of the gas can quickly escape to the atmosphere, which may introduce high levels of uncertainty to gas exchange proxies. Low solubility tracer gases are of particular concern when a potent greenhouse gas such as SF_6 is utilized (Benson *et al*., 2014). Third, reaeration may be underestimated when dispersion is neglected, which is a classic assumption in the majority of tracer studies (Knapp *et al*., 2015). Fourth, most tracer gas measurements are implemented during low-flow conditions. Empirical relationships are usually

derived for gas transfer velocity at a specific site based on the tracer injection made during low-flow. Then these equations are misapplied to higher flow conditions and often not corrected for differences in temperature (Melching and Flores, 1999; Riley and Dodds, 2013). Finally, gas tracer experiments are costly and labor intensive, which makes it difficult to directly measure gas exchange rates for a representative range of flow conditions (Morse *et al*., 2007).

Due to the difficulties working with tracer gases, there has been considerable effort to scale and relate gas transfer velocities based upon geomorphic features and physical principles (e.g. Melching and Flores, 1999; Morse *et al*., 2007; Alin *et al*., 2011; Wallin *et al*., 2011; Raymond *et al*., 2012). One controlling parameter in air-water gas exchange is the diffusion coefficient of that gas dissolved in water (Jähne *et al*., 1987). A gas's Schmidt number (Sc) is the ratio between its diffusion coefficient and the kinematic viscosity. The empirical temperature dependency of Sc for many gases has been described by Wanninkhof (1992) and was recently updated (2014). When researchers conduct experiments using a tracer gas to determine the reaeration coefficient or gas transfer velocity for another gas in a stream reach, they often apply the Sc dependence (Jähne *et al*., 1987):

$$K_{Lg}/K_{Lt} = (Sc_g/Sc_t)^{-n} \quad (2.8)$$

where K_{Lt} is the measured gas transfer velocity of the tracer, K_{Lg} is the transfer velocity of the gas of interest, and n is a property of the water surface ranging from 0.5 to 1. A value of 0.5 for n represents free mixing and a continual surface renewal model, while a value of 1 would indicate a thin film on the water's surface (Jähne *et al*., 1987). In free flowing waters, n is usually assumed to be 0.5 (Wallin *et al*., 2011; Raymond *et al*.,

2012). The Sc dependence for two gases could be altered if there were breaking waves present on the water's surface, which would facilitate bubble-mediated diffusion and decrease the gas transfer velocity of carbon dioxide (Asher and Wanninkhof, 1998) relative to oxygen as was observed by Guasch *et al*. (1998).

Empirical reaeration equations are popular alternatives to direct gas tracer measurements. However, they should be used with caution. Such equations are typically expressed in terms of relationships with hydraulic geometry (e.g. velocity, depth, width, and channel slope) and optimized for a specific water body under a constrained set of hydraulic or environmental conditions. Table 2.1 presents empirical reaeration equations that will be referred to throughout this chapter. Group 1 contains equations that are function of stream velocity and depth. These are classic equations that were originally expressed in log base 10 and English units. The following conversion was applied to produce the equations shown in Table 2.1:

$$C_{k1} = \frac{k_{O2}\left[d^{-1}\right]_{10}}{(U[\text{ft s}^{-1}])^{a}(H\,[\text{ft}])^{-b}} \tag{2.9a}$$

$$C_{k2} = \frac{k_{O2}\left[d^{-1}\right]_{10}}{(0.3048\,U[\text{m ft}^{-1}\ \text{ft s}^{-1}])^{a}(0.3048\,H\,[\text{m ft}^{-1}\text{ft}])^{-b}} \tag{2.9b}$$

$$k_{O2}\left[d^{-1}\right]_{e} = \ln(10)\,k_{O2}\left[d^{-1}\right]_{10} \tag{2.9c}$$

where C_{k1} is the English units constant, C_{k2} is the metric units constant, and a and b are constant exponents. This $C_k U^a H^{-b}$ form of the group 1 equations is derived from Streeter and Phelps (1925) biological oxygen demand (BOD) studies on the Ohio River. In 1956, O'Connor and Dobbins presented the film penetration theory for gas absorption and reasoned that the reaeration rate could be determined by the ratio of the vertical velocity

fluctuation and the mixing length. For shallow rivers with a pronounced velocity profile and non-isotropic turbulence, the reaeration coefficient would take the following form:

$$k_{O2} = C_{k3} D_m^{0.5} S^{0.25} H^{-1.25} \quad (2.10)$$

where C_{k3} is a constant, D_m is the molecular diffusivity, and S is the channel slope. The O'Connor and Dobbins equation presented in Table 2.1 was initially developed as a counterpart to equation 2.10 for moderately deep channels (0.3-9.1 m) approaching isotropic turbulence. However, O'Connor (1958) found insignificant differences between the two equations and concluded that the simpler form, equation OD in Table 2.1, should be applied to both systems. Churchill, Buckingham, and Elmore (1962) applied dimensional analysis and performed multiple regression techniques to develop 19 equations for k_{O2} containing combinations of the following hydraulic variables: stream velocity, mean depth, energy slope, fluid density, fluid viscosity, surface tension, molecular diffusion, vertical diffusion, and resistance coefficient. Ultimately, they recommended equation CH from Table 2.1 for channel depths between 0.6 and 3.4 m with average velocities between 0.55 and 1.52 m s^{-1}. Owens, Edwards, and Gibbs's equation (1964), OW, was developed for lowland streams with velocities ranging 0.03-1.5 m s^{-1} and depths from 0.129-3.35 m. Bennett and Rathbun's (1972), BR, equation is similar to OW but it was developed from regression analysis using a larger dataset than that of Owens *et al*. (1964) and showed the smallest standard error comparing direct reaeration measurements to hydraulic channel features for a range of natural streams.

The group 2 equations from Table 2.1 follow the general form of equation 2.10 and include channel slope. Moog and Jirka (1998) proposed a new method for evaluating the performance of reaeration equations via mean multiplicative error

(MME) as they found normalized mean error and standard error are biased toward equations that under-predict reaeration. MME is the geometric mean of the predicted reaeration (k_p) to measured reaeration (k_m) ratio and is defined as:

$$\mathrm{MME} = \exp\left[\frac{\sum_{i=1}^{N} \left|\ln\left(\frac{k_p}{k_m}\right)_i\right|}{N}\right] \tag{2.11}$$

where N is the number of reaeration measurements. Using MME, Moog and Jirka (1998) evaluated eleven of the most cited empirical reaeration equations and found that for channel slopes >0.0004, slope is a necessary term to include in the predictive equations and proposed equation MJ. Melching and Flores (1999) developed both empirical and semi-empirical equations to estimate the reaeration rate coefficient based upon a sizable United States Geological Survey (USGS) data set, which included 371 direct gas tracer measurements. Equations MFa and MFb were developed for channel-control streams for both low ($Q < 0.556$ m^3 s^{-1}) and high ($Q > 0.556$ m^3 s^{-1}) flows respectively. Channel-control reaches are those which are "generally devoid of unusual riffles or bars" (Leopold and Maddock, 1953, p. 8). For lower slopes and a pool and riffle geomorphology, wind may play a more important role in atmospheric gas exchange (Parker and DeSimone, 1992). Equations developed to represent reaeration for channel-control streams were selected for Table 2.1.

The first two groups of empirical equations were developed for specific channel morphologies. With respect to group 3, Raymond *et al*. (2012) set out to determine a set of gas transfer velocity equations that were scalable across different gases and hydraulic geometries for small streams and rivers. These are equations RAa-RAg in Table 2.1. They applied the Schmidt number dependence (equation 2.8) to scale equations for

many gases that are of interest to ecology and earth science. Since their original equations were presented in terms of the gas transfer velocity rather than the reaeration rate coefficient, the equations were divided by H under the assumption that V/A ~ H, to more closely match the form of the other equations in the table. Equations RAa-RAg were designed based on the theory that the gas transfer velocity is controlled by the turbulent dissipation rate at the air-water interface (i.e. surface turbulence), which is related to the geomorphic features of the channel (Zappa *et al.*, 2007; Raymond *et al.*, 2012). Raymond *et al*. found that RAa, RAb, and RAf generally had the lowest least square errors after comparing the predicted gas transfer velocities using regression analysis against 563 direct gas transfer release experiments.

The final two equations, AL and WA, from group 4 were initially developed to predict the gas transfer rates of CO_2 and are scaled to O_2 for Table 2.1 through the Schmidt number dependence. Alin *et al*. (2011) directly measured the gas transfer velocity of CO_2 in the Amazon and Mekong river systems in South America and found that the gas transfer velocities for small rivers and streams were significantly higher and more variable than those of large rivers. They combined their gas transfer velocity measurements with values reported in the literature to determine the primary physical drivers for gas transfer, which led to equation AL for small rivers. Wallin *et al.* (2011) measured carbon dioxide reaeration in boreal streams and found that it was best predicted by channel slope and the width to depth ratio.

Table 2.1 Empirical equations for oxygen reaeration rate coefficients k_{O2} (d^{-1}). Groups 1-2 were developed for a reference temperature of 20°C and can be adjusted with a temperature coefficient θ of 1.0241 (Elmore and West, 1961). Groups 3-4 are scalable to any temperature with the Schmidt number Sc. Variables included are velocity U (m s^{-1}), aeration or mean depth H (m), channel slope S (m m^{-1}), discharge Q (m^3 s^{-1}), Froude number ($Fr = U/(gH)^{0.5}$) where g is the acceleration due to gravity (9.81 m s^{-2}), and average channel width W (m).

ID	Reference	Reaeration Equation (day^{-1})
GROUP 1		
OD	O'Connor and Dobbins (1956)	$k_{O2} = 3.93U^{0.5}H^{-1.5}\theta^{T-20^oC}$
CH	Churchill *et al.* (1962)	$k_{O2} = 5.2UH^{-1.67}\theta^{T-20^oC}$
OW	Owens *et al*. (1964)	$k_{O2} = 5.33U^{0.67}H^{-1.85}\theta^{T-20^oC}$
BR	Bennett and Rathbun (1972)	$k_{O2} = 5.58U^{0.607}H^{-1.689}\theta^{T-20^oC}$
GROUP 2		
MJ	Moog and Jirka (1998)	$k_{O2} = 1740U^{0.46}S^{0.79}H^{0.74}\theta^{T-20^oC}$
MFa	Melching and Flores (1999)	$k_{O2} = 88(US)^{0.313}H^{-0.353}\theta^{T-20^oC}$ for $Q < 0.556$ m^3 s^{-1}
MFb	Melching and Flores (1999)	$k_{O2} = 142(US)^{0.333}H^{-0.66}W^{-0.243}\theta^{T-20^oC}$ for $Q > 0.556$ m^3 s^{-1}
GROUP 3		
RAa	Raymond *et al*. (2012)	$k_{O2} = 5037(US)^{0.89}H^{-0.46}(600/Sc_{O2})^{0.5}$
RAb	Raymond *et al*. (2012)	$k_{O2} = 5937(1-2.54Fr^2)(US)^{0.89}H^{-0.42}(600/Sc_{O2})^{0.5}$
RAc	Raymond *et al*. (2012)	$k_{O2} = 1162S^{0.77}U^{0.85}H^{-1}(600/Sc_{O2})^{0.5}$
RAd	Raymond *et al*. (2012)	$k_{O2} = 951.5(US)^{0.76}H^{-1}(600/Sc_{O2})^{0.5}$
RAe	Raymond *et al*. (2012)	$k_{O2} = (2841US + 2.02)H^{-1}(600/Sc_{O2})^{0.5}$
RAf	Raymond *et al*. (2012)	$k_{O2} = 929US^{0.75}Q^{0.011}H^{-1}(600/Sc_{O2})^{0.5}$
RAg	Raymond *et al*. (2012)	$k_{O2} = 4725(US)^{0.86}Q^{-0.14}H^{-0.34}(600/Sc_{O2})^{0.5}$
GROUP 4		
AL	Alin *et al.* (2011)	$k_{O2} = (3.32 + 8.4U)H^{-1}(600/Sc_{O2})^{0.5}$
WA	Wallin *et al.* (2011)	$k_{O2} = (1.9S + 0.3W/H - 0.0004)(Sc_{CO2}/Sc_{O2})^{0.5}$

2.1.2 The Nighttime Slope Method

The oxygen reaeration equations in Table 2.1 were selected due to either their applicability to small streams (e.g. Haider *et al*., 2013) or scalability to other gases. In this section, a graphical approach, the nighttime slope method (Hornberger and Kelly, 1975) is presented for determining reaeration and respiration from equation 2.1. Following the assumption of constant nighttime respiration and reaeration, R and k_{O2} can be solved graphically by plotting $\frac{dC_{DO}}{dt}$ against D (i.e. $C_{DOs} - C_{DO}$). For regular DO measurements collected at a single station with sampling interval $\delta = t_{i+1} - t_i$, an Eulerian flow scenario can be applied such that:

$$\int_{t_i}^{t_{i+1}} dC_{DO} = \int_{t_i}^{t_{i+1}} (k_{O2}(C_{DOs} - C_{DO}) - R)\, dt \qquad (2.12a)$$

$$C_{DO,i+1} - C_{DO,i} = \left(\overline{C}_{DOs} - C_{DO,i}\right) - \frac{R_o}{k_{O2}}(1 - e^{-k_{O2}\delta}) \qquad (2.12b)$$

where subscripts i and i+1 refer to times t_i and t_{i+1}, $\overline{C}_{DOs}$ is the average nighttime DO saturation concentration and R_o is the initial respiration at sunset, which is held constant throughout the night. Using the Euler approximation for $\frac{dC_{DO}}{dt}$, the application of the nighttime slope method to the idealized DO curve from Figure 1.1 would yield a solution to equation 2.12b of k_{O2} = 42 day^{-1} and R_o = 28 mg O_2 consumed L^{-1} d^{-1} as illustrated in Figure 2.1.

This method is applicable for non-polluted rivers and streams where the DO deficit D increases by at least 1 mg L^{-1} throughout the night (Thyssen *et al.*, 1987). Aristegi, Izagirre, and Elosegi (2009) studied oxygen reaeration in 21 streams in northern Spain. After calculating reaeration using three approaches, Hornberger and Kelly's nighttime method, the observed lag time between solar noon and the peak DO

concentration (e.g. the delta method, Chapra and Di Toro, 1991), and ten empirical equations including CH, OW, and BR from Table 2.1, they concluded that the nighttime slope method was the most robust and reliable for producing realistic estimates for stream metabolism.

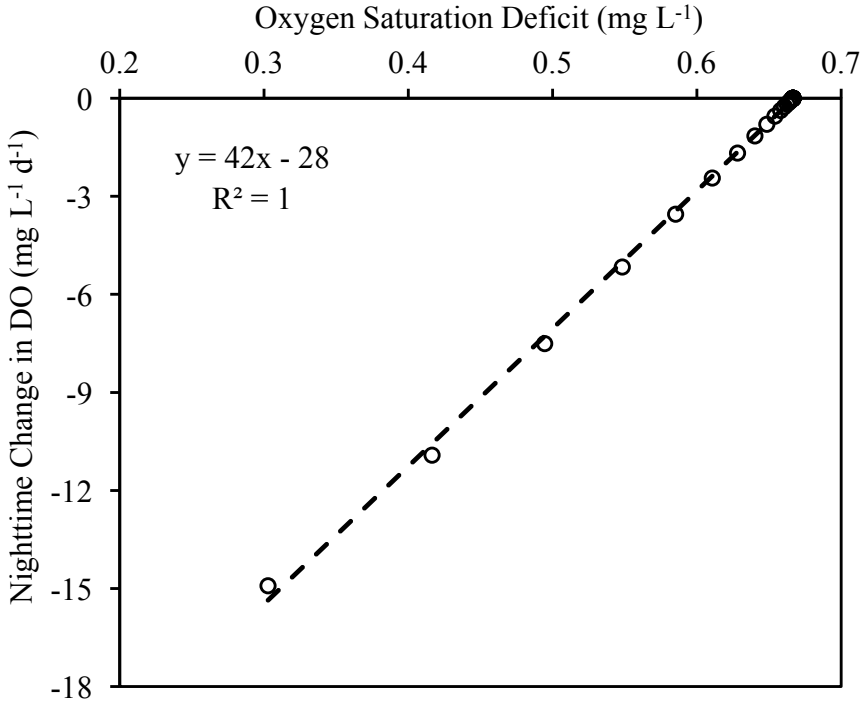

Figure 2.1 Example of the nighttime slope method applied to the idealized DO curve shown in Figure 1.1b. A linear fit regression line provides a solution to equation 2.12b with the slope representing the average reaeration rate coefficient and the ordinal intercept is the average rate of respiration. DO decreases fastest at sundown and the maximum DO deficit is reached before sunrise.

2.1.3 Temperature Effects on Reaeration and Respiration

Oxygen is more soluble in freshwater at cooler temperatures as described by Weiss's (1970) oxygen solubility-temperature function given in equation 2.5. Yet the rate of atmospheric oxygen absorption at the air-water interface increases with

increasing temperatures due to decreases in viscosity, density, and surface tension (Elmore and West, 1961). Through a series of controlled and high precision laboratory analyses, Elmore and West found that the rate of oxygen reaeration increases at a rate of 2.41% per ^{o}C so the relation between the reaeration coefficient at any temperature and the reaeration coefficient at a standard temperature of 20^{o}C ($k_{O2,20^{o}}$) can be described by the simplified Arrhenius formula:

$$k_{O2} = k_{O2,20^{o}} \theta^{T-20^{o}C} \qquad (2.13)$$

where $\theta = 1.0241$. Elmore and West's temperature correction coefficient of 1.0241 is assumed to be constant and frequently applied to empirical equations to standardize the reaeration rate coefficient to 20^{o}C (e.g. O'Connor and Dobbins, 1956; Churchill *et al*., 1962; Owens, 1964; Bennett and Rathbun, 1972). This constant has also been applied to recent studies to correct for the temperature dependence of reaeration on stream metabolism (e.g. Beaulieu *et al.*, 2013; Birkel *et al.*, 2013; Riley and Dodds, 2013). Butcher and Covington (1995) proposed using a van't-Hoff Arrhenius relation similar to equation 2.13 to correct each term in the oxygen mass balance and suggested the following:

$$\frac{dC_{DO}}{dt} = k_{O2}(C_{DOs} - C_{DO})\theta_{a}^{(T-20^{o}C)} + P(t)\theta_{P}^{(T-20^{o}C)} - R\theta_{R}^{(T-20^{o}C)} \qquad (2.14)$$

with temperature coefficients θ_a, θ_P, and θ_R for reaeration, photosynthesis, and respiration respectively. Butcher and Covington recommended $\theta_a = 1.02$ for reaeration, which was subsequently applied by Wang *et al.*, 2003 and Correa-González *et al*. (2014) in their metabolism modeling work.

Demars and Manson (2013) returned to Dobbins' classic film penetration model (1956) to test whether a constant temperature correction coefficient was a valid assumption for reaeration rates under a range of turbulence regimes and found that θ_a ranged from 1.005 to 1.042 for temperatures between 0°C and 35°C. Additionally, they noted that changes in turbulence had a greater impact on θ_a than temperature. Therefore, the application a turbulence correction factor may be appropriate for streams with self-aerated flows (e.g. white water rapids). The relation between θ_a, temperature, and turbulence is shown in Figure 2.2.

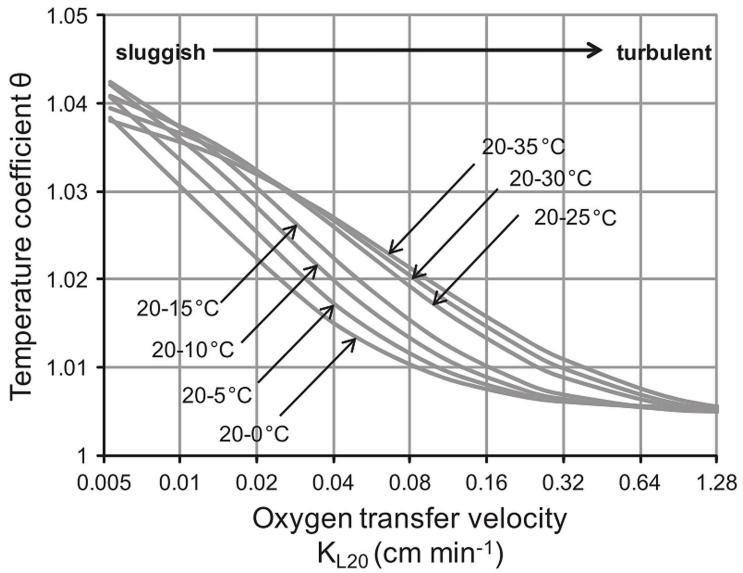

Figure 2.2 The relation between the temperature coefficient for reaeration, turbulence, temperature, and the oxygen transfer velocity. Reprinted from "Temperature dependence of stream aeration coefficients and the effect of water turbulence: A critical review," by B. O. L. Demars and J. R. Manson, 2013, *Water Research, 47,* p. 7. © 2012 Elsevier Ltd.

In their 2013 paper, Demars and Manson also carefully described Dobbins' theoretical film penetration model and proposed an empirical approximation to

determine θ_a as a function of the oxygen gas transfer velocity based upon Dobbins' model. Dobbins' model is unusual in that it is one of the few physically based reaeration models. Briefly, it is "based on the concept of 'an interfacial liquid film which maintains its existence in the statistical sense, that is the film is always present but the liquid content of the film is being continuously replaced in random manner by the liquid from the main body'" (Dobbins, 1963; Owens *et al.*, 1964, pp. 472-474). This is what is known as a surface renewal model and is the basis for the superscript n in the Schmidt number dependence (equation 2.8). Dobbins' film penetration theory is as follows:

$$K_{L_{O2}} = \sqrt{D_m s}\coth\sqrt{s\,L^2/D_m} \tag{2.15}$$

where $K_{L_{O2}}$ is the liquid film gas transfer velocity (cm s^{-1}), D_m is the molecular diffusivity (cm^2 s^{-1}), s is the average rate of surface renewal (s^{-1}), and L is the film thickness (cm). For high rates of renewal, equation 2.15 reduces to $K_{L_{O2}} = \sqrt{D_m s}$ giving way to the Schmidt number dependence of $K_L \propto (D_m)^n$ where $0.5 \leq n \leq 1$ (Demars and Manson, 2013). Assuming a constant two-dimensional bulk modulus, the surface renewal rate is:

$$s = \frac{1.3\,\rho\,\nu}{L^3} \tag{2.16}$$

where ρ is the density (g cm^{-3}) and ν is the kinematic viscosity of water (cm^2 s^{-1}). The product of kinematic viscosity and the density of a fluid gives the dynamic viscosity μ (g cm^{-1} s^{-1}). The diffusivity can be determined by the Stokes-Einstein equation:

$$D_m = \frac{k_B\,T}{3.491\,\pi\,\mu\,r} \tag{2.17}$$

where k_B is the Boltzmann constant ($1.3805 \cdot 10^{-16}$ g cm^2 s^{-2} K^{-1}), T is the absolute water temperature (K), and r is the radius of an oxygen molecule in water ($1.73 \cdot 10^{-8}$ cm; Edward, 1970). The film thickness $L \propto \nu^{3/4}$ where C_L is the constant of proportionality, a function of turbulence and independent of temperature. $C_L \propto E^{-1/4}$ where E is the energy dissipation in the fluid as a whole. Demars and Manson (2013) fit the following empirical functions for $\theta_a(C_L,T[^oC])$ and $\theta_a(K_{L_{O2}}[\text{cm hr}^{-1}],T[^oC])$:

$$\theta_a(C_L,T) = 1.39\cdot10^{-4}(C_L)^3 - 2.48\cdot10^{-3}(C_L)^2 + 1.55\cdot10^{-2}(C_L) + 1.61\cdot10^{-4}(T) + 1.011 \quad (2.18)$$

$$\theta_a(K_{L_{O2}},T) = 5.13\cdot10^{-5}\log_2(K_{L_{O2}})^3 + 9.12\cdot10^{-4}\log_2(K_{L_{O2}})^2 - 6.03\cdot10^{-4}\log_2(K_{L_{O2}}) + 3.31\cdot10^{-4}(T) + 0.9995 \quad (2.19)$$

These empirical relationships had R^2 values of 0.98 and 0.97, respectively, when compared with the exact solutions to Dobbins' theoretical equation.

Equation 2.4, the linearized Arrhenius function describes the temperature dependence on kinetic processes more precisely than the simplified version given in 2.13-2.14 and can also be used to determine the activation energy and temperature reaeration coefficient using equation 2.3 (Demars and Manson, 2013; Nguyen *et al*., 2015). González-Pinzón *et al*. (2016) suggest that it is incorrect to adjust for fast cycling diel temperature fluctuations using a steady state model such as the Q_{10} or van't Hoff-Arrhenius functions. After taking both day and nighttime respiration measurements in a headwater stream by injecting the bioreactive tracer resazurin, they concluded that there was not a significant difference between day and nighttime respiration rates and that applying a correction factor for diel temperature fluctuations for kinetic processes may be misleading.

2.2 Objectives

Prior to using the oxygen mass balance and van't Hoff-Arrhenius temperature correction coefficients to determine metabolic rates in aquatic systems, it is necessary to first characterize the activation energies associated with the kinetic processes for the particular site of interest. Additionally, holding reaeration and respiration constant over a diel period can lead to unrealistic parameter estimations, especially for shallow streams (Butcher and Covington, 1995). The goals of this chapter are as follows:

(1) Apply the nighttime slope method to two sites, one in the headwaters and the other near the mouth, to calculate respiration and reaeration rates.

(2) Determine whether Arrhenius kinetics is a valid assumption for both respiration and reaeration.

(3) Compare reaeration rate coefficients calculated from the nighttime slope method to the sixteen empirical equations presented in Table 2.1.

(4) Evaluate the sensitivity of the temperature correction coefficients for reaeration and respiration.

It is hypothesized that there will be a clear temperature dependence for respiration that can be described by Arrhenius kinetics when evaluating daily data over monthly to annual time scales. Turbulent flow conditions will minimize the temperature effect on reaeration so Elmore and West's temperature correction coefficient will generally overestimate the temperature sensitivity of reaeration. Although empirical equations are designed to describe reaeration rates for constrained sets of gas tracer studies, it is predicted that at least one of empirical equations will agree with the reaeration rate coefficients calculated from the nighttime slope method and be applicable to Fall Creek.

2.3 Methodology

In this section, the study sites and data collection methods will be described. The term baseflow will then be defined within the context of this investigation. Next, the detailed application of the nighttime slope method to determine respiration and reaeration rate coefficients will be outlined. Finally, the methods used to evaluate the temperature sensitivity and reaeration rate predictions will be described.

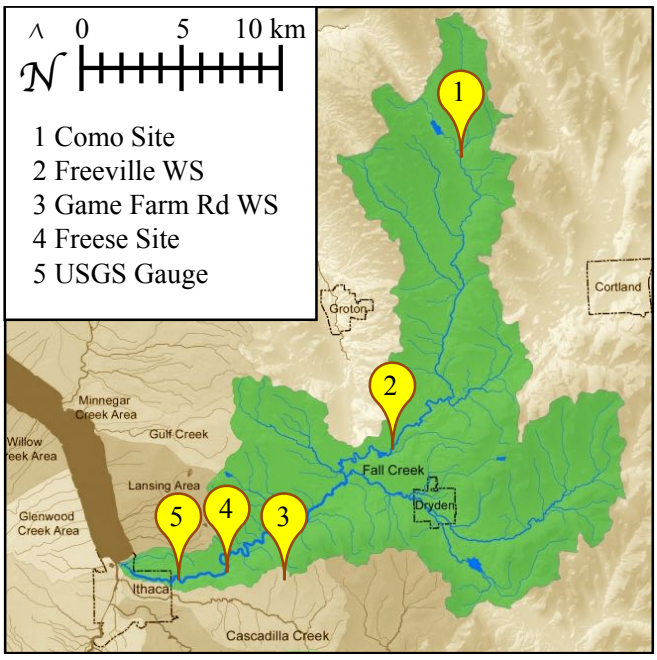

Figure 2.3 Fall Creek monitoring locations. Water quality monitoring was conducted at sites 1 and 4. Sites 2 and 3 are weather stations (WS). Site 5 is the USGS stream gauge (04234000)

2.3.1 Site Description and Data Collection

Fall Creek is a 33,086 ha watershed in the Finger Lakes region of upstate New York draining 48.2% agricultural, 39.7% forested, 10.7% urban land (Haith *et al.*, 2012). Its headwaters begin near Lake Como, northwest of Cortland, NY and it drains

into Cayuga Lake in Ithaca, NY. One study site was located three kilometers downstream of Lake Como Outlet, which will be referred to as "Como," while the other study site was located at Freese Road bridge, three kilometers upstream of the USGS Fall Creek gauging station (04234000); this site will be referred to as "Freese." These sites are shown on the map in Figure 2.3. Como has a drainage area of 29.3 km^2 with a slope of 0.0077 along the main channel (USGS StreamStats). Freese has a drainage area of 324 km^2 with an average channel slope of 0.0027 (USGS StreamStats). The Fall Creek drainage system has been impacted by the Pleistocene glaciation. The catchment is underlain by Devonian bedrock and consists primarily of siltstones and shales.

The USGS stream gauge on Fall Creek is located just downstream of Cornell's Water Filtration Plant (WFP) intake, twelve kilometers downstream of the combined effluent pipe for the Dryden and Freeville Waste Water Treatment Plants (WWTPs), and five kilometers upstream of Cayuga Lake. The USGS gauging station has a total drainage area of 326 km^2. There are two weather stations within the Fall Creek watershed (shown in Figure 2.3). The Northeast Regional Climate Center (NRCC), Cornell University, operates the station at Game Farm Road in Ithaca, which is approximately 2 km from Freese. The Network for Environment and Weather Applications (NEWA) operates the station in the village of Freeville, which is 19 km from Como. Stream discharge and gauge height (river stage) data was downloaded from the USGS website for the Fall Creek station for the period of interest (May 2015 – May 2016) at 15-minute recording intervals. Precipitation data from the Game Farm Road and Freeville weather stations was obtained from NRCC at an hourly sampling resolution.

Discrete and continuous (15 minute increments) water quality measurements were collected intermittently using multi-parameter sondes (YSI models 600 XLM and 6920 VS) at both Freese and Como from May 2015 – May 2016 for a total of 160 days of data coverage at Freese and 178 days of coverage at Como. Physiochemical water quality metrics included temperature, pH, specific conductance, and dissolved oxygen (DO). One day of coverage indicates that at least one full suite of water quality measurements was collected per day. Continuous measurements of water quality parameters were collected for 124 full days at Freese and 158 full days at Como. One full day of continuous coverage indicates that 96 sets of water quality measurements were collected over a 24-hour period.

The YSI 6920 VS sonde was linked to a handheld with display (YSI 650 MDS) for discrete measurements. This sonde was equipped with a reliable optical sensor (ROX) designed for drift-free long-term DO measurements in harsh environments. Two YSI 600 XLM sondes with rapid pulse oxygen sensors were deployed during the summer months (June – September) for continuous monitoring at both sites. From October 2015 – May 2016, one 600 XLM sonde was deployed at one of the field sites, while the 6920 VS sonde was utilized for continuous monitoring at the other. Each of these sondes was rotated from one site for a 1- to 2- week deployment to the next for the following deployment period. All physiochemical sensors were cleaned and calibrated bi-weekly in accordance with the YSI Environmental 6-Series Probes care and maintenance protocols (YSI, 2012). The rapid pulse DO sensors were calibrated with the ROX sensor prior to each long-term deployment and recalibrated against the ROX at the end of each deployment to adjust for drift (Bales and Nardi, 2007).

In addition to monitoring water quality, channel hydraulic geometric features (e.g. cross sectional depth and width) were measured from June – October 2015 on a weekly to bi-weekly basis. These parameters were related to discharge as demonstrated by Leopold and Maddock (1953). Because the total drainage area for the Freese site is close to that of the USGS gauge (324 km^2/326 km^2 ~ 1), the discharge at Freese was assumed to be approximately equal to the discharge recorded at the gauge station. The USGS gauge height was also conveniently similar to the average measured depth at Freese (H_{gauge}/H_{Freese} = 1.02). Channel width was best predicted by discharge via a logarithmic function for Freese rather than through a power function as Leopold and Maddock had proposed. To model discharge for Como (Q_{Como}), a proportional relationship between the comparative drainage area for Como and the USGS gauge was applied such that:

$$Q_{Como} = Q_{gauge}^{A_{D_{Como}} / A_{D_{gauge}}} \tag{2.20}$$

where A_{DComo} is the drainage area for Como and A_{Dgauge} is the drainage area for the USGS station yielding a proportion of 0.09. Like Freese, the measured channel width for Como was related to its discharge through a logarithmic function. This was also the case for average channel depth at Como. The equations relating Q_{gauge}, W_{Freese}, Q_{Como}, W_{Como}, and H_{Como} are provided in Appendix A.

2.3.2 Defining Baseflow

Baseflow is a term that is not easily quantified in hydrology. It is generally considered to be the sustained low-flow rate that is reached during dry conditions. For gaining streams, such as Fall Creek, that have channel floors at a lower elevation than

the groundwater table, baseflow is primarily sourced from groundwater seepage. In snowmelt-dominant streams, it may also be sourced from the long-term storage and slow release of snowmelt (Miller *et al*., 2014). Ultimately, baseflow is sourced from water entering a stream reach via subsurface flow paths as opposed to overland flow (e.g. runoff) or direct flow via precipitation. For the purposes of this study, baseflow is considered the portion of streamflow which is sourced from groundwater.

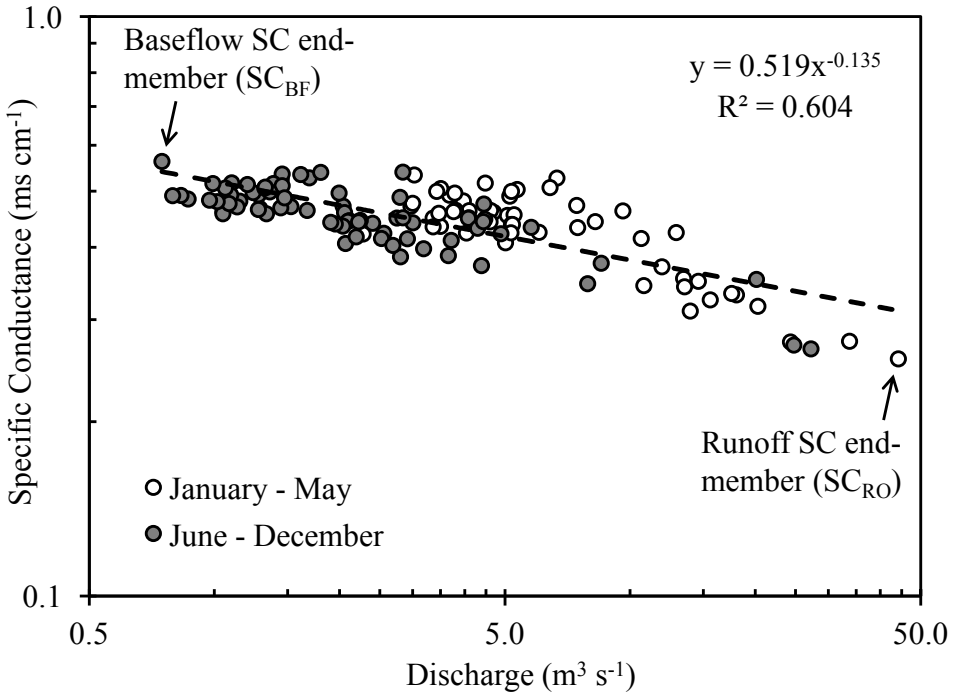

Figure 2.4 Baseflow and runoff SC end-member selection for Freese

In order to separate the baseflow component of discharge from runoff, a classic chemical hydrograph separation approach using daily average specific conductance (SC) and streamflow measurements was utilized (Miller *et al.*, 2014; Miller *et al.*, 2015). SC describes the concentration of salts (e.g. chlorides, sulfides, alkalis, and carbonates)

in water that have been dissolved into ions (electrolytes). SC is considered a conservative mass tracer, which means that it does not react with other chemical constituents in water so it can essentially be tracked throughout a watershed. During low-flow conditions, SC concentrations will generally be greater than during higher flow conditions since groundwater has a higher SC concentration than precipitation. During storm events, SC will be diluted from the added volume of lower SC water from rainfall-runoff. Through analyzing the daily average SC concentration for a stream against its discharge, two end-members, one representative of baseflow and the other of runoff, can be extracted. The baseflow end-member is the SC for lowest flow and highest observed SC, while the runoff end-member is the SC for the highest flow and lowest observed SC.

Once the two end-members have been determined, daily baseflow (Q_{BF}) can be calculated using the following conductivity mass balance (Pinder and Jones, 1969):

$$Q_{BF} = Q\left(\frac{SC - SC_{RO}}{SC_{BF} - SC_{RO}}\right) \tag{2.21}$$

where Q is the daily average discharge, SC is the daily average specific conductance, SC_{RO} is the runoff specific conductance end-member, and SC_{BF} is the baseflow specific conductance end-member. The baseflow-runoff end-member analysis for Fall Creek is shown in Figure 2.4. The daily average SC data comes from the combined discrete and continuous sonde measurements taken at both sites. For days with only one SC measurement, the value was assumed to be representative of the average discharge for that date (Miller *et al*., 2015). The daily average discharge data for Freese and Como are the averaged 15-minute discharge at each site obtained via the methods described in section 2.2.1. Since SC data were not available for the entire recording period, a

regression curve was fit to describe SC as a function of Q (R^2 = 0.60 for Freese, Figure 2.4; R^2 = 0.77 for Como, Appendix A) to model baseflow for May 2015-16. For Freese, SC_{BF} was 0.563 ms cm^{-1} and the SC_{RO} was 0.257 ms cm^{-1} (Figure 2.4). For Como, SC_{BF} was 0.330 ms cm^{-1} and SC_{RO} was 0.166 ms cm^{-1} for the study period.

This conductivity mass balance (CMB) method may become more challenging to use in the future with the marked increase in salinization of freshwaters from road salt application in the Northeastern United States (Kaushal *et al.*, 2005), which could make the SC signature of snowmelt-runoff difficult to discern from the baseflow SC signature. Though there is a clearly defined runoff end-member in Figure 2.4, the presence of high SC concentrations observed between January and May, when much of the runoff for Fall Creek is derived from snowmelt, is suggestive of increased salinity from road salts as ascertained by Shaw *et al*. (2012). While this CMB may not be appropriate for Fall Creek in the context of assessing impacts of climate and land use change on Fall Creek's hydrological budget, the purpose of separating baseflow in this chapter is to select measurement dates where DO is minimally impacted by precipitation and runoff in preparation for the nighttime slope method as described in the following section. Thus, the CMB is applied to Freese and Como to isolate days for which most of the stream discharge is composed of baseflow (e.g. $Q_{BF}/Q > 0.6$). Throughout the rest of this chapter "baseflow" will refer to any monitoring date where the streamflow is made up of at least 60% baseflow as determined by the CMB (equation 2.21).

2.3.3 Characterizing Respiration and Reaeration

The nighttime slope method (NSM), as introduced in section 2.1.2, was applied to monitoring dates for Freese and Como, which contained a full set of nighttime water quality measurements (from sunset to sunrise), met the qualifications for baseflow defined in the previous section, did not receive significant precipitation, and for which there was not ice coverage on the water surface. Time of sunset and sunrise were calculated with the National Oceanic and Atmospheric Administration (NOAA) solar calculations spreadsheet to determine solar data for any day for a specified site and year. The calculations are based on the equations from *Astronomical Algorithms* by Jean Meeus (1991) and are accurate to within a minute for locations between +/- 72^{o} latitude. The spreadsheets and solar calculation details are available at http://www.esrl.noaa.gov/gmd/grad/solcalc/calcdetails.html. The NSM was modified from its original form for the summer months when the maximum DO deficit (i.e. minimum DO concentration) was reached well before sunrise. Instead of being applied throughout the entire nighttime duration, it was carried out from sunset up through the time of the minimum DO concentration to minimize the scatter associated with decreasing DO deficits. All NSM plots are provided in Appendix B.

A linear trend was fit to the NSM plots. The respiration (ordinal intercept) and reaeration rate coefficient (slope) were extracted from each measurement date. For dates where the NSM yielded an $R^2 > 0.5$, the respiration was normalized from a concentration to a mass flux density (mg O_2 consumed m^{-2} d^{-1}) by multiplying by average channel depth. Then the natural log of the normalized respiration was plotted against standardized temperature (equation 2.4), for the average nighttime water temperature,

to test whether an Arrhenius temperature dependence on respiration is a valid assumption and to check that the NSM provided realistic estimates for respiration.

2.3.4 Evaluating Temperature Sensitivity and Reaeration Rate Predictions

The reaeration rate coefficients (k_{O2}) derived from the NSM provide the surface water-atmosphere mixing rates for the average nighttime water temperature on each measurement date. In order to determine whether there is a relationship between k_{O2} and discharge, k_{O2} must be referenced to a standard temperature so that the values can be appropriately compared. As discussed in section 2.1.4, the standard reference temperature for reaeration is 20^{o}C, which is somewhat inconvenient considering the common standardized reference temperature for respiration is 15^{o}C in the literature. For consistency with past works, 20^{o}C will be maintained as the standard temperature for reaeration and 15^{o}C for respiration throughout this dissertation.

Two temperature correction factors (θ_a) were applied to standardize the reaeration rate coefficients from the NSM to 20^{o}C: (1) Elmore and West's empirical θ_a of 1.0241 and (2) Demars and Manson's (2013) θ_a based on an empirical simplification (eqn. 2.19) of Dobbins' film penetration model. Since Demars and Manson's empirical approximation breaks down for the lower limit of the theoretical range ($\theta_a = 1.005$), any θ_a that was predicted to be out of range for turbulent flows was forced equal to 1.005 in this study. Figure 2.5 illustrates the performance of equation 2.19 as compared to Dobbins' theoretical model. Equation 2.3 relates the temperature correction factor to the activation energy (E_a) for Arrhenius kinetics. The underlying assumption in Elmore and West's θ_a is that simplified Arrhenius kinetics can describe the effect of temperature on

reaeration rates—that reaeration rates increase with increasing temperature. To test this assumption, the natural log of reaeration rates under a constant flow regime were plotted against standardized temperature following the same linearized Arrhenius form that was applied to respiration in the previous section. The slope of this relation (equation 2.4) is the activation energy for the kinetic process, which can then be used to calculate the temperature correction coefficient.

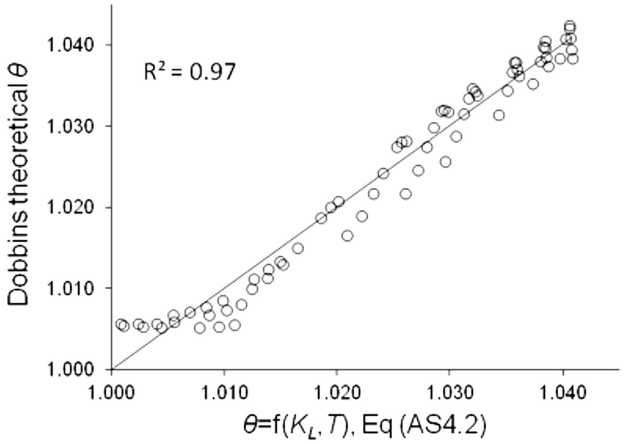

Figure 2.5 Dobbins' theoretical temperature coefficient for reaeration (θ_a) versus the temperature coefficient calculated from the empirical function. Reprinted from "Temperature dependence of stream aeration coefficients and the effect of water turbulence: A critical review," by B. O. L. Demars and J. R. Manson, 2013, *Water Research, 47,* App. A. © 2012 Elsevier Ltd.

After the reaeration rate coefficients were standardized to 20°C by rearranging equation 2.13 to give $k_{O2,20^o} = k_{O2}\theta^{20^oC-T}$, a regression curve was fitted. The mean multiplicative error MME (Moog and Jirka, 1998), described in section 2.1.1 was then applied to assess the fit of the regression curve and sixteen empirical reaeration equations from Table 2.1 to the standardized reaeration rates from the NSM for both Freese and Como.

2.4 Results

Daily average discharge for Fall Creek from the USGS gauging station and the Freese daily baseflow hydrograph generated from the CMB are shown in Figure 2.6. There were ultimately 46 sampling dates for Freese and 47 dates for Como that met the criteria specified in section 2.3.3 for the nighttime slope method. Respiration rates calculated from the NSM follow a strong Arrhenius temperature dependence as displayed in Figure 2.7 with an R_o (at 15^{o}C) of 11.5 g O_2 consumed m^{-2} and coefficient of determination of 0.94 for Freese and an R_o of 3.46 g O_2 m^{-2} with a coefficient of determination of 0.88 for Como. The activation energies for respiration at Freese and Como were 0.67 eV and 0.61 eV respectively. Reaeration rate coefficients calculated from the NSM are provided as a function of discharge in Figure 2.8 for Freese and Figure 2.9 for Como. NSM k_{O2} in Figures 2.8-2.9 are normalized to 20^{o}C using Dobbins' θ_a, which provided regression coefficients of 0.71 and 0.21 for Freese and Como respectively. Dobbins' θ_a ranged from 1.005 to 1.009 for Freese and from 1.011 to 1.020 for Como. Elmore and West's θ_a of 1.0241 yielded an R^2 of 0.66 when fit to the Freese temperature adjusted data and an R^2 of 0.15 for Como. There was a strong correlation between k_{O2} and discharge for Freese with the highest non-temperature adjusted reaeration rates occurring in the summer (k_{O2max} = 56 d^{-1}) and lowest in the winter (k_{O2min} = 5.6 d^{-1}). The highest reaeration rates during baseflow for Como also took place in summer (k_{O2max} = 14.7 d^{-1}) with the lowest in the winter (k_{O2min} = 5.6 d^{-1}). However, there was not a distinct relation between k_{O2} and discharge at Como. On average, reaeration rates were 4.7 times higher and more variable at Freese (k_{O2avg} = 12.5 $\pm$ 12.3 d^{-1}) than at Como (k_{O2avg} = 5.63 $\pm$ 2.61 d^{-1}).

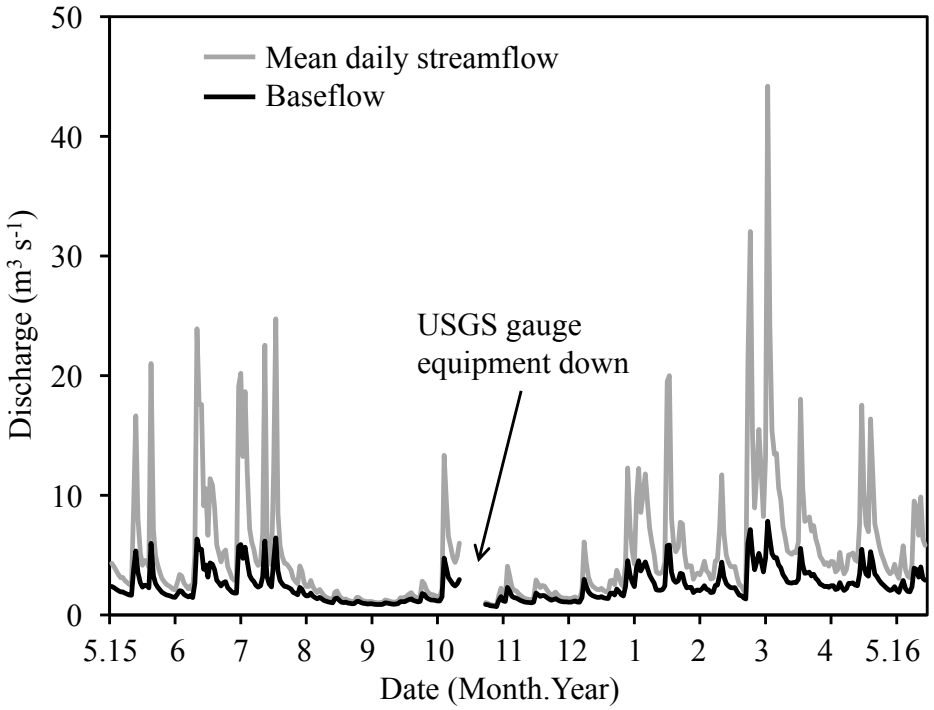

Figure 2.6 Mean daily discharge and baseflow for Fall Creek calculated from the conductivity mass balance at Freese

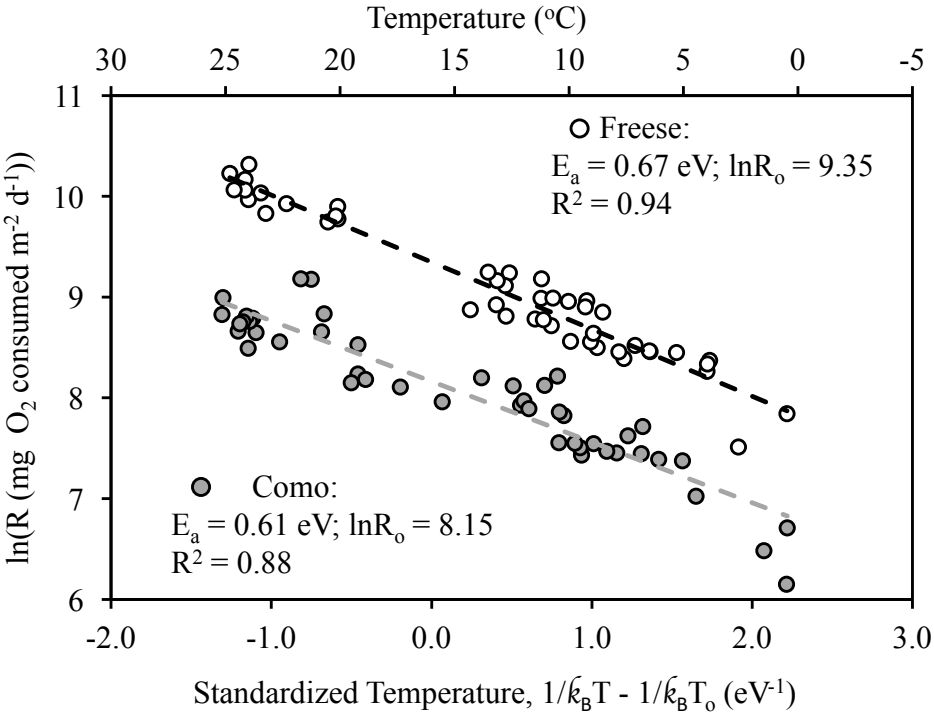

Figure 2.7 Arrhenius plots for stream respiration at Freese and Como for a reference temperature of 15°C

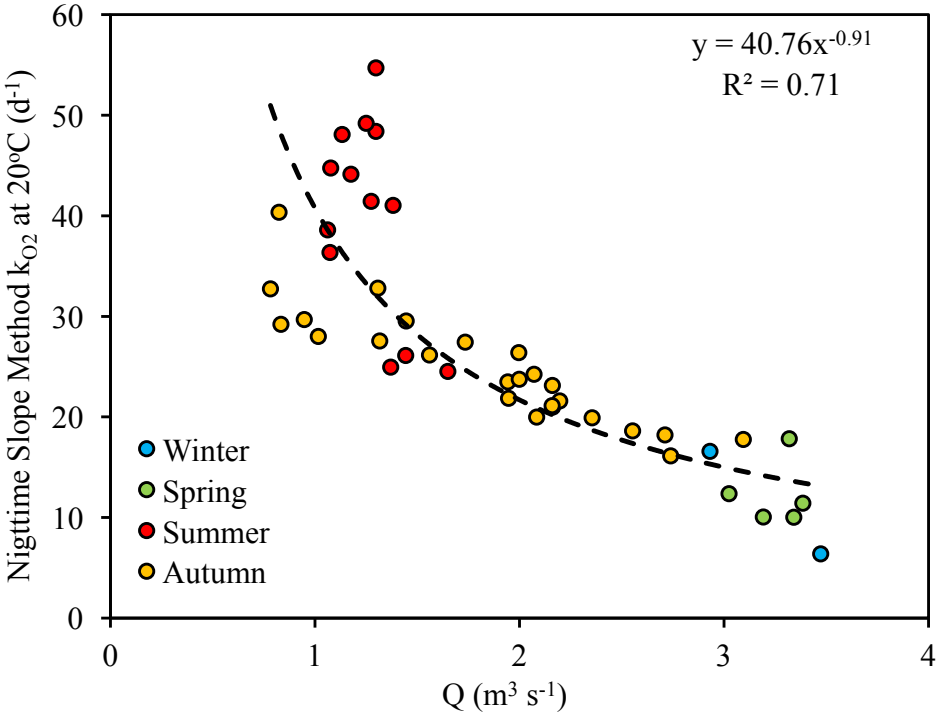

Figure 2.8 Reaeration rate coefficients calculated from the nighttime slope method for Freese normalized to 20°C with Dobbins' θ_a

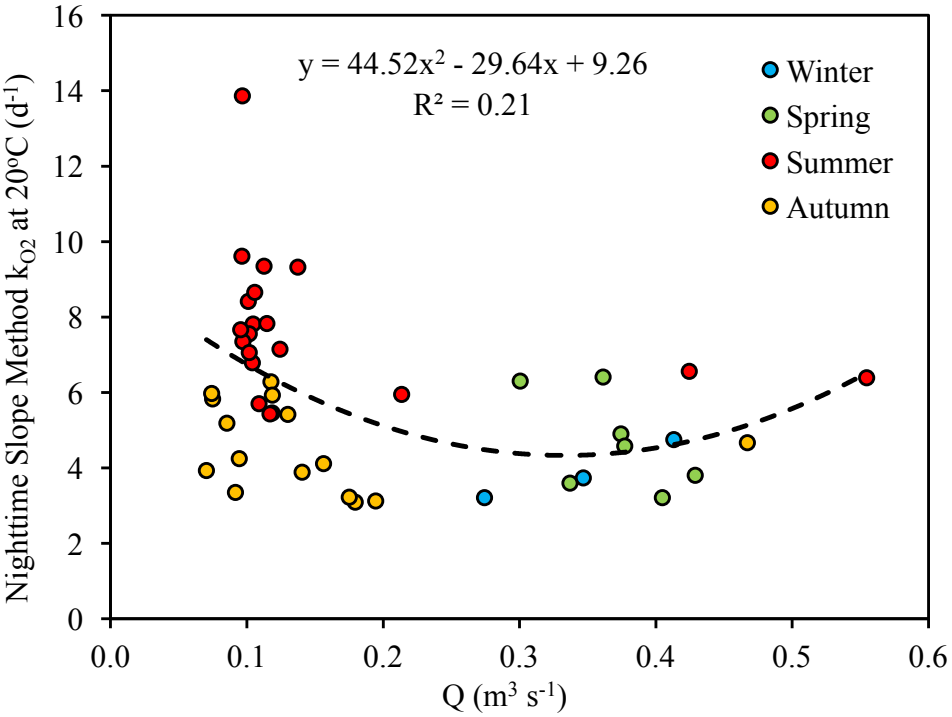

Figure 2.9 Reaeration rate coefficients calculated from the nighttime slope method for Como normalized to 20°C with Dobbins' θ_a

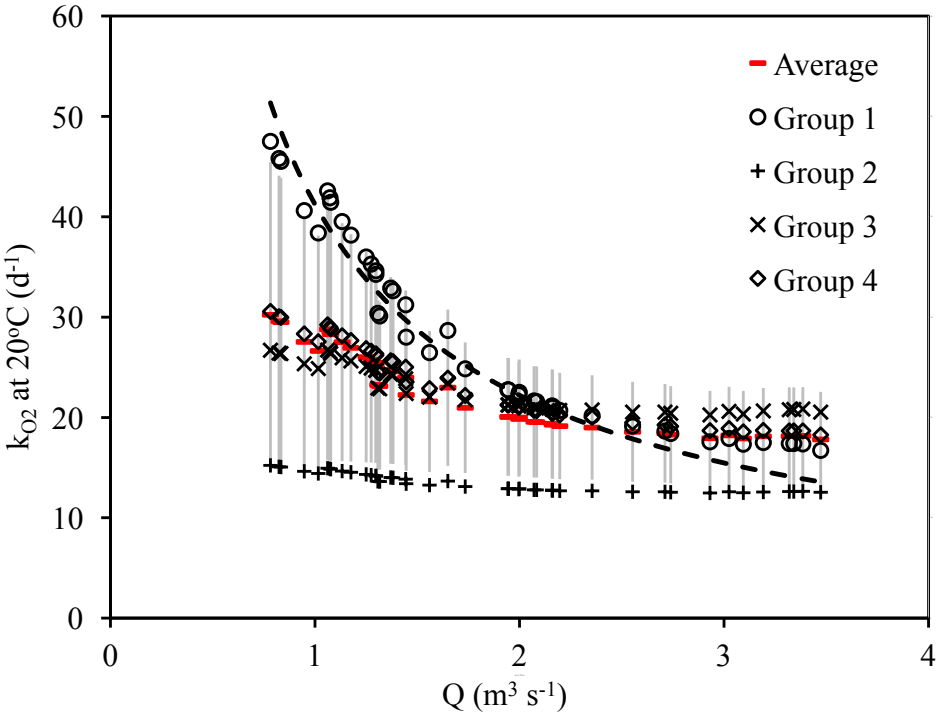

Figure 2.10 Average reaeration rate coefficients calculated from empirical equations presented in Table 2.1 during baseflow for Freese. The average represents the average reaeration rate coefficient of all sixteen empirical equations and the error bars are one standard deviation of the average of all the empirical equations. The empirical equations averaged within each group are organized as shown in Table 2.1. The dashed curve represents the reaeration rate calculated form the equation presented in Figure 2.8.

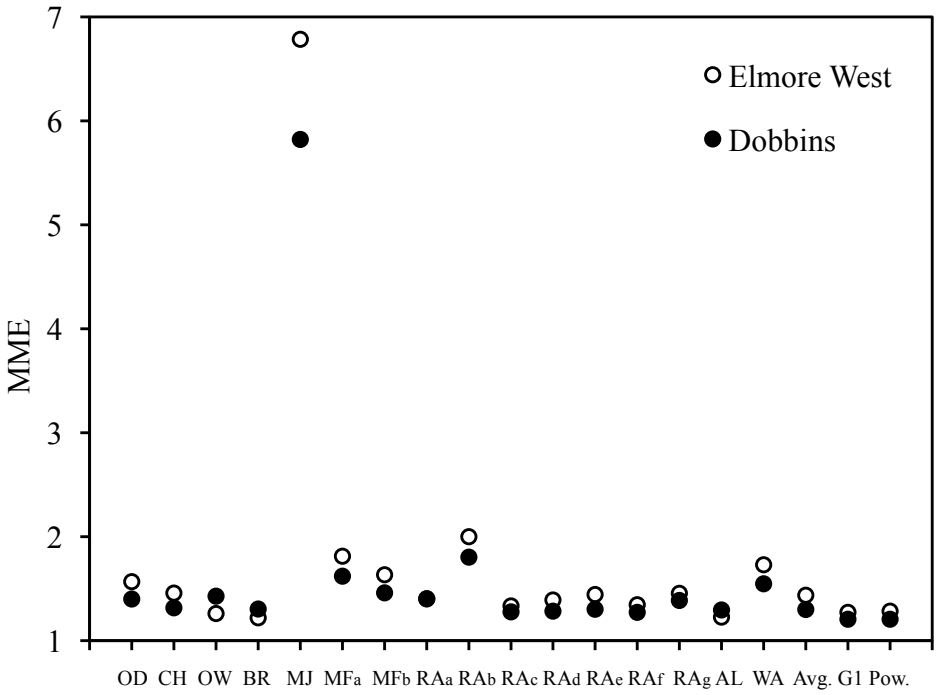

Figure 2.11 Mean multiplicative error for reaeration rate coefficients calculated from empirical equations (symbols are described in Table 2.1) compared to reaeration rate coefficients calculated from the nighttime slope method for Freese. "Avg." is the average MME from all sixteen empirical equations as illustrated in Figure 2.10, "G1" is the group 1 empirical equation average, and "Pow." is the regression fit from Figure 2.8.

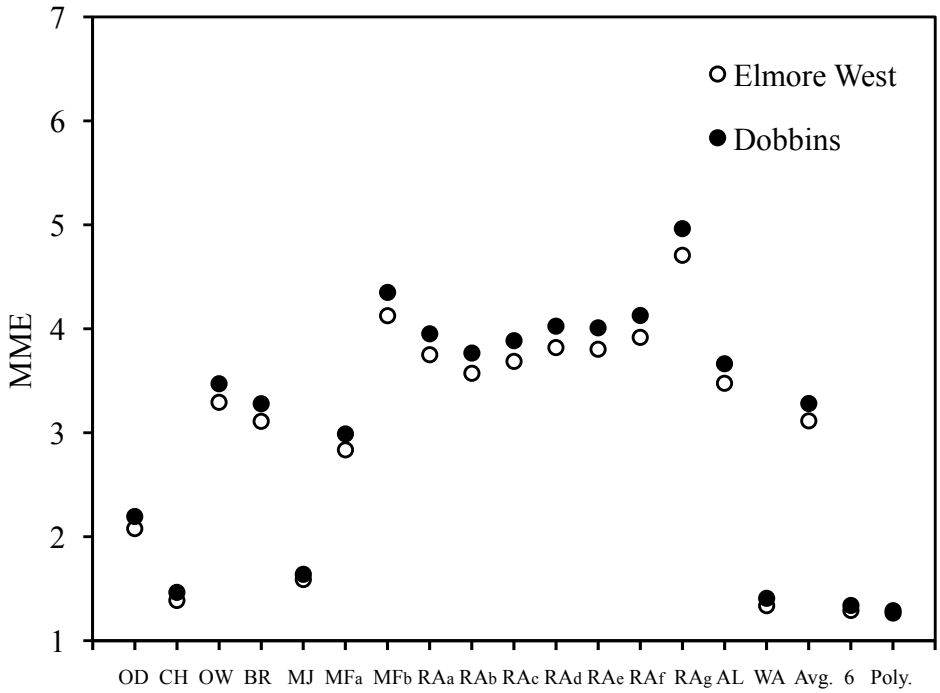

Figure 2.12 Mean multiplicative error for reaeration rate coefficients calculated from empirical equations (symbols are described in Table 2.1) compared to reaeration rate coefficients calculated from the nighttime slope method for Como. "Avg." is the average MME from all sixteen empirical equations, "6" assumes a constant reaeration rate coefficient of 6 day^{-1}, and "Poly." is the regression fit from Figure 2.9.

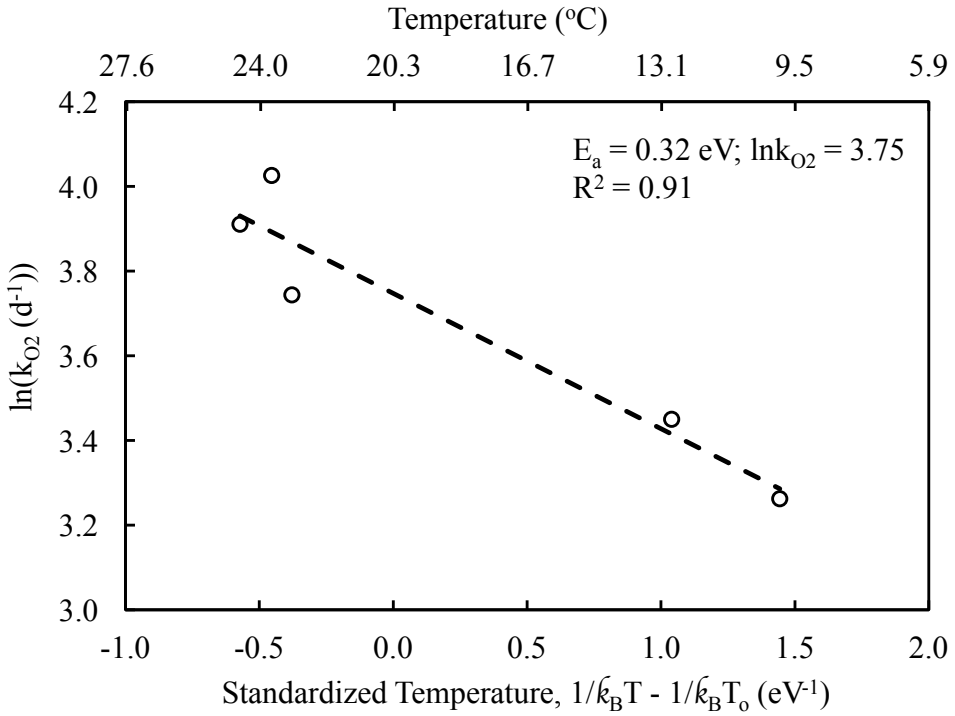

Figure 2.13 Arrhenius plot for stream reaeration at Freese for Q ~ 1.3 m^3 s^{-1} and a reference temperature of 20°C

2.5 Discussion

2.5.1 Respiration

There was a strong temperature dependence on respiration that could be described by Arrhenius kinetics for both Como and Freese. Respiration at Freese required an E_a of 0.67 eV as compared to 0.61 eV at Como. While it requires more energy for respiration to occur at Freese, the respiration mass flux of O_2 at Freese was nearly 3.4 times greater on an area basis than that of Como. The activation energies for both sites were within the theoretical range of 0.6-0.7 eV for heterotrophic respiration in aquatic ecosystems (Gillooly *et al*., 2001; Demars *et al*., 2011; Perkins *et al*., 2012; Yvon-Durocher, 2012; Jankowski *et al*., 2014).

While Yvon-Durocher (2012) expected R_o and E_a to vary seasonally due to the availability of reduced carbon substrates and changes in net primary production, this was not the case for Fall Creek. A constant, site specific R_o and E_a described respiration kinetics at both Freese and Como over the course of one year. This suggests that benthic heterotrophic communities vary from site to site within a stream, but do not change substantially at each site seasonally. However, because of the effect of El Niño, the mild 2015-16 New York winter may have been a special case. Conversely, if the bulk of stream respiration takes place within the hyporheic zone and, therefore, does not fluctuate significantly on a daily timescale (González-Pinzón *et al.*, 2016), then it could be reasoned that the temperature changes would be attenuated on a seasonal timescale so the hyporheic community would remain relatively static.

Perkins *et al*. (2012) found that the core biochemistry that drives respiration kinetics may be conserved across diverse taxa suggesting there is an intrinsic sensitivity of metabolic respiration based on the size of an organism (e.g. Gillooly *et al*., 2001). This implies that the sensitivity of respiration on temperature, as quantified by the E_a, will not change with changes in temperature or even necessarily with changes in the types of organisms that make up a community. However, absolute rates of respiration may be impacted by changes in biofilm biomass.

The activation energy describes temperature sensitivity according to equations 2.2-2.3. Therefore, the higher the required E_a is for a kinetic process, the more sensitive that process is to changes in temperature. This suggests that the downstream locations (e.g. Freese) may be more sensitive to temperature, and therefore climate, changes than that of the upstream headwaters (e.g. Como). E_a is also indicative of the type of

ecosystem in which respiration is taking place. Lower activation energies (~0.32 eV) are characteristic of terrestrial ecosystems, while higher activation energies (~0.65 eV) are characteristic of aquatic ecosystems (Yvon-Durocher *et al*, 2012). An abundance of aquatic plants at a given site may decrease E_a. As illustrated in Figure 2.14, Como has a greater volume of aquatic vegetation than that of Freese, which supports the lower observed E_a at Como.

Figure 2.14 Observed summer and autumn baseflow on Fall Creek.
(a.) Freese, 9.01.15; **(b.)** Como, 9.01.15; **(c.)** Freese, 11.08.15; **(d.)** Como, 11.08.15

2.5.2 Reaeration

Figure 2.14 also displays the differences in baseflow conditions for Freese and Como. Freese has a rocky substrate compared to the sand, silts, and flat rocks that line Como's sediment floor. Shallow channel depths combined with a large contact area for friction provided by the benthic rocks facilitates mixing and turbulence even during low flow regimes. This supports the high reaeration rates observed at Freese. The reaeration at Como was, on average, half that of Freese. As shown in Figure 2.14, the water surface at Como tended to be flat and calm with only mild ripples occurring in the November image as compared to the rough water surface characteristic of Freese. Based on their appearance, Como's ripples were likely wind driven. In streams, turbulence from wind shear at the water's surface yields a shallower effective mixing depth and lower gas transfer rates than that of turbulence derived from benthic boundary layer friction (Lorke and Peeters, 2006; Zappa *et al.*, 2007; Alin *et al.*, 2011). The bountiful vegetation at Como may have also played a role in suppressing air-water gas exchange.

The narrow range of discharge and k_{O2} calculated from the NSM during baseflow for Como made it difficult to discern a trend between flow and reaeration. Reaeration at Freese, on the other hand, was highly correlated with discharge. The generally low MME for the empirical reaeration rate equations calculated from geomorphic features at Freese show that the equations were more reliable in predicting reaeration at Freese than at Como. This is not surprising since the empirical equations require knowledge of channel width, average channel depth, and reach slope, which are all hydraulic geometric features that can be described by discharge (Leopold and Maddock, 1953). From the beginning, discharge at Como was approximated so

uncertainties in this approximation would propagate through to the reaeration rate coefficients determined by the empirical equations. Selecting a constant reaeration rate coefficient of 6 d^{-1}, independent of discharge, yielded the lowest MME for predicting reaeration at Como (besides the regression fit). This result further illustrates the unpredictability and scatter of describing the reaeration calculated at Como from the NSM.

Equation WA (Wallin *et al*., 2011) performed surprisingly well at both sites considering it was developed to describe the gas transfer coefficient of CO_2 in boreal streams. This equation was scaled by the Schmidt dependence specifically for use in this dissertation; not by Wallin *et al*. The low MME values for both Freese and Como from WA support the application of the Schmidt number for scaling gas transfer rates between different gases (Jähne *et al*., 1987; Raymond *et al*., 2012). The RAa-RAg and AL equations were specifically designed for scalability between gases. While RAa, RAc-RAg, and AL performed reasonably well at Freese, they did not perform nearly as well as WA at Como as indicated by MME. Raymond *et al*. (2012) are careful to point out that their scalable gas transfer equations were designed specifically for scaling gas fluxes across broad regions not for individual stream reaches.

Of all the empirical reaeration equations tested, the average of the classic group 1 equations produced the lowest MME when compared to the reaeration rates calculated by the NSM at Freese. This suggests that stream velocity and average channel depth are more influential controls on reaeration than reach slope at Freese. Due to the gentle step-like nature of the flat shales that underlay the lower portion of Fall Creek, slope would not be expected to be a major control on reaeration. While the group 1 equation CH

appears to be a relatively good indicator of reaeration rates at Como, the slightly smaller MME produced by equation WA suggests that slope may play a more important role at Como. Overall, when DO measurements are not available to carry out the NSM, the combined use of equations CH and WA may be applied to estimate reaeration rates during baseflow on Fall Creek keeping in mind that the use of these empirical equations will likely overestimate k_{O2} at upstream locations (e.g. Como) and underestimate k_{O2} at more turbulent downstream locations (e.g. Freese) as shown in Appendix C.

2.5.3 Temperature Coefficient for Reaeration

In general, the temperature coefficient (θ) is not constant throughout a range of temperatures as exemplified by equation 2.3 (Schneiter and Grenney, 1983). Even if Arrhenius kinetics do appear to describe reaeration (Figure 2.13), the application of the simplified Arrhenius form (equation 2.13) does not appropriately describe Arrhenius kinetics if a constant temperature coefficient is assumed (Schneiter and Grenney, 1983; Sheridan *et al*., 2012). Although, water temperature does not vary nearly as much as air temperature, it is by no means constant on seasonal (or even daily) time scales. Under their careful laboratory experiments, Elmore and West (1961) found that the reaeration rate increased geometrically with increasing temperature producing a constant θ_a of 1.0241 for use in equation 2.13—a form of the simplified Arrhenius. In this case, a constant temperature coefficient is applied to Arrhenius kinetics, which does not make sense physically. Elmore and West do not mention the Arrhenius by name in their manuscript and may have chosen equation 2.13 simply to describe their laboratory observations. Even so, their θ_a has been interpreted as a temperature correction for use

in the DO mass balance to describe reaeration under simplified Arrhenius kinetics by other researchers (e.g. Butcher and Covington, 1995). Butcher and Covington's suggested temperature corrections have additionally been applied to respiration and photosynthesis under the assumption of a constant θ for all temperatures in numerous reaeration and metabolism studies (e.g. McBride and Chapra, 2005; Kent *et al*., 2006; Birkel *et al*., 2013; Riley and Dodds, 2013; Correa-González, 2014).

Dobbins' θ_a proposed by Demars and Manson (2013) is a function of both temperature and turbulence. For sites characterized by turbulent flow, such as Freese, the effect of temperature on reaeration is smaller ($1.005 \leq \theta_a < 1.009$) than that of sites characterized by sluggish or laminar flow like Como ($1.011 < \theta_a < 1.020$). Even at Como, Elmore and West's θ_a of 1.0241 would over predict the sensitivity of reaeration rates to changes in temperature. At 20^{o}C, the θ_a calculated from the linearized Arrhenius for Q ~ 1.3 m^3 s^{-2} at Freese, was 1.0081, which is within the range of temperature coefficients predicted by Dobbins' film penetration theory. Correcting for temperature by arbitrarily using Elmore and West's θ_a may overestimate reaeration during low temperatures or for turbulent flow regimes. Additionally, reaeration rates may be underestimated for temperatures > 20^{o}C. In the case of overestimating reaeration for lower temperatures, respiration rates would also be overestimated, while the reverse would be the case for underestimating reaeration for higher temperatures. If respiration rates were determined entirely on the basis of equation 2.1 and an empirical equation with an inappropriate θ_a, an Arrhenius plot for respiration (e.g. Figure 2.7) would likely

have a shallower slope influenced by the assumed temperature dependence from the chosen θ_a providing unrealistic activation energies for respiration in aquatic ecosystems.

2.6 Conclusion

The nighttime slope method was a viable technique for predicting reaeration and respiration rates for Fall Creek. Resulting respiration rates from the NSM displayed a strong temperature dependence that could be described by Arrhenius kinetics. Constant activation energies and reference respiration ($T_o = 15^oC$) throughout a year determined from an Arrhenius plot suggests that seasonality may not influence basal respiration kinetics and heterotrophic communities may not vary substantially on seasonal time scales at each site. Differences in activation energies between Freese and Como implies that each site supports a distinctive community composition of heterotrophs.

Reaeration rates, as determined from the NSM, were best described by a regression fit against discharge for Freese and a constant value of 6 d^{-1} for Como. As a whole, reaeration rates for Fall Creek may be predicted empirically by either the equations of Churchill *et al*. (1962) or Wallin *et al*. (2011) provided in Table 2.1. The low MME for both Freese and Como from the Wallin *et al*. equation combined with the low MME for Freese from the Alin *et al*. equation supports scalability between oxygen and carbon dioxide reaeration described by the Schmidt number dependence.

It is critical to characterize respiration and reaeration rates, which can be accomplished via the NSM for unpolluted streams, prior to assigning a temperature correction coefficient. For respiration, temperature sensitivity can be determined from from the activation energy, which is between 0.6 and 0.7 eV for aquatic ecosystems;

heavily vegetated stream reaches may fall at the lower end of this range. However, the R_o for any site is not so easy to approximate and may be determined from an Arrhenius plot or by measuring respiration at 15^oC. For reaeration, the temperature coefficient may be determined by Demars and Manson's (2013) approximation of Dobbins' theoretical θ_a since reaeration is a function of both temperature and turbulence. Applying Elmore and West's θ_a without physical justification may overestimate reaeration and respiration in turbulent streams and at temperatures lower than 20^oC.

CHAPTER 3

SPATIOTEMPORAL VARIABILITY OF AND HYDROLOGICAL CONTROLS ON REAERATION AND CARBON DIOXIDE EVASION

3.1 Introduction

Oxygen consumption during respiration depletes rivers and streams in dissolved oxygen (DO) during the nighttime. Reaeration can recharge the DO deficit in surface waters with atmospheric O_2. During the daytime, rivers and streams may become supersaturated in oxygen from photosynthesis and release O_2 back to the atmosphere. While surface waters tend to oscillate between DO supersaturation during the day and depletion at night, they often remain supersaturated in free carbon dioxide (pCO_2) and may be net sources of CO_2 to the atmosphere.

Due to their small areal coverage (< 1%) of Earth's surface, inland waters had long been neglected from the global carbon cycle (Cole *et al*., 2007; Battin *et al*., 2009). This neglect has begun to be addressed over the past decade. Inland waters are now estimated to emit at least an order of magnitude more CO_2 to the atmosphere (2.1 Pg C yr^{-1}) than volcanic outgassing (0.1 Pg C yr^{-1}) on the global scale (Raymond *et al*., 2013; Ciais *et al.*, 2013). Rivers and streams contribute at least three quarters of the global CO_2 efflux from inland waters (Raymond *et al*., 2013). An estimated 0.54 Pg C yr^{-1} is emitted to the atmosphere from northern temperate rivers and streams alone (Butman and Raymond, 2011).

Similar to the diffusion term in the oxygen mass balance (eqn. 2.1, 2.7), the surface water-atmosphere flux of CO_2 ($\mathcal{F}_{CO2}$, mg CO_2-C m^{-2} d^{-1}) can be described by:

$$\mathcal{F}_{CO_2} = k_{CO2} K_H H \left(pCO_{2_w} - pCO_{2_{atm}}\right) \quad (3.1)$$

where k_{CO2} is the reaeration rate coefficient for carbon dioxide, K_H is the Henry's law solubility coefficient for CO_2 (mg C L^{-1} μatm^{-1}), H is the average channel depth (m), pCO_{2w} is the partial pressure of free CO_2 in the water (μatm), and pCO_{2atm} is the partial pressure of atmospheric CO_2 (400 μatm). K_H can be approximated from the following empirical equation as a function of temperature (K) in freshwater at standard atmospheric pressure (Weiss, 1974):

$$K_H = \frac{0.012 \text{ mg C}}{\text{L } \mu\text{atm } CO_2} \exp\left[-58.0931 + 90.5069\left(\frac{100}{T}\right) + 22.294 \ln\left(\frac{T}{100}\right)\right] \quad (3.2)$$

To quantify the contribution of the CO_2 efflux from rivers and streams on a global scale (e.g. Pg CO_2-C yr^{-1}), pCO_2, k_{CO2}, and the areal extent of rivers and streams must be known. Butman and Raymond (2011) found increases in pCO_2 and k_{CO2} with decreasing stream order. This would make headwaters, all first- and second-order streams (Leopold *et al*., 1964), potential hotspots for CO_2 evasion. While the smallest streams have the potential to produce the most CO_2 emissions, they have been shown to exhibit the greatest variability in fluxes of CO_2 to the atmosphere (Alin *et al*., 2011; Crawford *et al*., 2013) and their areal extent is difficult to quantify (Melack, 2011). For these reasons, the magnitude of the net terrestrial carbon sink remains uncertain and may be much smaller than once thought. The focus of this chapter will be on the hydrological controls on and spatiotemporal variability of reaeration (k_{O2}, k_{CO2}) and pCO_2 for Fall Creek, the stream described in chapter 2. Additionally, implications for CO_2 evasion will be discussed.

3.1.1 Spatiotemporal Variability and the Influence of Precipitation on Reaeration

Oxygen reaeration was characterized for two sites on Fall Creek during baseflow in chapter 2 using the nighttime slope method (NSM) described in section 2.1.3. The results showed that on average k_{O2} at Freese, the more turbulent downstream location, was nearly five times higher and more variable than Como, the upstream headwaters location. The importance of both temperature and turbulence on the sensitivity of reaeration to changes in temperature was also emphasized. Furthermore, two empirical equations from Churchill *et al*. (1962) and Wallin *et al.* (2011), shown in Table 2.1, were identified as appropriate for estimating reaeration on Fall creek on the basis of producing low mean multiplicative errors (MME, Moog and Jirka, 1998) against reaeration predicted by the NSM. The applicability of these empirical equations suggest that stream velocity, average channel depth, catchment slope, and stream width to depth index (Wallin *et al*., 2011) may be significant hydraulic and geomorphic controls on reaeration rates for baseflow at Fall Creek. However, the effect of precipitation and stormflow on reaeration rates for Fall Creek are still unknown and will be analyzed in this chapter.

It can be reasoned that precipitation would increase reaeration rates due to more turbulent mixing (Zappa *et al*., 2007), and increasing surface roughness, which will also increase the stream surface area. Belanger and Korzun (1990) tested the effects of rainfall on reaeration for lentic systems (i.e. still water) and found a linear relationship between reaeration rates and rainfall intensity. They also speculated that the effect would be less pronounced in lotic systems (i.e. flowing waters) since turbulence due to flow rates and channel slope were expected to be the more influential factors.

Additionally, direct inputs from oxygen saturated raindrops accounted for 80% of the DO increase observed in their pools. While Belanger and Korzun's results align with physical intuition for oxygen dynamics in lentic systems, it is critical to recognize that both oxygen and carbon dioxide reaeration rates are expected to be less predictable for lotic systems.

The primary purpose of characterizing the reaeration rate coefficients for oxygen and carbon dioxide is to quantify surface water-atmosphere gas fluxes. Since precipitation is likely saturated in atmospheric gases, as identified by Belanger and Korzun with oxygen, then precipitation would recharge depleted dissolved gases in surface waters. For supersaturated gases, an increase in reaeration from precipitation would facilitate outgassing from the water column.

3.1.2 Spatiotemporal and Hydrological Controls on CO_2 Evasion

Carbon dioxide evasion ($\mathcal{F}_{CO2}$) has been shown to be strongly correlated with precipitation (Butman and Raymond, 2011; Khadka *et al*., 2014) and discharge (Kokic *et al*., 2015). However, Li *et al*. (2012) only detected a weak correlation between riverine CO_2 efflux and stream discharge. Since the primary controls on CO_2 evasion are the concentration gradient of CO_2 at the surface water-atmosphere boundary layer and the reaeration rate coefficient for carbon dioxide, it remains unclear whether elevated pCO_2 or k_{CO2} has the greater influence on CO_2 outgassing from rivers and streams. Wallin *et al.* (2011) observed high spatiotemporal variability of k_{CO2} in boreal headwater streams and concluded that the variation of k_{CO2} rather than pCO_2 drove CO_2 evasion. Crawford *et al*. (2013) found that both CO_2 efflux from and pCO_2 in two first-

order Boreal streams in Alaska were highly variable with opposing responses of pCO_2 to storm events. For a five catchment study consisting of a coastal western hemlock climatic zone, two temperate oceanic peatlands, a forested boreal region, and a mixed forest and mire site, the highest CO_2 concentrations were observed in the peatlands and pCO_2-discharge dynamics were inconsistent across catchments (Dinsmore *et al*., 2013). In the semi-arid continental climate of Montana, maximum pCO_2 was detected in autumn and precipitation contributed pCO_2-enriched pulses throughout the year. Small rivers and streams, with widths <100 m, in the tropical Amazon and Mekong river systems of South America and Southeast Asia, had larger and more variable $\mathcal{F}_{CO2}$ and k_{CO2} than large rivers (Alin *et al*., 2011). For a sub-tropical river in China, Li *et al*. (2012) found elevated pCO_2 during the dry season compared to the wet season throughout the course of a year with a daily sampling interval, which is contrary to the elevated pCO_2 observed by Khadka *et al*. (2014) during storm events for a river in a sub-tropical karst system.

3.2 Objectives

Northern temperate regions have been identified as potential hotspots for CO_2 evasion at the global scale due to the large areal coverage of headwater streams with super saturated pCO_2 (Raymond *et al*., 2013). CO_2 evasion is primarily dependent on both k_{CO2} and pCO_2, which are highly variable and catchment specific. In this chapter the controls on CO_2 outgassing will be characterized for Fall Creek through completion of the following objectives:

(1) Calculate oxygen and carbon dioxide reaeration rate coefficients for all flow regimes and identify an empirical reaeration equation from Table 2.1 that can appropriately describe reaeration at Fall Creek.

(2) Analyze the spatiotemporal variability of and hydrological controls on pCO_2 and CO_2 evasion at daily and seasonal timescales.

(3) Determine whether k_{CO2} or pCO_2 has greater influence on the CO_2 efflux from Fall Creek.

It is hypothesized that reaeration rates, pCO_2, and CO_2 outgassing will be controlled by discharge and precipitation. CO_2 evasion will be greatest at upstream locations (e.g. Como) following summer storm events due to elevated pCO_2 and lowest at all sites during winter baseflow due to the increased solubility of CO_2 in cold water.

3.3 Methodology

In this section, the field procedures for monitoring pCO_2 in Fall Creek will be described, a unique application of the extreme value method will be introduced for determining oxygen reaeration for all flow regimes, and the procedure for scaling oxygen reaeration to carbon dioxide reaeration will be detailed.

3.3.1 Site Description and Carbon Dioxide Sampling

In addition to water quality measurements, discrete and continuous pCO_2 monitoring was conducted on Fall Creek. A description of the Fall Creek watershed along with field procedures and weather and hydrological data sources are provided in section 2.3.1. The partial pressure of carbon dioxide in Fall Creek was measured using

a rugged non-dispersive infrared (NDIR) sensor with visual display (Vaisala GMT221 CO_2 transmitter, Helsinki, Finland), which was protected with a gas permeable, water impermeable polytetrafluoroethylene (PTFE) membrane (International Polymer Engineering, Tempe, AZ) following procedures detailed by Johnson *et al*. (2010). One lightweight 12V 20AH lithium ion battery (Smart Battery, Tampa, FL) was used to power the CO_2 transmitter for discrete sampling that took place between May and October 2015 at fourteen locations on Fall Creek (shown in Figure 3.1) providing a total of 326 pCO_2 measurements. These measurements were accompanied by the suite of physiochemical water quality parameters and channel geometry measurements described in section 2.3.1. Continuous (15-minute sampling interval) CO_2 monitoring was conducted July 2015-May 2016 at the Como and Freese sites indicated by the stars in Figure 3.1. For these measurements, the CO_2 transmitter was connected to two 12V 20AH lithium ion Smart Batteries in series, a data logger (Campbell Scientific 21x, Logan, UT), and HOBO air temperature logger (Onset Computer Corporation, Bourne, MA). While 124 full days (with 96 measurements per day) of water quality and air temperature data were collected at Freese and 158 full days at Como, only 45 full days of CO_2 data was collected at Freese and 39 days at Como due to resource limitations and technical setbacks encountered with the batteries. Every month except for November and June had at least one full day of continuous CO_2 measurements at Freese and every month except December and June was accounted for at Como.

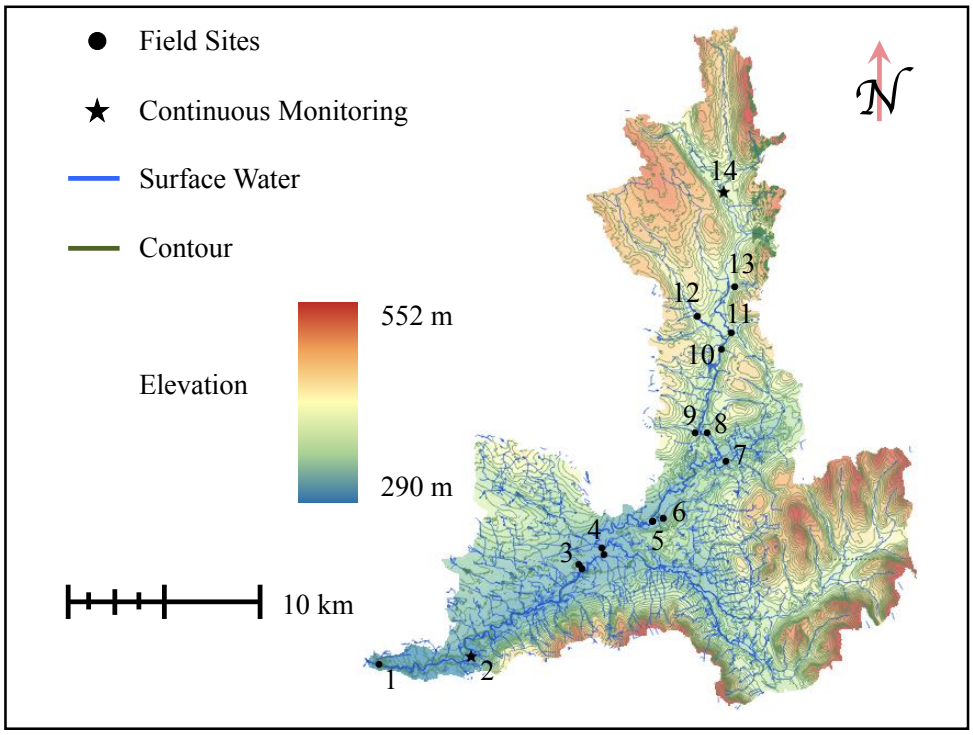

Figure 3.1 Fall Creek watershed and sampling schematic. Discrete pCO_2 and water quality measurements were collected at all field sites between May and October 2015. Continuous monitoring was conducted June 2015 – May 2016 (water quality) and July 2015 – May 2016 (pCO_2) for Como (upper star) and Freese (lower star).

3.3.2 The Extreme Value Method

While the nighttime slope method (NSM) was useful for characterizing oxygen reaeration for Fall Creek during baseflow, it was not applicable to storm events due to substantial scatter in the DO data. Respiration rates calculated from the NSM at both Freese and Como displayed a strong temperature dependence that could be described by Arrhenius kinetics during baseflow. Since the bulk of stream respiration is likely from benthic organisms, it is assumed that respiration rates will maintain the temperature dependence shown in Figure 2.7 under storm flow conditions. With this assumption, reaeration rates can be determined from the extreme value method (EVM).

The EVM developed by Wang *et al*. (2003) was inspired by Chapra and Di Toro's (1991) delta method for determining reaeration, primary production, and respiration in streams via a graphical approach to solve the oxygen mass balance (eqn. 1.2). Chapra and Di Toro reasoned that the daytime lag observed between solar noon and the maximum DO (i.e. minimum oxygen deficit) would be indicative of the reaeration rate, primary productivity could be determined from the daily change in DO, and respiration could be computed by closing the mass balance. Wang *et al*. proposed a more rapid and quantitative approach for calculating stream metabolism parameters using the maximum and minimum daily oxygen deficits (i.e. extreme values). Rather than extracting reaeration rates from the Chapra and Di Toro's daytime lag procedure, which is problematic for high reaeration rates, cloudy conditions, and not applicable after autotrophic senescence in the late autumn through early spring, Wang *et al*. suggested Owen's (1956) empirical reaeration equation (Table 2.1) as originally endorsed by Chapra and Di Toro to supplement their daytime lag procedure.

The procedures for the nighttime portion of the EVM were modified to determine reaeration from respiration. Beginning with the nighttime oxygen mass balance from equation 2.1:

$$\frac{dC_{DO}}{dt} = k_{O2}(C_{DOs} - C_{DO}) - R = k_{O2}\,D - R$$

where C_{DO} is the concentration of dissolved oxygen (mg L^{-1}), t is time (d), k_{O2} is the reaeration rate coefficient for oxygen (d^{-1}), C_{DOs} is the concentration of dissolved oxygen at saturation (mg L^{-1}), and D is the dissolved oxygen deficit (mg L^{-1}). Wang *et*

al. indicate that the maximum oxygen deficit (D_{max}) would occur at the minimum DO concentration (DO_{min}) where $\frac{dC_{DO}}{dt}$ is zero, so:

$$0 = k_{O2} D_{max} - R \tag{3.3}$$

Then, Wang *et al*. proceed to rearrange the equation to solve for respiration by calculating k_{O2} from Owen's empirical equation. However, in this study, equation 2.3 was rearranged to solve for k_{O2} rather than R:

$$k_{O2} = R/D_{max} \tag{3.4}$$

Substituting in the Arrhenius equation for R gives:

$$k_{O2} = \frac{R_o \exp\left[\frac{-E_a}{k_B}\left(\frac{1}{T} - \frac{1}{T_o}\right)\right]}{D_{max} H} \tag{3.5}$$

where R_o is the reference respiration rate (g O_2 consumed m^{-2} d^{-1}) at T_o = 288.15 K, E_a is the activation energy (eV), k_B is the Boltzmann constant (8.62 x 10^{-5} eV K^{-1}), T is the water temperature (K), and H is the average channel depth (m). For Freese, R_o is 11.5 g O_2 consumed m^{-2} d^{-1} and E_a is 0.67 eV. For Como, R_o is 3.46 g O_2 consumed m^{-2} d^{-1} and E_a is 0.61 eV.

Prior to calculating k_{O2} for all flow regimes from equation 3.5, it was applied to DO, temperature, and channel depth data from Como and Freese during baseflow to evaluate the performance of k_{O2} calculated from the NSM against k_{O2} calculated from the modified EVM (eqn. 3.5). The correlation diagram for Freese is presented in Figure 3.2 and the correlation diagram for Como is provided in Appendix D. The EVM k_{O2} had adequate agreement with the NSM k_{O2} for both sites (Freese R^2 = 0.87 and Como R^2 = 0.70). The modified EVM was then applied to all flow regimes for Freese and Como to

characterize oxygen reaeration as a function of stream hydraulics and channel morphology. The performance of the empirical reaeration rate equations presented in Table 2.1 for predicting the EVM k_{O2} were assessed using Moog and Jirka's MME. Note that equation 3.5 produces k_{O2} at temperature T. In order to compare k_{O2} between sampling dates, it should be normalized to a standard temperature (e.g. 20^{o}C). This can be accomplished using Dobbins' temperature correction coefficient θ_a calculated from Demars and Manson's (2013) empirical approximation as detailed in chapter 2 (eqns. 2.13, 2.19).

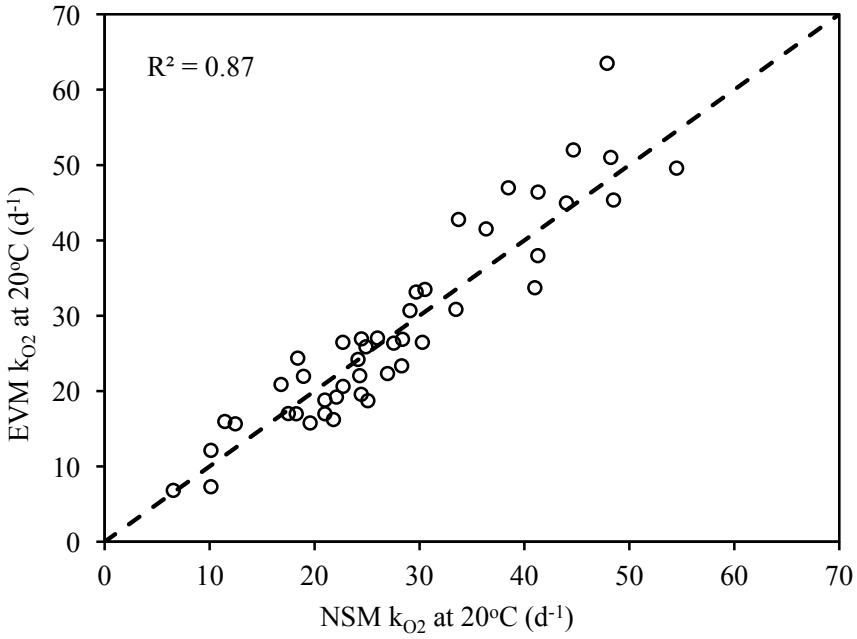

Figure 3.2 Comparison of k_{O2} calculated from the nighttime slope method with k_{O2} calculated from the modified extreme value method (eqn. 3.5) for Freese baseflow

3.3.3 Carbon Dioxide Evasion

The NSM method could not be applied to the diel carbon dioxide curve at Fall Creek. Unlike the parabolic form of the nighttime oxygen curve, which provides a linear derivative (i.e. $\frac{dC_{DO}}{dt} = \text{slope} \cdot D(t) + \text{const.}$), carbon dioxide accumulates at a nearly constant rate following sunset as indicated by the grey curve in Figure 3.3 (i.e. $\frac{dC_{CO2}}{dt} = \text{const.}$). For this reason, the Schmidt relation was applied to convert oxygen reaeration to carbon dioxide reaeration from the following (Raymond *et al*., 2012; Jähne, 1987):

$$k_{CO2} = k_{O2} \left(\frac{Sc_{CO2}}{Sc_{O2}}\right)^{-0.5} \tag{3.6}$$

where k_{CO2} is the CO_2 reaeration rate coefficient (d^{-1}), k_{O2} is the O_2 reaeration rate coefficient (d^{-1}), Sc_{CO2} is the CO_2 Schmidt number, and Sc_{O2} is the O_2 Schmidt number. The Schmidt number (Sc, dimensionless), which describes the ratio of kinematic viscosity to diffusivity for a gas, can be empirically calculated as a function of temperature (^oC) for CO_2 and O_2 in freshwater (Wanninkhof, 2014):

$$Sc_{CO2} = 1923.6 - 125.06T + 4.3773T^2 - 0.085681T^3 + 0.00070284T^4 \tag{3.7}$$

$$Sc_{O2} = 1745.1 - 124.34T + 4.8055T^2 - 0.10115T^3 + 0.00086842T^4 \tag{3.8}$$

For reference, $Sc_{CO2}(20^oC)$ is 600 and $Sc_{O2}(20^oC)$ is 510.

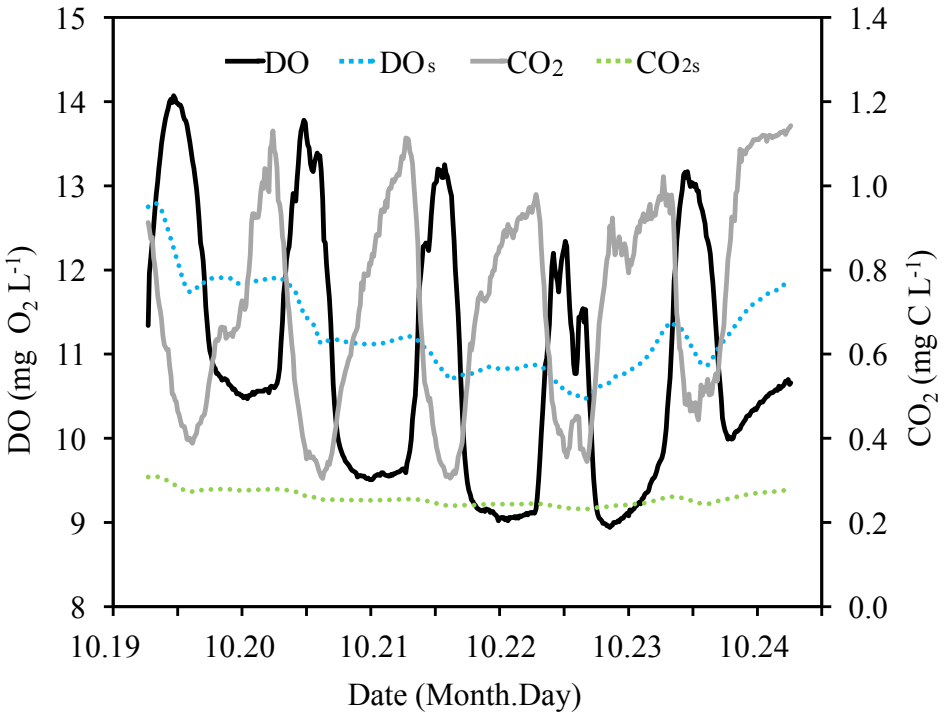

Figure 3.3 Diurnal DO and CO_2 for Freese, October 2015. Following sunset CO_2 accumulates at a constant rate until the maximum concentration is reached while DO declines at a linear rate. Dotted lines represent saturation values for DO and CO_2.

CO_2 evasion was calculated using the carbon dioxide reaeration coefficient determined from the modified EVM for oxygen (eqn. 3.5) along with equation 3.1 for continuous pCO_2 measurements collected at Freese and Como. For sites with discrete measurements, pCO_2 was normalized to solar noon by applying a linear correction factor calculated from the average decrease in pCO_2 before its minimum value was reached around solar noon and the average increase in pCO_2 in the afternoon. The average before noon and afternoon slopes between May and October 2015, were taken for Freese and Como to develop upper and lower limits to this correction factor. The correction factor for before noon (CF_{BN}) and after noon (CF_{AN}) can be described mathematically as follows:

$$CF_{BN} = \frac{(pCO_{2_n} - pCO_{2_{SR}}) \cdot (t_n - t_m)}{t_n} + pCO_{2_m} \quad (3.9)$$

$$CF_{AN} = \frac{(pCO_{2_n} - pCO_{2_{SS}}) \cdot (t_n - t_m)}{t_{SS} - t_n} + pCO_{2_m} \quad (3.10)$$

where time (t) is referenced in terms of days after sunrise, time of sunrise is 0 d and the time just before sunrise for the following day would be 0.99 d (i.e. a diel cycle ranges from 0 to 1 d). pCO_{2SR} is the partial pressure of CO_2 (μatm) at sunrise for the reference locations (Freese and Como), pCO_{2n} is pCO_2 at solar noon for the reference locations, t_m is the time the measurement was collected at the site of interest (d), t_n is solar noon, and pCO_{2m} is the measured pCO_2 at the site of interest.

3.4 Results

Discharge and precipitation are controls on reaeration. The oxygen reaeration rate coefficients (k_{O2}) calculated from the modified EVM (eqn. 3.5) for Freese and Como during all streamflow regimes between June 2015 and May 2016 are shown in Figures 3.4-3.5 as a function of discharge (Q). Three flow regimes were defined by the fraction total flow (Q) composed of baseflow (Q_{BF}): stormflow ("storm," $Q_{BF} < 0.5Q$), transitional flow ("trans.," $0.5Q \leq Q_{BF} < 0.6Q$), and baseflow ("base," $Q_{BF} \geq 0.6Q$). Baseflow was calculated using the conductivity mass balance (CMB) described in section 2.3.2. "Ice" refers to dates where the water temperature was less than 2°C and there was moderate ice coverage on the surface of the water, which substantially reduced reaeration (as illustrated by the blue stars). These data points were not included in the regression fit.

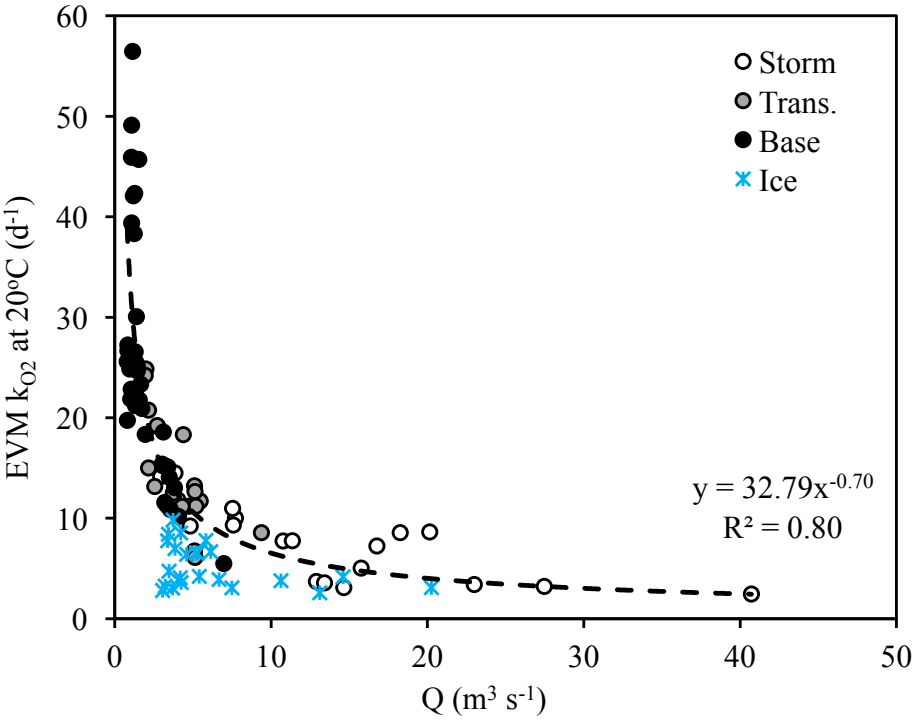

Figure 3.4 Oxygen reaeration rate coefficients (k_{O2}) for Freese

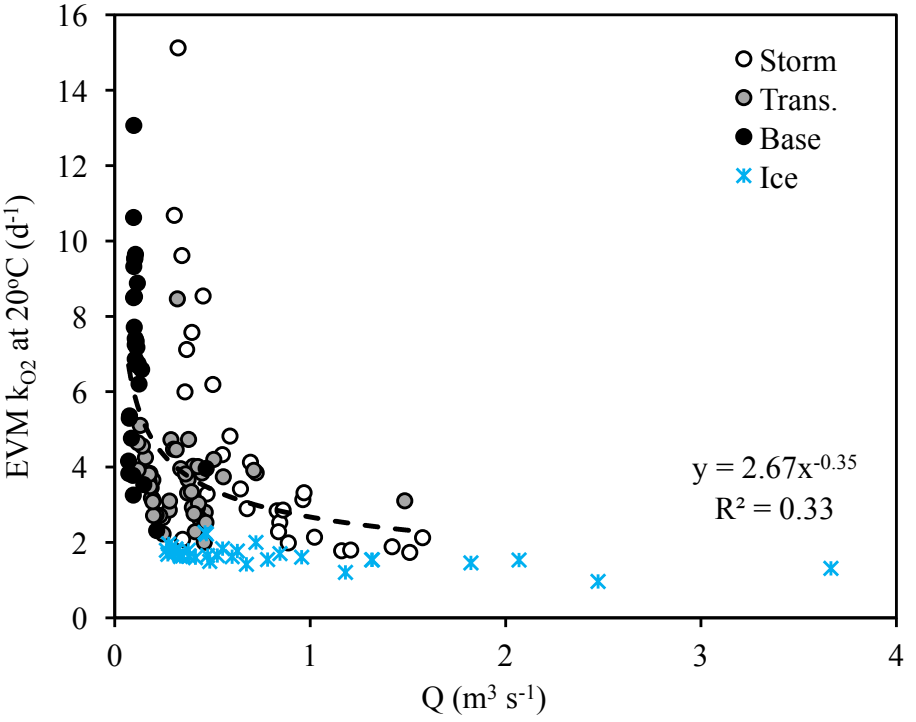

Figure 3.5 Oxygen reaeration rate coefficients (k_{O2}) for Como

Reaeration at Freese was strongly related to discharge ($R^2 = 0.8$) during all flow events and maintained a similar dependence on Q as during baseflow (Figure 2.8) with the greatest reaeration rates occurring during the lowest flows ($k_{O2max} = 56.5\ d^{-1}$). The lowest reaeration rates were calculated for periods of ice coverage with k_{O2} between 2.8 d^{-1} and 10 d^{-1}. For Como, there was not a clear relation between k_{O2} and Q during baseflow (Figure 2.9), but a distinct pattern did emerge once all flow events were considered (Figure 3.5). However, k_{O2} was still only weakly related to Q at Como ($R^2 = 0.33$). The maximum k_{O2} occurred during stormflow with a rate of 15.1 d^{-1}. Like Freese, the lowest reaeration rates were observed during ice coverage at Como with k_{O2} of 0.97 – 2.2 d^{-1}.

With the goal of identifying an empirical equation able to predict the reaeration rate coefficient for Fall Creek, sixteen empirical equations (Table 2.1) were evaluated using Moog and Jirka's (1998) mean multiplicative error (MME) metric. The MME for two additional scenarios for Freese and Como was also calculated as a comparison against the MME values from the empirical equations. The additional predictive scenarios tested for Freese were the group 1 empirical equation average, which yielded one of the lowest MME for baseflow in chapter 2, and the equation from the regression fit provided in Figure 3.4. The regression fit (Figure 3.5) was also tested for Como in addition to a constant reaeration rate of 6 d^{-1}, which produced a low MME for baseflow at Como in chapter 2. These results are summarized in Table 3.1.

Table 3.1 Mean multiplicative error (MME) for the sixteen empirical equations from Table 2.1 (and two additional scenarios) compared to k_{O2} calculated from the modified EVM at Freese and Como. "G1" scenario refers to the group 1 empirical equations average for Freese and "6" refers to a null k_{O2} of 6 d^{-1} for Como. The regression fit are the equations shown in Figures 3.4-3.5. Bolded MME emphasize the scenarios with the best predictive power (lowest MME values for each site) against the modified EVM.

		MME	
Group	**ID**	**Freese**	**Como**
1	OD	**1.35**	**2.98**
	CH	**1.46**	**2.29**
	OW	1.82	4.74
	BR	1.68	4.47
2	MJ	3.15	**2.15**
	MFa	1.70	4.32
	MFb	**1.53**	5.97
3	RAa	2.31	6.96
	RAb	2.03	6.24
	RAc	1.87	6.30
	RAd	1.74	6.31
	RAe	**1.66**	6.07
	RAf	1.81	6.48
	RAg	2.01	8.09
4	AL	1.94	4.90
	WA	**1.45**	**1.83**
G1 (Freese); 6 (Como)		**1.50**	**1.71**
Regress. Fit		**1.27**	**1.39**

Second to the regression fits, O'Connor and Dobbins' (1956) equation, OD, produced the lowest MME against the modified EVM k_{O2} for Freese, while the null reaeration assumption of 6 d^{-1} yielded the second lowest MME for Como. Overall, the equation developed for the CO_2 gas transfer coefficient by Wallin *et al*. (2011), eqn. WA, performed the best for determining the oxygen reaeration rate coefficient for both Freese and Como. WA is a function of channel slope and the average channel width to

depth ratio. Plots showing the top three empirical equation fits, including eqn. WA, compared to the EVM k_{O2} as a function of temperature are given in Appendix D. The second and third best fit empirical equations for both sites were eqn. OD and the Churchill *et al*. (1962) equation, CH, from group one.

CO_2 evasion is controlled by the concentration of dissolved carbon dioxide in the water and the rate of carbon dioxide reaeration, which was calculated from the oxygen reaeration rate coefficients summarized in Figures 3.4-3.5 using the Schmidt relation (eqn. 3.6). k_{CO2} ranged from an average of 5.3-22.6 d^{-1} at Freese and 1-6.2 d^{-1} at Como. The seasonal variability for the average diurnal pCO_2 and $\mathcal{F}_{CO2}$ patterns are depicted in Figures 3.6-3.7 for Freese and Figures 3.8-3.9 for Como. Winter included data collected between 1 January 2016 – 20 March 2016, spring included 21 March 2016 – 10 May 2016, summer included 1 July 2015 – 22 September 2015, and autumn included 23 September 2015 – 20 December 2015.

Patterns of diurnal fluctuations in pCO_2 varied throughout the year for both Freese and Como with the greatest diurnal fluctuations occurring in the summer and the least in the winter. The maximum pCO_2 was observed in the summer for both sites with similar minimum values in the spring, summer, and autumn for Freese and the lowest pCO_2 in the spring for Como. Winter pCO_2 was more variable at Freese than it was at Como, fluctuating between 840 and 4040 μatm. The average winter pCO_2 was similar at both sites with an average of 1660 μatm at Freese and 1430 μatm at Como. The diurnal pCO_2 trend was also similar at both sites during the spring with average diurnal fluctuations of 850 μatm at Freese and 655 μatm at Como. However, there were marked

differences in pCO_2 during the summer at the two sites. The pCO_2 at Freese was more variable from day to day than that of Como (illustrated by the sizeable standard deviations in Figure 3.6), but the pCO_2 at Como varied much more over a diel cycle (3410 μatm d^{-1} compared to 1410 μatm d^{-1} at Freese). The pCO_2 at Como was more than twice as high as the pCO_2 at Freese (3260:1480 μatm) in the summer and autumn (2750:1100 μatm). The diurnal variations on the other hand were nearly equivalent at both sites (810 μatm d^{-1} for Freese and 820 μatm d^{-1} for Como). On average, both sites were supersaturated in CO_2 throughout the entire year compared to the atmospheric concentration of 400 μatm indicated by the black dotted line in Figures 3.6 and 3.8.

The seasonal trends in the average diurnal efflux of CO_2 are provided for Freese in Figure 3.7 and for Como in Figure 3.9. Comparable diurnal patterns are evident between pCO_2 and $\mathcal{F}_{CO2}$. However, the proportional magnitude for the variability is much different for $\mathcal{F}_{CO2}$. The scales for the y-axis (CO_2 emissions) for Freese and Como are equivalent for Figures 3.7 and 3.9 to make the comparison clearer. While Freese tends to have lower pCO_2 than Como, it has greater rates of CO_2 evasion (2-3 times higher throughout the year). On average, the highest evasion rates occur during summer nights at both Freese (6.8 g CO_2-C m^{-2} d^{-1}) and Como (3.1 g CO_2-C m^{-2} d^{-1}) with the lowest rates occurring during the daytime in spring at Freese (0.45 g CO_2-C m^{-2} d^{-1}) and at a nearly constant low rate over the entire diurnal cycle during the winter at Como (0.3 g CO_2-C m^{-2} d^{-1}). Autumn has the second highest CO_2 emissions for both sites. These results suggest that the carbon dioxide reaeration rate coefficient may be a greater influence on CO_2 evasion than pCO_2 for Fall Creek.

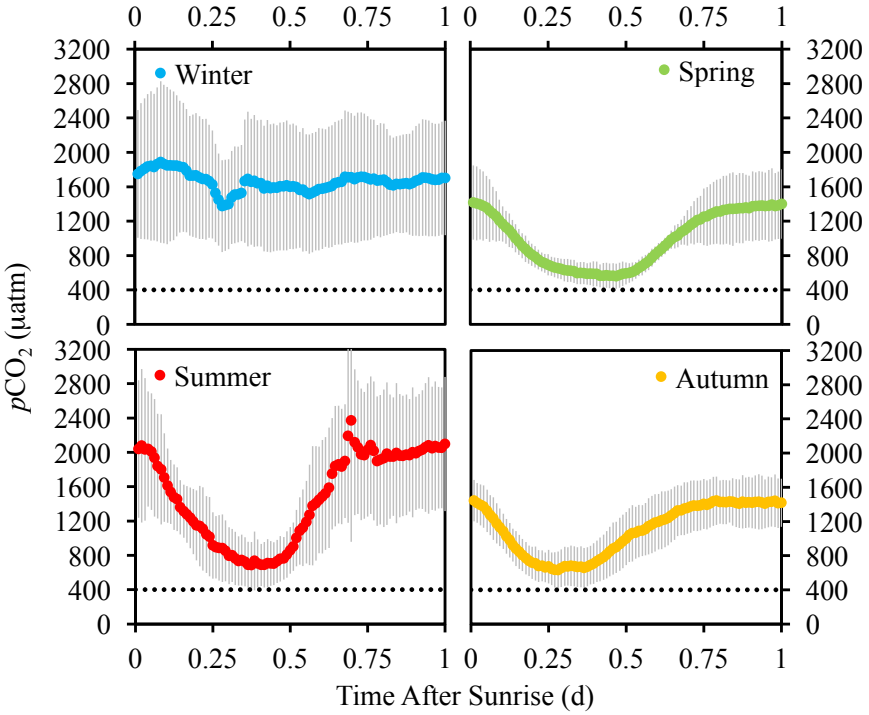

Figure 3.6 Seasonal average diurnal variability in pCO_2 at Freese. The black dotted line represents the atmospheric concentration of CO_2.

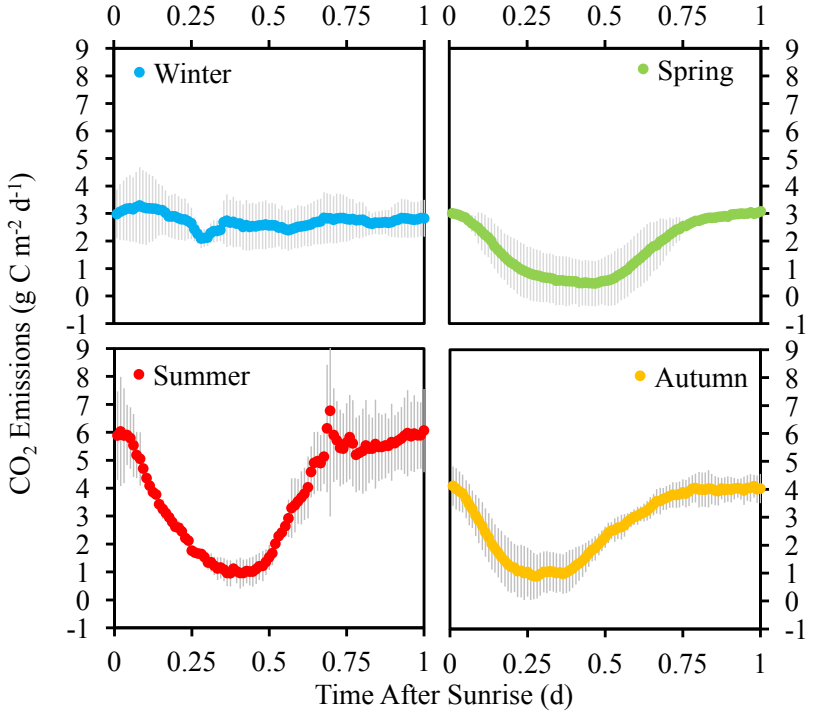

Figure 3.7 Seasonal average diurnal variability in $\mathcal{F}_{CO2}$ at Freese.

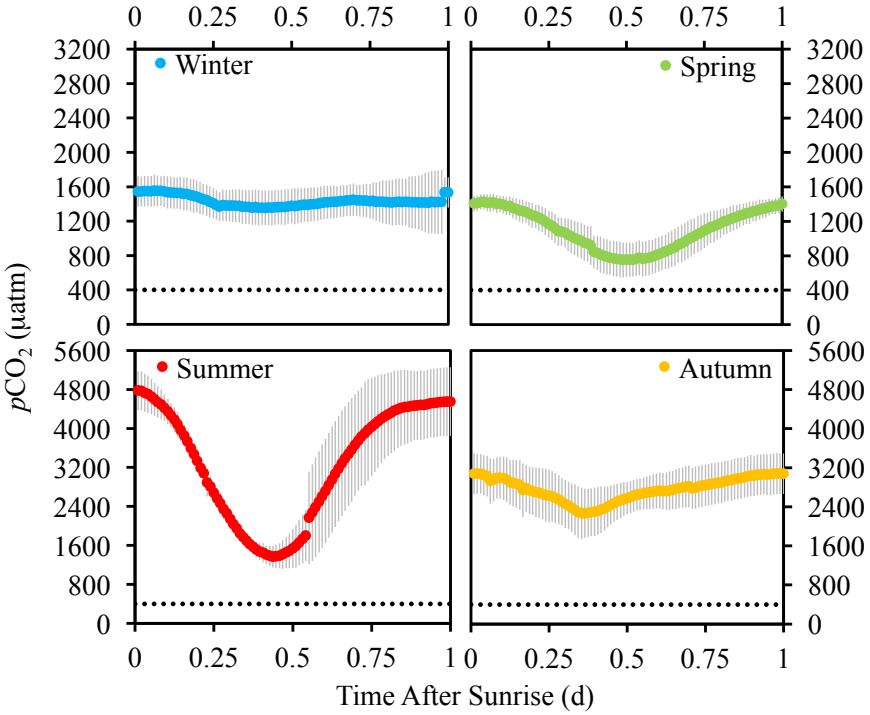

3.8 Seasonal average diurnal variability in pCO_2 at Como. The black dotted line represents the atmospheric concentration of CO_2.

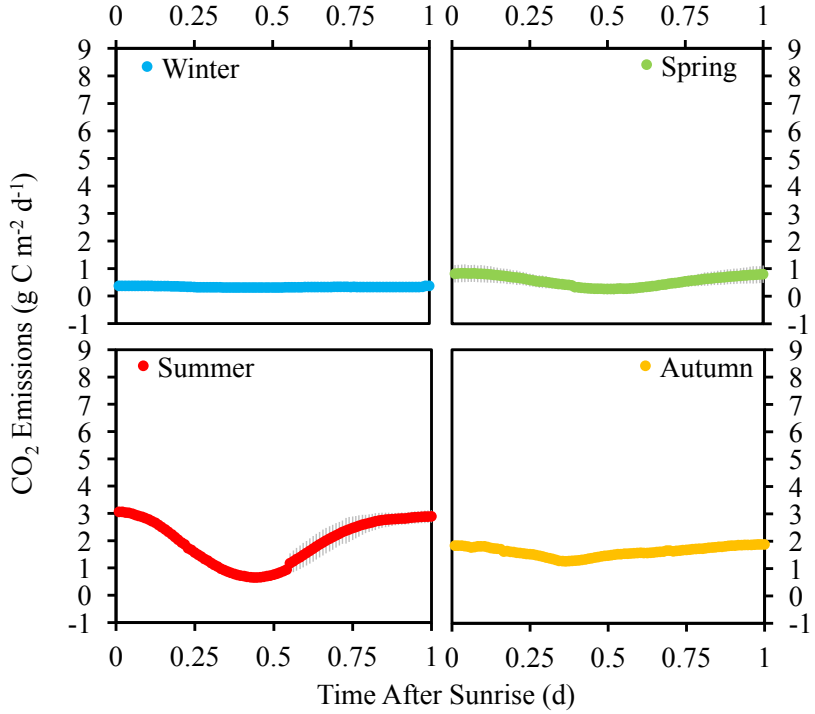

Figure 3.9 Seasonal average diurnal variability in $\mathcal{F}_{CO2}$ at Como.

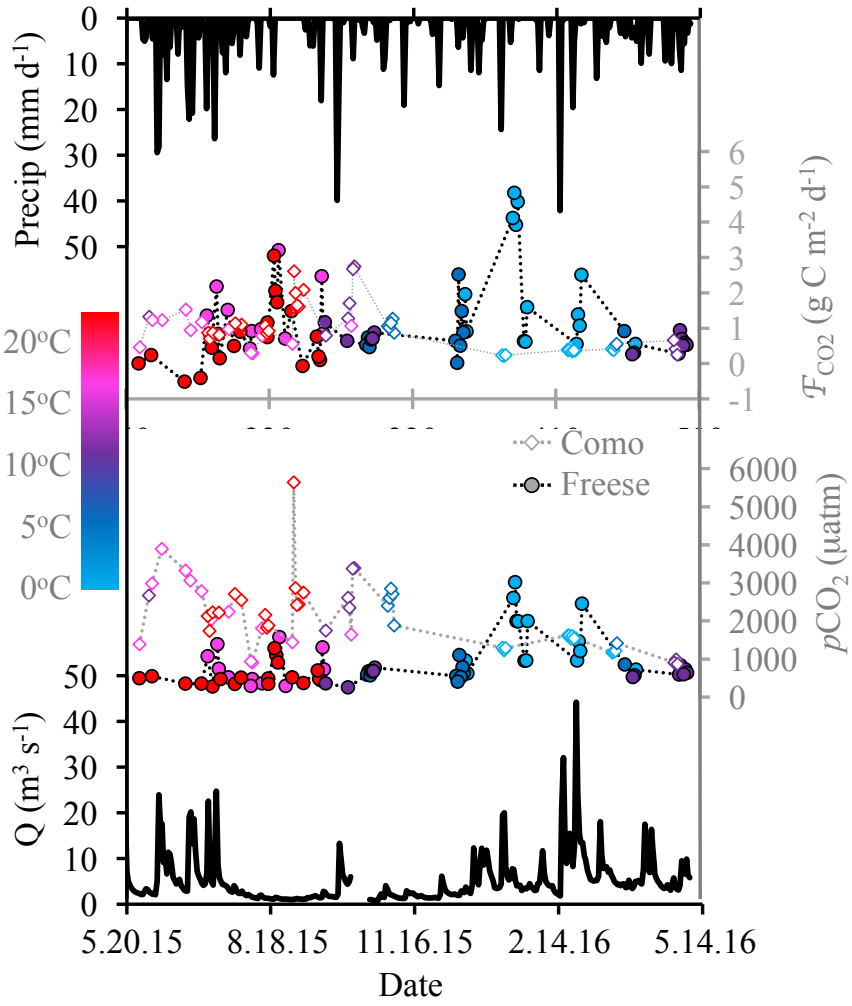

Figure 3.10 Relationship between daily average precipitation, discharge, pCO_2, and CO_2 evasion for Freese and Como from May 2015 – May 2016 normalized to solar noon. The blue to red gradient scale represents the water temperature.

Another pCO_2 – $\mathcal{F}_{CO2}$ comparison is depicted in Figure 3.10 for Freese and Como. In this figure, pCO_2 collected from both discrete and continuous measurements are combined to illustrate CO_2 variability in Fall Creek on an annual scale from May 2015 to May 2016. To normalize the discrete pCO_2 measurements to solar noon so the values would be comparable from day-to-day, equations 3.9-3.10 and the figures in Appendix E were applied to the data. Based on the continuous measurements, from

sunrise until the minimum pCO_2 concentration was reached just after noon, pCO_2 dropped at a rate of 2290 μatm d^{-1} in the late-spring to early-summer and 4760 μatm d^{-1} in the mid-summer to early-autumn at Freese. In the afternoon, pCO_2 increased at an average rate of 1110 μatm d^{-1} from late-spring to early-autumn at Freese (Figure E.2). Since the spring-summer (lower limit) and summer-autumn (upper limit) slopes converged by mid-morning (Figure E.1), and to prevent normalizing the Freese pCO_2 data to negative values, the lower limit slope was applied to all Freese discrete pCO_2 measurements. For Como, the upper limit (summer-autumn) for the morning decline in pCO_2 was 6180 μatm d^{-1} and the lower limit (spring-summer) pCO_2 decline was 5450 μatm d^{-1} (Figure E.3). The average spring-autumn afternoon increase in pCO_2 was 1830 μatm d^{-1} (Figure E.4). The lower limit morning slope was also applied to discrete measurements at Como to conservatively normalize the pCO_2 values to solar noon.

As observed in Figures 3.6 and 3.8, pCO_2 at Como (diamonds in Figure 3.10) was generally higher than at Freese (circles in Figure 3.10) during summer and autumn, lower during winter, and similar during spring. CO_2 evasion rates at solar noon were similar in the summer at both sites, but greater in the winter at Freese. It appears that precipitation led to local peak effluxes in CO_2 at Freese in the winter and summer. During late spring, local maxima in CO_2 evasion at Como corresponds to precipitation, but evasion at Freese does not follow the same trend. pCO_2 at Freese tends to decrease with increasing discharge while pCO_2 at Como frequently increases with increasing discharge. Additionally, pCO_2 generally increased with decreasing temperature at Freese and decreased with decreasing temperature at Como.

Figure 3.11 shows the longitudinal pattern of pCO_2 on Fall Creek for discrete measurements collected between May and October 2015 normalized to solar noon. Como data (site 14) were adjusted using the lower limit morning slope specific to Como described previously. Freese data were adjusted using the lower limit morning slope for Freese as described previously. The remaining sites were also adjusted using the lower limit Freese slope to maintain conservative adjustments and to prevent negative pCO_2 values. This normalization significantly changed the original pCO_2 values for sites 6-8 and 12-14 shown in Table 3.2 ($p > 0.05$) where the measurements were made earlier in the morning.

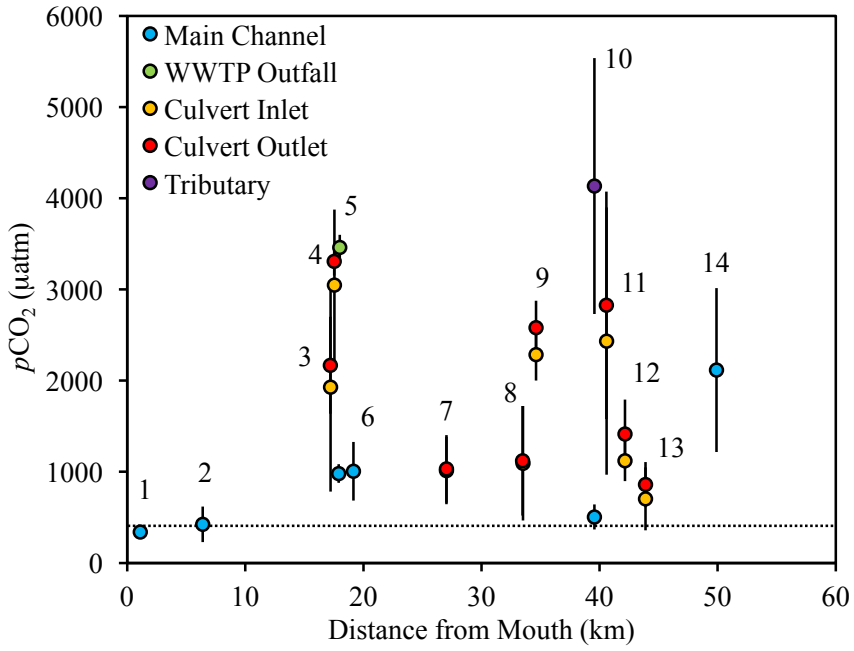

Figure 3.11 Longitudinal patterns of pCO_2 in Fall Creek normalized to solar noon, May 2015 – October 2015. Field sites are indicated on map in Figure 3.1 and correspond to numbers in Table 2.2. Site 14 is Como and furthest away from the mouth (upstream). Site 2 is Freese and second closest to the mouth (downstream). Wastewater treatment plant (WWTP) measurements were collected directly from the effluent pipe (green circle). The dotted black line represents atmospheric CO_2.

Table 3.2 Summary of average measured and solar noon adjusted discrete pCO_2 measurements at each site with standard deviation (SD). pCO_2 is recorded in μatm. P-value from two-tailed paired t-test compares measurements before and after standardization at 0.05 significance.

ID	Name	Type	pCO_2 measured		pCO_2 solar noon		p-value
			Avg.	SD	Avg.	SD	
14	Como	Channel	2718	959	2115	899	< 0.05
13	Hinman Inlet	Culvert	916	325	703	345	< 0.05
13	Hinman Outlet	Culvert	1059	242	860	247	< 0.05
12	Clark Inlet	Culvert	1263	227	1121	225	< 0.05
12	Clark Outlet	Culvert	1525	362	1414	378	< 0.05
11	Groton City Inlet	Culvert	2451	1412	2434	1466	0.68
11	Groton City Outlet	Culvert	2819	1193	2826	1247	0.87
10	Lafayette	Channel	545	156	504	137	0.18
10	Lafayette	Tributary	4128	1394	4134	1403	0.83
9	Cemetery Inlet	Culvert	2227	314	2284	283	0.32
9	Cemetery Outlet	Culvert	2500	319	2580	295	0.18
8	Gulf Inlet	Culvert	1228	649	1093	629	< 0.05
8	Gulf Outlet	Culvert	1240	628	1121	600	< 0.05
7	Cady Inlet	Culvert	1073	356	1013	369	< 0.05
7	Cady Outlet	Culvert	1066	345	1032	371	0.15
6	Freeville	Channel	1122	319	1005	322	< 0.05
5	Dryden-Freeville	WWTP Outfall	3460	139	3460	139	
5	Dryden-Freeville	Channel	983	150	981	102	0.94
4	Kingdom Inlet	Culvert	3047	829	3047	829	0.10
4	Kingdom Outlet	Culvert	3227	125	3307	154	0.11
3	Upper Creek Inlet	Culvert	1830	1157	1928	1147	0.07
3	Upper Creek Outlet	Culvert	2060	561	2168	532	0.07
2	Freese	Channel	674	311	424	195	< 0.05
1	Lake	Channel	552	47	338	30	< 0.05

On the main channel in Figure 3.11 (blue circles), pCO_2 generally decreases from upstream to downstream. The yellow circles represent culvert inlets and the red circles represent culvert outlets. These culverts intercept the stream channel on major tributaries and tend to be more supersaturated in pCO_2 at the outlets compared to the inlets. The purple circle has the highest recorded pCO_2 concentrations on Fall Creek. It is a ground-water fed tributary that drains into the main channel at site 10. The green circle represents the Dryden-Freeville Wastewater Treatment Plant (WWTP) outfall, which is supersaturated in CO_2 compared to the main channel. The WWTP outfall was the only discrete sampling location not normalized to solar noon.

3.5 Discussion

3.5.1 Controls on Oxygen and Carbon Dioxide Reaeration

The empirical reaeration equation developed to determine the gas transfer coefficient for CO_2 by Wallin *et al*. (2011) had the lowest MME of the sixteen equations introduced in chapter 2 for all stream flow regimes at Freese (MME = 1.45) and Como (MME = 1.83). Thus, this equation may be appropriate to generally apply to Fall Creek. It can be written as follows to directly determine the reaeration rate coefficient (d^{-1}) for carbon dioxide (k_{CO2}):

$$k_{CO_2} = 1.9S + 0.3\frac{W}{H} - 0.0004 \qquad (3.11)$$

where S is the reach slope ($m\ m^{-1}$) and W/H is the mean width to depth ratio ($m\ m^{-1}$) for the channel. The applicability of equation 3.11 to Fall Creek suggests that channel morphology is a major control on reaeration for the catchment. A wide, shallow channel would have a high W/H index and facilitate gas exchange with the atmosphere. Slope

has been identified as a significant control on reaeration in the theoretical energy dissipation model (Grant, 1976; Tsivoglou and Neal, 1976). Wallin *et al*. found that W/H was highly correlated with specific discharge (m d^{-1}) at the majority of boreal stream reaches they studied and that reach slope was able to describe the higher gas exchange rates observed in steeper stream sections. While Como has a steeper reach slope (S = 0.0077) than Freese (S = 0.0027), Freese has a greater W/H index (41.83) compared to 20.98 for Como. Equation 3.11 provides an average k_{CO2} for Freese of 12.6 d^{-1} and 6.2 d^{-1} for Como from May 2015 – May 2016 at 20°C. The mean seasonal k_{CO2} calculated for Freese using the modified EVM (eqn. 3.5) ranged from a winter low of 5.3 d^{-1} (5.9 d^{-1} at 20°C) to a summer high of 22.6 d^{-1} (22.7 d^{-1} at 20°C). Como had a winter low modified EVM k_{CO2} of 1.0 d^{-1} (1.4 d^{-1} at 20°C) and a summer high rate of 6.3 d^{-1} (6.0 d^{-1} at 20°C). For reference, Wallin *et al*. measured k_{CO2} between 1.44 d^{-1} and 298 d^{-1} in their study.

Discharge and precipitation are hydrological controls on reaeration for Fall Creek as exemplified by Figures 3.4-3.5. Como displays an interesting double curve when the reaeration rate coefficient is plotted against discharge. High reaeration rates are generally characteristic of baseflow largely due to a shallower mixing depth and, perhaps, because of added turbulence from exposed rocks and benthic vegetation during low flows that increase the effective surface area of streams at the stream-atmosphere boundary layer. At Como, there is a clear departure from the baseflow curve (Figure 3.5) during stormflows. Como is located in the headwaters of Fall Creek and it has a large benthic surface area to water volume ratio. Its baseflow is characterized by a smooth stream-atmosphere boundary layer (as shown in Figure 2.14). The added

volume from precipitation would be substantial compared to baseflow at Como. Direct-flow from precipitation would increase the surface roughness (e.g. Figure 3.12b.) on Como's usually smooth surface producing the higher reaeration rates observed during stormflows in Figure 3.5.

Figure 3.12 Observed winter stormflow and ice coverage on Fall Creek.
(a.) Freese, 1.10.16; **(b.)** Como, 1.10.16; **(c.)** Freese, 1.31.16; **(d.)** Como, 1.31.16

A double-curve does not appear in the k_{O2} versus Q plot for Freese between baseflow and stormflow. Rather, baseflow, stormflow, and transitional flows sit along the same regression curve. The surface-atmosphere boundary layer at Freese tends to be rough during all flow regimes. Images of Como and Freese during baseflow are provided in Figure 2.14. Though surface roughness at Freese does increase during

stormflow (Figure 3.12a.), its effective mixing depth also increases since W/H becomes smaller so reaeration generally decreases with increasing discharge. However, there is a noted departure from the regression curve between flows of 18 and 20 m^3 s^{-1}. This narrow range may indicate an ideal regime for the effective mixing depth and energy dissipation to produce higher reaeration rates. Temperature is another critical control on reaeration, since ice coverage reduces the contact area for reaeration (Figure 3.12c-d.).

3.5.2 Spatiotemporal Variability of pCO_2

Seasonal patterns of daily mean pCO_2 revealed that both Freese and Como sites were consistently supersaturated in CO_2 (Figures 3.6 and 3.8). Both sites had similar diurnal pCO_2 trends in the winter and spring. Nighttime maximum pCO_2 values in the summer and autumn were twice as high at Como as those at Freese. Minimum daytime CO_2 concentrations were also twice as high at Como compared to Freese. pCO_2 could be expected to be greater at Como than at Freese due to its high benthic surface area to water volume ratio. However, the Arrhenius plot for respiration in chapter 2 (Figure 2.7) shows that Freese consumes substantially more oxygen during respiration than Como. Assuming benthic organisms at both sites are consuming similar quality substrates (i.e. the ratio of the moles oxygen consumed to moles carbon dioxide produced during respiration are equivalent (Berggren *et al*., 2012)), Freese should be producing more CO_2 than Como. Then, logically, it would be expected that Freese would have greater pCO_2 than Como as well.

One explanation for the contradiction between the expected and the observed pCO_2 at the two sites is that Como could be gaining allochthonous CO_2 inputs from

groundwater seepage (Crawford *et al*, 2014; Peter *et al*., 2014; Hotchkiss *et al*., 2015). This is plausible since Como's large benthic surface area to volume ratio could facilitate detectable increases in pCO_2 from CO_2-enriched groundwater. Another possible explanation is that Freese is emitting a greater flux of CO_2 to the atmosphere than Como because of its higher gas transfer coefficient. The gas transfer coefficient and controls on CO_2 evasion will be the focus of the remainder of this chapter. Chapter 4 will address allochthonous CO_2 sources.

It could be expected that pCO_2 would decrease longitudinally down a stream channel. Downstream pCO_2 losses could be intensified by high reaeration rates in steeply sloped headwaters, either through an increase in the W/H index as a stream widens at downstream locations, an increase in specific discharge, or through downstream slopes, falls, or rapids. This decreasing downstream trend in pCO_2 is representative of Fall Creek's main channel as shown in Figure 3.11. There may be allochthonous CO_2 inputs along the way that drive pCO_2 up at select locations (e.g. the WWTP outfall at site 5, which discharges effluent enriched in organic acids into the creek). Locations where tributaries join the main channel may additionally influence pCO_2.

Culverts that cover portions of stream reaches could also be sites of elevated pCO_2 as exemplified by Figure 3.11. It is interesting to note that the culvert outlet locations (red circles) often had higher pCO_2 than the culvert inlets (yellow circles). Since photosynthesis, and carbon dioxide assimilation, will not take place within the dark confines of a culvert, respiration and CO_2 production would dominate. Additionally, or alternatively, the air inside a culvert may have a higher concentration

of CO_2 than the outside atmosphere so the equilibrium dissolved CO_2 may be elevated inside culverts.

A brief word on sampling strategies… Figures 3.6 and 3.8 display considerable variability in pCO_2 over a diurnal cycle with the most extreme changes taking place between sunrise and solar noon. Along with pCO_2, other physiochemical parameters such as DO, pH, temperature, and even nitrate (e.g. Rusjan and Mikos, 2010) have diel cycles. For pCO_2, afternoon variability is not nearly as drastic as the morning decline (see Appendix E). Therefore, if continuous pCO_2 monitoring is not possible, it is recommended that discrete pCO_2 measurements are made in the afternoon for summer sampling campaigns for comparability between sites. For the northeast, the time of day for discrete pCO_2 measurements should not make as much of a difference from late autumn through early spring due to a flattening out of the diurnal pCO_2 curve.

3.5.3 Implications for CO_2 Evasion

The results shown in Figures 3.7 and 3.9 suggest that the carbon dioxide gas transfer coefficient has a greater influence on CO_2 evasion than the concentration gradient of dissolved carbon dioxide at the stream surface-atmosphere boundary layer for Fall Creek. While pCO_2 is twice as high at Como compared to Freese throughout the summer and autumn, the $\mathcal{F}_{CO2}$ is a least two times larger at Freese than at Como. Carbon dioxide gas exchange rates are primarily controlled by channel slope and the W/H index at Fall Creek, which is correlated with specific discharge and energy dissipation (Wallin *et al*., 2011). The year-long pCO_2 and $\mathcal{F}_{CO2}$ patterns normalized to

solar noon in Figure 3.10 demonstrate that precipitation in the spring along with the resulting increase in discharge may also increase pCO_2 and $\mathcal{F}_{CO2}$ at Como compared to Freese. This suggests that CO_2 sourced from groundwater and runoff may be responsible for the observed spring increase in pCO_2 at Como. The double-peaked response curve between k_{O2} and Q in Figure 3.5 during baseflows and stormflows for Como additionally suggests that precipitation is an important control on reaeration and CO_2 evasion for Como. For Freese, on the other hand, precipitation may decrease reaeration rates by decreasing the W/H ratio.

Longitudinal patterns of pCO_2 alone from Figure 3.11 may not provide much insight into patterns of CO_2 evasion on Fall Creek. Since the greatest pCO_2 values occur during the nighttime, even if k_{CO2} was known at each site, $\mathcal{F}_{CO2}$ would be under-estimated. However, k_{CO2} calculated from equation 3.11 can still highlight potential CO_2 hotspots for emissions if channel slope, width, and depth are known at each location. Culverts usually have a shallow water depth, steeper slope, and often rough surface features that can cause turbulence (see Figure 3.13). These are all physical properties that produce high gas transfer rates. Furthermore, the water inside culverts often has elevated pCO_2 compared to the main channel on Fall Creek. Increased discharge from precipitation has the potential to flush out and degas the culverts, emitting pulses of CO_2 to the atmosphere so storm events may be "hot moments" (McClain *et al*., 2003) for CO_2 evasion on Fall Creek. The sharp increase in $\mathcal{F}_{CO2}$ following storm events in the winter at Freese may represent another hot moment for CO_2 outgassing from melting ice on the water's surface and releasing trapped CO_2. In addition to the increased

solubility of CO_2 in cold water, ice coverage may account for the high and constant pCO_2 displayed throughout a diel cycle at both sites in the winter that nearly matches the nighttime maximum pCO_2 at Freese in the summer.

Figure 3.13 Site 7 culvert on Fall Creek, 10 July 2015. A potential hotspot for CO_2 evasion.

3.6 Conclusion

While pCO_2 is easier to directly measure in the field than k_{CO2}, oxygen reaeration can be characterized for baseflow using continuous DO measurements and following the NSM procedure in chapter 2, applied to all flow regimes using the Arrhenius respiration dependence from chapter 2 and the modified EVM presented earlier in this chapter, evaluated against existing empirical reaeration rate equations to select one that is appropriate for the watershed of interest, and converted to k_{CO2} through the Schmidt relation. Once an empirical equation is selected, controls on CO_2 evasion can be studied in depth.

An empirical carbon dioxide gas transfer equation was selected from Wallin *et al*. (2011) to describe reaeration on Fall Creek. Channel morphology (slope, width, depth), discharge, precipitation, and temperature are all controls on k_{CO2} for Fall Creek. Additionally, the k_{CO2} had a greater influence on $\mathcal{F}_{CO2}$ than that of pCO_2 as indicated by greater CO_2 evasion occurring at Freese, which generally had lower pCO_2 than Como. Since Freese has a higher standard respiration rate than Como, described by Arrhenius kinetics in chapter 2, the elevated pCO_2 at Como is likely due to allochthonous groundwater inputs of CO_2, which will be explored in the following chapter.

CHAPTER 4

ALLOCHTHONOUS CARBON DIOXIDE SOURCES AND BIOPHYSICAL CONTROLS ON COUPLED O_2-CO_2 DYNAMICS

4.1 Introduction

Carbon dioxide in rivers and streams (pCO_2) may be derived from internal metabolic processes (i.e. autochthonous sources) or from terrestrial carbon mineralization and subsequent transport by groundwater or overland flow paths (i.e. allochthonous sources). Here, autochthonous pCO_2 refers to CO_2 that is produced within a stream ecosystem and includes the metabolic processing of allochthonous *organic* carbon. The aquatic carbon cycle is illustrated in Figure 4.1. A sizeable fraction of organic carbon received from the terrestrial landscape may be buried in aquatic sediments, metabolized, and released to the atmosphere, while the remainder is transported downstream (Cole *et al*., 2007). Streambed topography and channel geomorphology control the subsurface retention of organic carbon, organisms, and the rate of exchange with the water column (Battin *et al*., 2009). A watershed's degree of hydrologic connectivity, "the water-mediated transport of matter, energy and organisms within or between elements of the hydrologic cycle" (Freeman *et al*., 2007, p. 5), controls the import of allochthonous organic and inorganic carbon sources to rivers and streams. In this chapter, the ratio of autochthonous to allochthonous pCO_2 will be quantified and the biophysical controls on O_2-CO_2 dynamics will be discussed for Fall Creek.

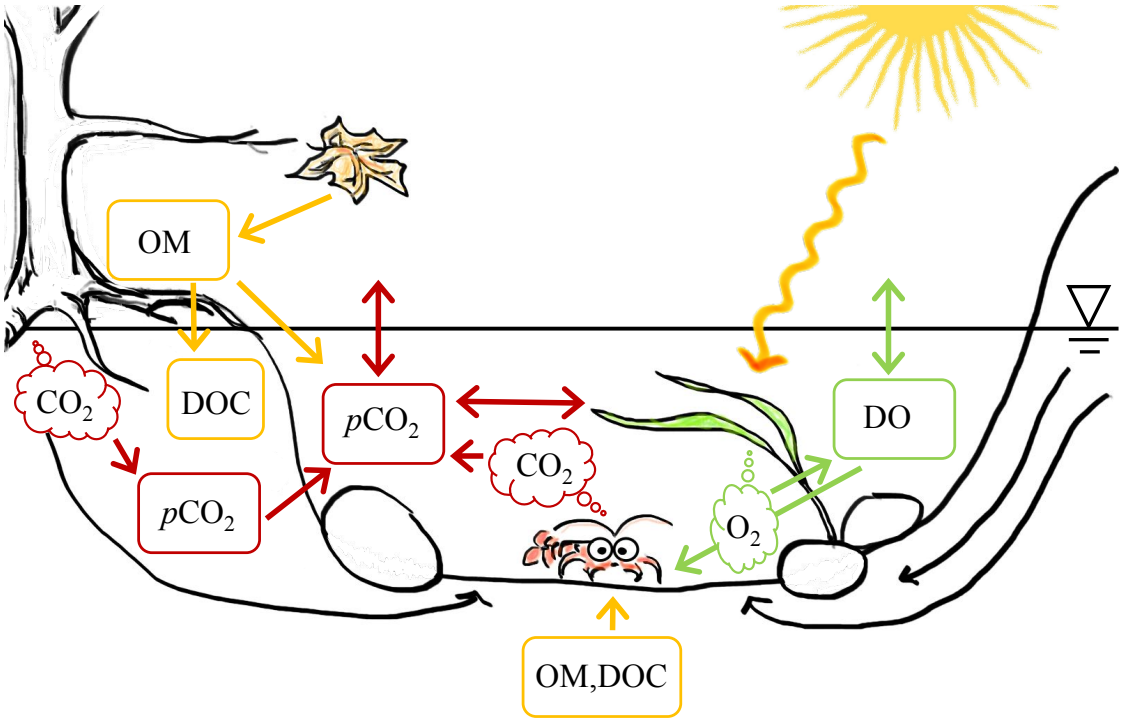

Figure 4.1 Aquatic carbon cycle. The free CO_2 pool (pCO_2) within the stream is a product of autochthonous CO_2 from respiration, inputs from groundwater, atmospheric exchange, and autotrophic uptake during photosynthesis. The DO pool within the stream is a product of oxygen from photosynthesis, atmospheric exchange, and consumption during respiration. Internal metabolic processes may be fueled by allochthonous sources of organic matter (OM) comprised of carbon and nutrients along with dissolved organic carbon (DOC). The black arrows indicate groundwater flowpaths. The groundwater pCO_2 pool is sourced from heterotrophic and root respiration within the soil and provides an allochthonous source of CO_2 to the in-stream pCO_2 pool.

The supersaturation of CO_2 in inland waters occurs from the inflow of CO_2-enriched groundwater and when respiration rates exceed photosynthetic uptake (Jones *et al.*, 2003). In other words, when the aquatic ecosystem is net heterotrophic—a status that can be quantified by net daily metabolism (NDM) traditionally determined in terms of net daily oxygen production from Odum's (1956) open-channel diel oxygen method and an oxygen mass balance, eqn. 1.2 (e.g. Uehlinger *et al.*, 2000; Wang *et al.*, 2003; Izagirre *et al.*, 2007; Aristegi *et al.*, 2009; Beaulieu *et al.*, 2013; Riley and Dodds, 2013;

Correa-González *et al*., 2014; Knapp *et al*., 2015; Hall *et al*., 2016 and many others). NDM has also been determined from the oxygen mass balance, converted through the use of respiratory quotients (RQ) and photosynthetic quotients (PQ), which describe the efficiency of O_2-CO_2 conversions in respiration and photosynthesis, and reported in terms of carbon equivalents (e.g. Johnson *et al*., 2012; Perkins *et al*., 2012; Birkel *et al*., 2013; Roley *et al*., 2014). Others have estimated NDM in terms of carbon by applying the open channel approach to diel pCO_2 and solving a carbon dioxide mass balance (e.g. Wright and Mills, 1967; Lynch *et al*., 2010), but this approach is rare.

4.1.1 A Brief History of Coupled O_2-CO_2 NDM Studies

While few researchers have utilized CO_2 measurements to quantify metabolic rates in aquatic ecosystems, even fewer have compared NDM using both O_2 and CO_2 data. Odum (1957) collected grab samples to capture the diurnal curves for both DO and dissolved CO_2 from Silver Springs, FL on seven sampling dates. He used Winkler titrations to measure DO and phenolphthalein titrations to initially quantify CO_2. After reporting low analytical accuracy for the phenolphthalein titrations, Odum calculated CO_2 from pH and alkalinity. Overall, he found that NDM was similar from both gas methods considering the levels of uncertainty in his analytical techniques. Many years later, Guasch *et al*. (1998) investigated the diurnal variation of DO and dissolved CO_2 in two undisturbed Mediterranean streams during four sampling dates by directly measuring O_2 and indirectly calculating CO_2 from alkalinity and pH, which is a method now known to misrepresent CO_2 and introduce substantial error (Hunt *et al*., 2011; Wallin *et al*., 2014). They observed similar and distinct daily patterns from both gases

in one highly aerated stream during low-flow conditions and no relation between the two gases in the second stream, which was more turbulent than the first. Guasch *et al*. concluded that the difference in solubility between O_2 and CO_2 led to disparate gas exchange rates for the two gases in turbulent waters and speculated that bubbles formed at the surface by turbulence decreased the gas transfer velocity of CO_2.

Hanson *et al*., (2003) deployed an O_2 and CO_2 sensor package to measure NDM in the surface waters of lakes in the Northern Highland Lake District (NHLD) of Wisconsin and the Upper Peninsula of Michigan. They found that NDM calculated from both O_2 and CO_2 agreed on approximately a 1:1 molar ratio with the exception of lakes with high pH where Hanson *et al*. speculated that the CO_2-carbonate system interactions dampened the diel CO_2 cycle. One decade later, Crawford *et al*., (2014) reported NDM for small streams in the NHLD based on dual O_2-CO_2 measurements and found NDM calculated from CO_2 was 1.35 times larger than that of O_2 on a molar basis. Crawford *et al*. indicated that this discrepancy could have been caused by external groundwater inputs, variability in RQ and PQ, and differences in the diffusivity of O_2 and CO_2 as Guasch *et al*. (1998) had also concluded. Data was collected for both of these studies during the summers of 2000-2001.

Field seasons for all of the previously described O_2-CO_2 NDM studies were short. Odum's (1957) productivity investigation had seven sampling dates, the work of Guasch *et al*. (1998) covered four dates, and the NDM analysis of NHLD lakes (Hanson *et al*., 2003) and streams (Crawford *et al*., 2014) only covered the summer months. In order to better understand coupled O_2-CO_2 dynamics and the controls on pCO_2 in

aquatic systems, NDM studies including DO and pCO_2 observations covering longer time spans to better represent daily and seasonal variability are needed.

4.1.2 Carbon Dioxide in Groundwater

Groundwater inputs may influence NDM. Partial pressures of CO_2 in groundwater are typically ~10-100 times higher than atmospheric (Macpherson, 2009). Considering depths less than half a kilometer, pCO_2 generally decreases with increasing depth from the water table surface (Macpherson, 2009; Öquist *et al*., 2009) since carbon dioxide is produced within the soil by both autotrophic and heterotrophic respiration from roots and microbial activity. Direct diffusion of CO_2 from groundwater to the atmosphere may be restricted by the presence of water-filled pores and limited by tortuosity within the soil matrix (Jassal *et al*, 2004). However, CO_2 from groundwater can take an indirect route to the atmosphere by first passing through surface waters.

Groundwater fuels baseflow in gaining streams (Dingman, 2002), transporting supersaturated pCO_2 through thin seepage faces into surface waters. It is an important contributor to in-stream dissolved CO_2 in temperate (Worrall *et al*., 2005), arid (Choi *et al*., 1998), boreal (Öquist *et al*., 2009), and tropical systems (Johnson *et al*., 2008). It is an especially significant conduit for allochthonous carbon transport to headwater streams (Johnson *et al*., 2008; Öquist *et al*., 2009; Peter *et al*., 2014; Hotchkiss *et al*., 2015). For a tidal creek in Australia, Atkins *et al*. (2013) found that groundwater inputs were a primary driver of pCO_2 at an upstream sampling location, while pCO_2 dynamics at a downstream site were governed by more complex processes. Additionally, groundwater displayed the strongest influence on in-stream CO_2 following a flood event.

Groundwater has been shown to provide spatially and temporally consistent longitudinal patterns and background CO_2 concentrations in diverse settings including Alaskan boreal (Crawford *et al*., 2013), Danish lowland (Sand-Jensen and Staehr, 2012), upland Scottish peatland (Hope *et al*., 2001), and Vermont temperate forest (Doctor *et al*., 2008) streams. Since groundwater can contribute a consistent source of CO_2-rich and O_2-poor effluxes to inland waters, it can bias NDM evaluations by over-estimating respiration (Hall and Tank, 2005). Thus, coupled O_2-CO_2 dynamics should be considered when calculating NDM.

4.1.3 O_2-CO_2 Conversion Efficiency: RQ and PQ

One difficulty encountered when relating coupled O_2-CO_2 dynamics in metabolic processes is in converting oxygen to carbon equivalents. The respiratory quotient, RQ, describes the molar ratio of CO_2 produced to O_2 consumed during respiration. Similarly, the photosynthetic quotient, PQ, expresses the efficiency of moles O_2 produced to moles CO_2 consumed in photosynthesis. The conversion is described as follows (Bott, 2007):

$$m_C = RQ \cdot m_{O_2} \left(\frac{12 \text{ g C}}{32 \text{ g } O_2} \right) \tag{4.1}$$

$$m_C = \frac{m_{O_2}}{PQ} \left(\frac{12 \text{ g C}}{32 \text{ g } O_2} \right) \tag{4.2}$$

where m_C is the mass of carbon (g), m_{O2} is the mass of oxygen (g), and 12/32 is the molar ratio of carbon to oxygen.

Most often either an RQ of 0.85 (Bott, 2007; Johnson *et al*., 2012; Perkins *et al*., 2012; Roley *et al*., 2014) or 1.0 (Birkel *et al*., 2013) is assumed. Hanson *et al*. (2003)

found that for lakes with pH $\leq$ 7, RQ ~ 1 and for lakes with pH > 7, RQ < 1. In response to the many metabolism studies that apply an RQ without biophysical justification, Berggren *et al*. (2012) directly measured bacterioplankton RQ at 52 different freshwater sites in Québec and discovered high variability with RQ converging around 1.2 $\pm$ 0.45. The observed RQ ranged from 0.25-2.26. Berggren *et al*. hypothesized that RQ < 1 in net autotrophic systems and > 1 in net heterotrophic systems since RQ would depend on substrate quality and should be ~1 for glucose respiration, below 1 for the oxidation of phytoplanktonic material, and above 1 for metabolizing simple organic acids. In subalpine soils, Jenkins and Adams (2011) found that RQ << 1 in grassland soils likely due to the decomposition of aliphatic organic compounds, amino acids, or refractory or highly reduced compounds; RQ ~ 1 in woodland soils where there is a greater availability of carbohydrates in its larger extractable carbon pool. Additionally, RQ declined over a 120-day incubation period in the grassland soils and began to decline near the end of the 120-day incubation period in the woodland soils. This shows that RQ may not only vary with difference in substrate quality between locations, but also over time at each location as the composition of the carbon pool changes.

A PQ of 1.2 is applied in most ecosystem studies (Bott, 2007; Johnson *et al*, 2012; Roley *et al*., 2014). Hanson *et al*. (2003) noted a PQ of 1.25 in their lake systems. A PQ of ~1 was determined for seaweeds (Rosenberg *et al*., 1995) and assumed for submerged macrophytes in lowland streams in Denmark (Baattrup-Pedersen *et al.*, 2013). In Narragansett Bay, RI, the observed PQ increased from 1.24 in the 1980's to a value of 1.42 $\pm$ 0.09 nearly thirty years later (Smith *et al*., 2012). It is noted that photosynthetic quotients vary widely in aquatic systems. In Lake Erie, Ostrom *et al*.,

(2005) found the PQ was 1.93. It has been proposed that nutrient availability drives differences in PQ (Smith *et al*., 2012).

4.2 Objectives

For an RQ and PQ of 1 and no groundwater inputs, the NDM calculated from the oxygen mass balance (eqn. 2.1) and a similar mass balance with carbon dioxide should be equivalent on a molar basis. However, this is not likely the case for most systems. In this chapter, Odum's (1956) single-station open channel diel mass balance approach will be applied to both diurnal O_2 and CO_2 curves to achieve the following objectives:

(1) Apply the modified extreme value method (EVM) from chapter 3 to calculate NDM on an O_2 mass basis for the upstream Como site and downstream Freese site on Fall Creek assuming negligible groundwater O_2 inputs.

(2) Parameterize an O_2-CO_2 mass balance model to estimate the allochthonous pCO_2 inputs from groundwater and determine RQ and PQ for Fall Creek.

(3) Assess biophysical controls on O_2-CO_2 dynamics.

In terms of volumetric influence, allochthonous pCO_2 inputs from groundwater is expected to dominate over autochthonous CO_2 production at Como, while pCO_2 derived from in-stream respiration is predicted to be the primary pCO_2 source at the downstream Freese site. NDM will likely be greater at Como than Freese during the growing season, due to its substantial mass of aquatic vegetation. RQ and PQ are expected to differ between Freese and Como and also vary seasonally.

4.3 Methodology

In this section, the procedure for calculating NDM from the modified EVM will be described. Additionally, an O_2-CO_2 NDM model will be detailed emphasizing its parameterization of RQ, allochthonous pCO_2 inputs, and PQ. This NDM study took place on Fall Creek at the Freese and Como sites introduced in chapter 2. Field and auxiliary data collection procedures were described in chapters 2-3.

4.3.1 Net Daily Metabolism

Net daily metabolism (NDM) is defined as:

$$NDM = GPP - ER \tag{4.3}$$

where GPP is gross primary production (g O_2 produced or g CO_2 consumed m^{-2} d^{-1}) and ER is ecosystem respiration (g CO_2 produced or g O_2 consumed m^{-2} d^{-1}). This section will outline the steps for calculating NDM in terms of the oxygen mass balance.

As introduced in chapter 1 (eqn. 2.1), the oxygen mass balance for lotic ecosystems using the assumption that the mass of oxygen contributed by groundwater seepage is negligible, can be described by:

$$\frac{dC_{DO}}{dt} = k_{O2}(C_{DOs} - C_{DO}) + \frac{P(t)_{O2} - R_{O2}}{H} = k_{O2}(D) + \frac{P(t)_{O2} - R_{O2}}{H} \tag{4.4}$$

where $\frac{dC_{DO}}{dt}$ is the change in the DO concentration in a day (mg L^{-1} d^{-1}), k_{O2} is the reaeration rate coefficient (day^{-1}), C_{DOs} is the concentration of DO at saturation (mg L^{-1}), C_{DO} is the concentration of dissolved oxygen (mg L^{-1}), the difference between C_{DOs} and C_{DO} is the oxygen deficit D (mg L^{-1}), $P(t)_{O2}$ is the rate of photosynthesis (g O_2 m^{-2} d^{-1}), R_{O2} is the rate of respiration (g O_2 m^{-2} d^{-1}) and H is the average channel depth (m), which gives daily rates of $P(t)_{O2}$ and R_{O2} in terms of concentrations (mg O_2 L^{-1} d^{-1}).

The proportion of the day with sunlight can be defined as the photoperiod, f (d^{-1}), where sunrise occurs at t = 0, sunset occurs at t = f, and the length of a diel-cycle (1 d) is τ. At nighttime, when $f \leq t \leq \tau$, P(t) = 0 as first discussed in chapter 2, so the oxygen mass balance becomes:

$$\frac{dC_{DO}}{dt} = k_{O2}(D) - \frac{R_{O2}}{H} \tag{4.5}$$

Then, as indicated by Wang *et al*. (2003) in their EVM, the maximum oxygen deficit (D_{max}) occurs at the minimum DO concentration ($C_{DO,min}$) where $\frac{dC_{DO}}{dt}$ is zero. The reaeration rate coefficient can be determined through the modified EVM (eqn. 3.5) by substituting in the Arrhenius respiration relation, a function of temperature R(T), and solving for k_{O2}. The oxygen reaeration coefficient can be normalized to 20°C using Demars and Manson's (2013) empirical approximation of the temperature coefficient θ_a, a function of temperature and turbulence, (eqns. 2.13, 2.19) to allow k_{O2} to vary with temperature:

$$k_{O2,20^o} = \left(\frac{R_o \exp\left[\frac{-E_a}{k_B}\left(\frac{1}{T} - \frac{1}{T_o}\right)\right]}{D_{max}\, H} \right) \theta_a^{\,293.15\ K - T} \tag{4.6}$$

where $k_{O2,20^o}$ is the oxygen reaeration rate coefficient (d^{-1}) normalized to 20°C, R_o is the reference respiration rate (g O_2 consumed m^{-2} d^{-1}) at T_o = 288.15 K, E_a is the activation energy (eV), k_B is the Boltzmann constant (8.62 x 10^{-5} eV K^{-1}), and T is the water temperature (K).

For $0 \leq t < f$, the full oxygen mass balance (eqn. 4.4) becomes:

$$\frac{dC_{DO}}{dt} = \left(k_{O2,20^o}\theta_a^{T-293.15\ K}\right)\cdot D + \frac{P(t)_{O2} - R_o \exp\left[\frac{-E_a}{\kappa_B}\left(\frac{1}{T} - \frac{1}{T_o}\right)\right]}{H} \quad (4.7)$$

where T is the water temperature (K), which varies throughout a diurnal period. The minimum oxygen deficit (D_{min}) is reached at the observed maximum DO concentration ($C_{DO,min}$), which takes place at the time of the minimum oxygen deficit (t_{minD}) and corresponds to $\frac{dC_{DO}}{dt} = 0$ (Wang *et al*., 2003). Therefore, at t_{minD}:

$$P(t_{minD})_{O2} = R_o \exp\left[\frac{-E_a}{\kappa_B}\left(\frac{1}{T} - \frac{1}{T_o}\right)\right] - H\left(k_{O2,20^o}\theta_a^{T-293.15\ K}\right)\cdot D_{min} \quad (4.8)$$

where $P(t_{minD})_{O2}$ is the rate of photosynthesis (g O_2 produced m^{-2} d^{-1}) at the time of the minimum DO deficit. Assuming photosynthesis can be described by a half-sine wave during the photoperiod f, the maximum photosynthesis P_{max} is:

$$P_{O2,max} = \frac{P(t_{minD})_{O2}}{\sin\left[\frac{\pi\, t_{minD}}{f}\right]} \quad (4.9)$$

Since solar noon corresponds to $0.5f$, the average daily photosynthesis ($P_{O2,avg}$) can be approximated by:

$$P_{O2,avg} = P_{O2,max}\left(\frac{2f}{\pi\,\tau}\right) \quad (4.10)$$

where τ is 1 day. Finally, at the average daily water temperature (T_{avg}) NDM can be determined from:

$$NDM = P_{O2,avg} - R(T_{avg})_{O2} \quad (4.11)$$

4.3.2 Modeling O_2-CO_2 Dynamics

While a negligible contribution of O_2 from groundwater seepage is a common assumption for the oxygen mass balance, it may not be a valid assumption for the CO_2

mass balance since a significant mass influx of dissolved CO_2 is expected from supersaturated groundwater. The following presents a procedure for determining RQ, the mass loading of allochthonous CO_2-C, and PQ for streams based on the daily metabolic rates described in terms of oxygen in section 4.3.1.

The CO_2 mass balance can be described in similar form as equation 4.4:

$$\frac{dC_{CO2}}{dt} = \frac{R_{CO2} - P(t)_{CO2} - \mathcal{F}_{CO2}}{H} + C_{CO2,alloc} \quad (4.12)$$

where $\frac{dC_{CO2}}{dt}$ is the daily change in the CO_2 concentration (mg L^{-1} d^{-1}), R_{CO2} and $P(t)_{CO2}$ are the CO_2-C fluxes from respiration and photosynthesis (g C m^{-2} d^{-1}), $\mathcal{F}_{CO2}$ is the CO_2 efflux at the air-water interface (g C m^{-2} d^{-1}) from eqn. 3.1, and $C_{CO2,alloc}$ is the dissolved concentration of allochthonous CO_2 (mg L^{-1}).

When $f \leq t \leq \tau$ during nighttime, equation 4.12 becomes:

$$\frac{dC_{CO2}}{dt} = \frac{R_{CO2} - \mathcal{F}_{CO2}}{H} + C_{CO2,alloc} \quad (4.13)$$

However, because $\frac{dC_{CO2}}{dt}$ is nearly constant throughout the night as discussed in chapter 3, the EVM cannot be invoked to solve the CO_2 mass balance. Thus, the rate of change of CO_2 at nighttime can be approximated by:

$$\frac{dC_{CO2}}{dt} = \frac{K_H(pCO_{2,max} - pCO_{2,min})}{\tau - f} \quad (4.14)$$

where K_H is Henry's law solubility coefficient for CO_2 (mg C L^{-1} μatm^{-1}) given in eqn. 3.2, $pCO_{2,max}$ is the maximum partial pressure of CO_2 at night usually at $t = \tau$ (μatm), and $pCO_{2,min}$ is the minimum partial pressure of CO_2 measured at night usually at $t = f$ (μatm).

The average nighttime $\mathcal{F}_{CO2}$ can be determined following the procedure outlined in chapter 3 by converting k_{O2} calculated from the modified EVM to k_{CO2} using the Schmidt number dependence (eqn. 3.6), so:

$$\mathcal{F}_{CO2} = k_{O2}\left(\frac{Sc_{CO2}}{Sc_{O2}}\right)^{-0.5} K_H H\,(pCO_{2,avg} - pCO_{2,atm}) \qquad (4.15)$$

where Sc_{CO2} is the Schmidt number for CO_2 (eqn. 3.7), Sc_{O2} is the Schmidt number for O_2 (eqn. 3.8), $pCO_{2,avg}$ is the nighttime average partial pressure of CO_2 (μatm), and $pCO_{2,atm}$ is the partial pressure of CO_2 in the atmosphere (400 μatm).

The respiration term (R_{CO2}) in equation 4.13 can be related to R_{O2}, calculated from Arrhenius kinetics as shown in eqn. 4.6, by the respiratory quotient on a molar basis:

$$\frac{R_{CO2}}{12} = RQ\frac{R_{O2}}{32} \qquad (4.16)$$

By first solving 4.13 for the case of $C_{CO2,alloc} = 0$, R_{CO2} can be initially characterized for several sampling dates. Then these $R_{CO2}/12$ (mol m^{-3} d^{-1}) values can be plotted against $R_{O2}/32$ (mol m^{-3} d^{-1}) where the slope is RQ.

Once RQ is known, substituting 4.14-4.16 back into 4.18, and solving for $C_{CO2,alloc}$ yields:

$$C_{CO2,alloc} = \left\{ K_H \left[\begin{array}{c} \left(\frac{(pCO_{2,max} - pCO_{2,min})}{\tau - f} + k_{O2}\left(\frac{Sc_{CO2}}{Sc_{O2}}\right)^{-0.5}\right] \\ \cdot \left(pCO_{2,avg} - pCO_{2,atm}\right) \\ - \frac{12}{32}\frac{RQ}{H}\frac{R_{O2}}{} \end{array} \right] \right\} \qquad (4.17)$$

$C_{CO2,alloc}$ is expected to remain nearly constant on daily timescales. Next, the EVM is applied during the day to solve for $P(t)_{CO2}$ at the minimum daytime pCO_2 ($pCO_{2,minD}$) since $\frac{dC_{CO2}}{dt} = 0$:

$$P(t)_{CO2,minD} = \frac{12\ RQ}{32} R_{O2} - \left[K_H k_{O2} \left(\frac{Sc_{CO2}}{Sc_{O2}} \right)^{-0.5} \cdot (pCO_{2,minD} - pCO_{2,atm}) \right] \quad (4.18)$$

where R_{O2}, K_H, K_{O2}, and Sc correspond to the temperature at the time of $pCO_{2,minD}$ ($t_{minD,C}$). $t_{minD,C}$ is not necessarily the same as t_{minD}. $P_{CO2,max}$ and $P_{CO2,avg}$ can then be determined from equations 4.9-4.10. Finally, the photosynthetic quotient (PQ) can be found from relating $P_{CO2,avg}$ to $P_{O2,avg}$:

$$PQ = \frac{12\ P_{O2,avg}}{32\ P_{CO2,avg}} \quad (4.19)$$

The procedure outlined in sections 4.3.1-4.3.2 may also be applied to timesteps < 1 day once the daily rates have been initially characterized for a site to simulated O_2-CO_2 dynamics.

4.4 Results

Daily photosynthesis and respiration rates in terms of oxygen determined by the EVM are shown in Figure 4.2. Photosynthesis and respiration displayed a strong relationship for both Freese ($R^2 = 0.95$) and Como ($R^2 = 0.91$) for data collected between June 2015 – May 2016. Oxygen production rates ranged from 0.2-101 mg L^{-1} d^{-1} with a mean rate of 16 $\pm$ 22 mg L^{-1} d^{-1} for Freese and from 0.1-30 mg L^{-1} d^{-1} with a mean rate of 5 $\pm$ 6 mg L^{-1} d^{-1} for Como. Respiration exceeded gross primary production (GPP) at both sites indicating net heterotrophy for Fall Creek (Figure 4.3). Net heterotrophy

increased (i.e. NDM decreased) during low flow conditions. The average NDM at Como (-1.1 ± 0.66 g O_2 m^{-2} d^{-1}) was higher than at Freese (-3.6 ± 2.5 g O_2 m^{-2} d^{-1}).

The respiratory quotient (RQ) at Como was 0.95 ($R^2 = 0.92$), while RQ at Freese was 0.73 ($R^2 = 0.80$) as illustrated in Figure 4.4. Figure 4.5 presents a photosynthetic quotient (PQ) of 1.6 for Como ($R^2 = 0.69$) and 2.1 for Freese. The concentration of CO_2 contributed by allochthonous sources was calculated from RQ at nighttime using the CO_2 mass balance (eqn. 4.17). These results are displayed in Figure 4.6. Allochthonous CO_2 was clearly related to the fraction of streamflow attributed to baseflow (as defined in section 2.3.2) with higher allochthonous CO_2 concentrations during baseflow than stormflow. Como, on the other hand, appeared to have a consistent concentration of externally sourced CO_2 for all flow regimes with the exception of two outliers that occurred following a summer storm event. Autochthonous CO_2 production exceeded allochthonous inputs at both Freese (1.7:1, $R^2 = 0.70$) and Como (2.6:1, $R^2 = 0.95$) as shown in Figure 4.7.

After the RQ, PQ, and allochthonous CO_2 parameters had been determined, they were used to calculated NDM in terms of carbon (Figure 4.8). Carbon NDM results were similar to those from the oxygen NDM and indicated net heterotrophy for Fall Creek. However, the carbon NDM trend appeared more normalized than that of the oxygen NDM flattening out the extreme low values calculated during the summer and decreasing the higher winter values. Figure 4.8 also shows a clear temperature dependence of the carbon NDM on the average daily air temperature. The GPP pattern for both Freese and Como (Figure 4.9) resembled the shape of the incoming net solar radiation curve.

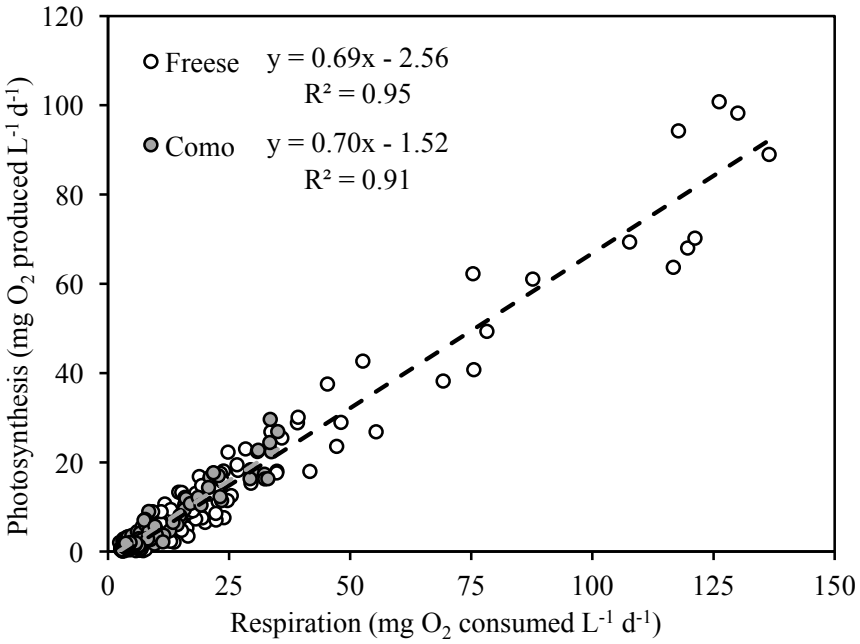

Figure 4.2 Oxygen produced during photosynthesis against oxygen consumed during respiration for Fall Creek, June 2015 – May 2016

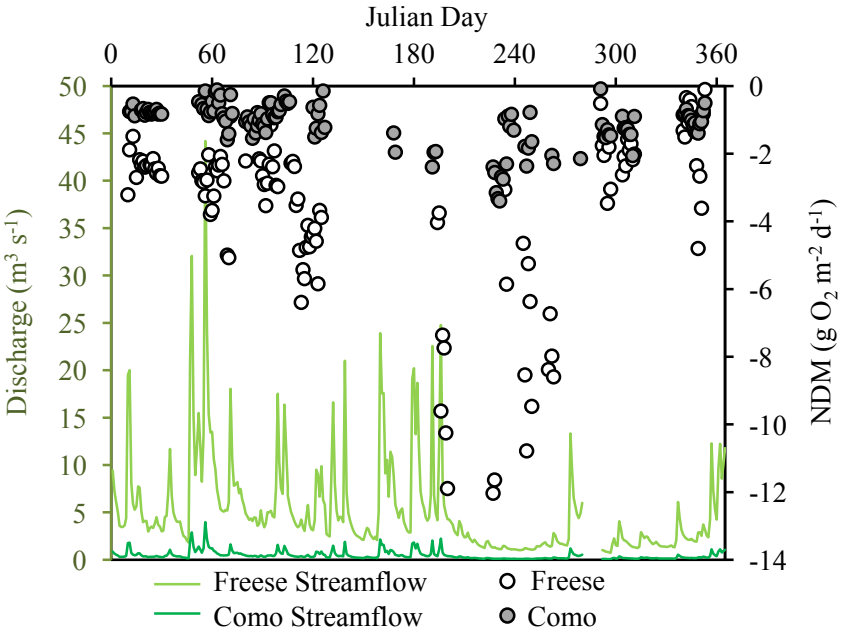

Figure 4.3 Net daily metabolism (NDM) as an oxygen flux and daily average streamflow for Fall Creek, June 2015 – May 2016

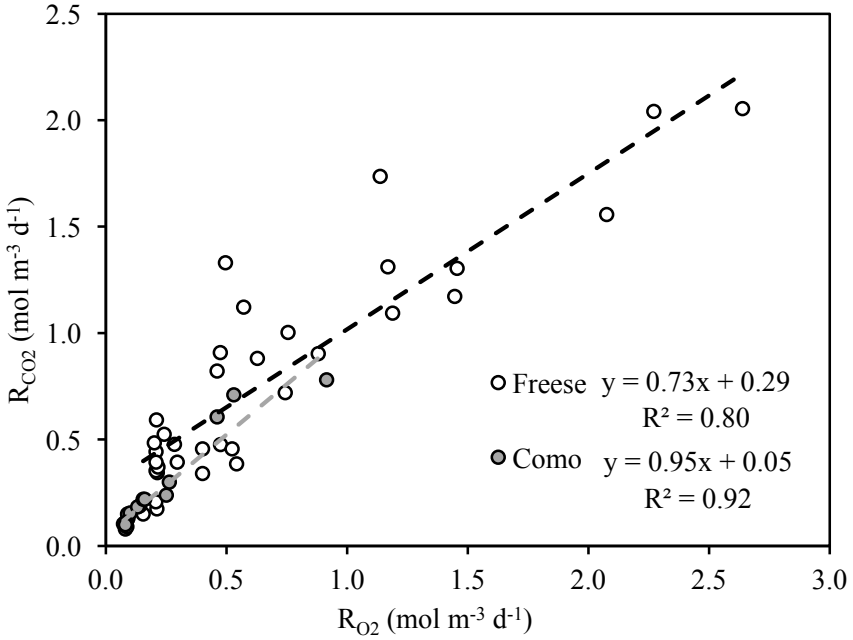

Figure 4.4 Moles of carbon produced during respiration vs. moles of oxygen consumed. The slope is the respiratory quotient (RQ).

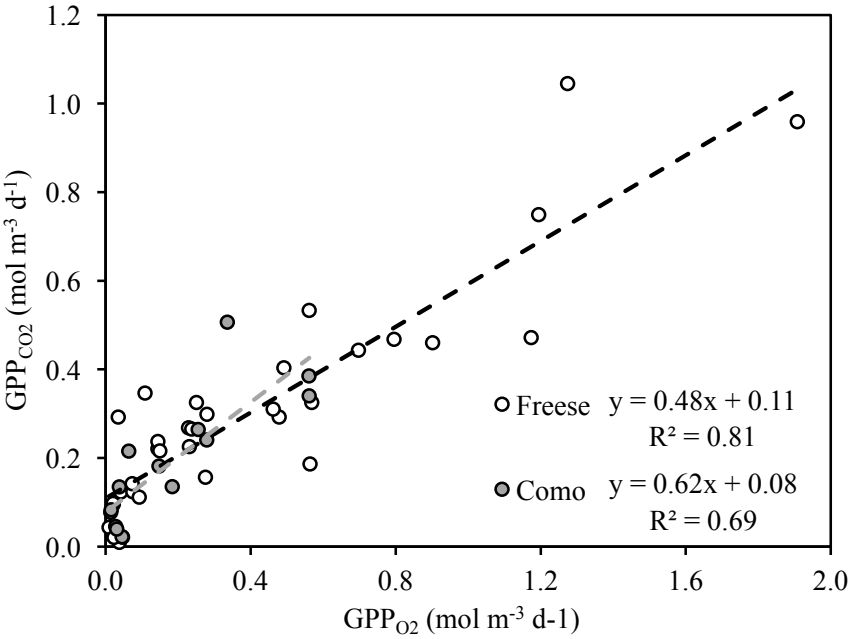

Figure 4.5 Moles of carbon consumed during photosynthesis vs. moles of oxygen produced. The slope is the 1/photosynthetic quotient (1/PQ).

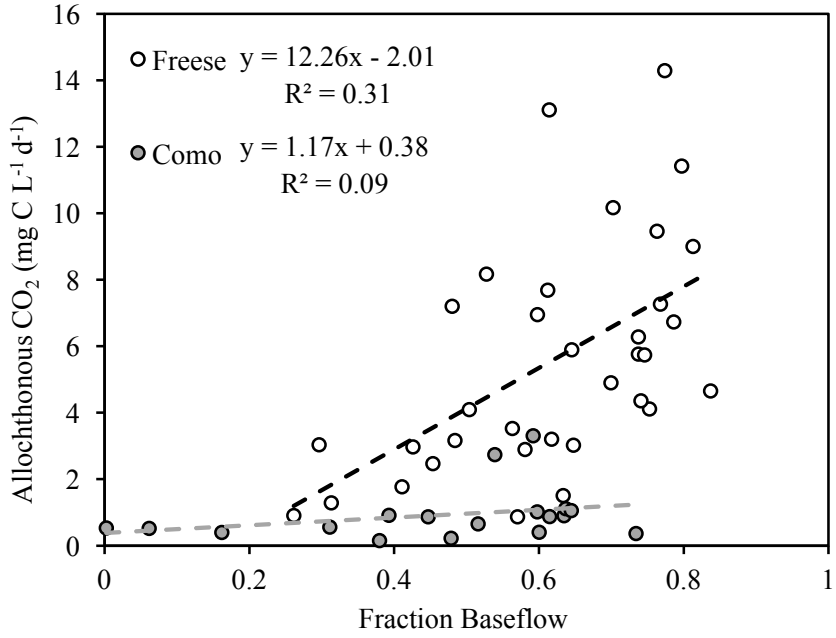

Figure 4.6 Concentration of allochthonous CO_2-C in relation to the fraction of streamflow comprised of baseflow for Fall Creek

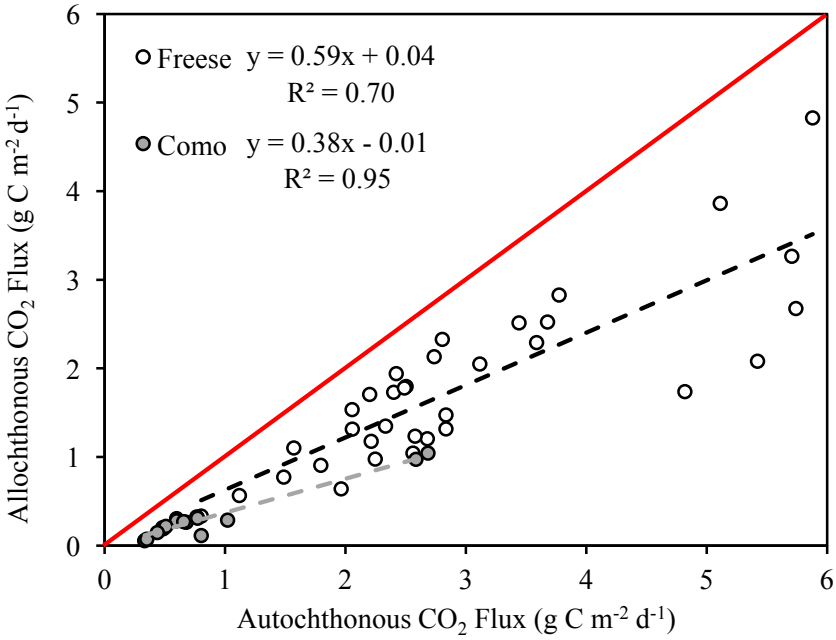

Figure 4.7 Externally sourced vs. internally derived CO_2 for Fall Creek. Red line represents 1:1.

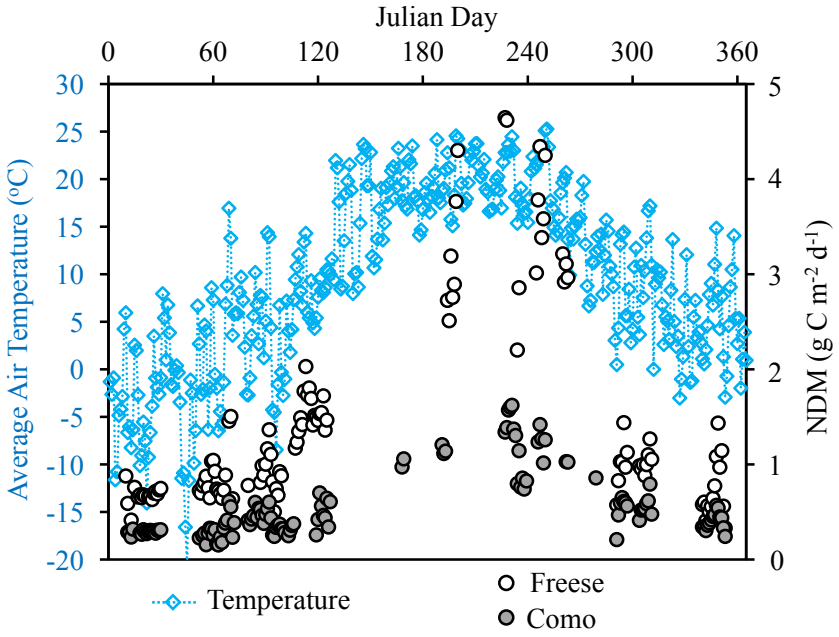

Figure 4.8 Net daily metabolism (NDM) as a carbon flux and average air temperature for Fall Creek, June 2015 – May 2016

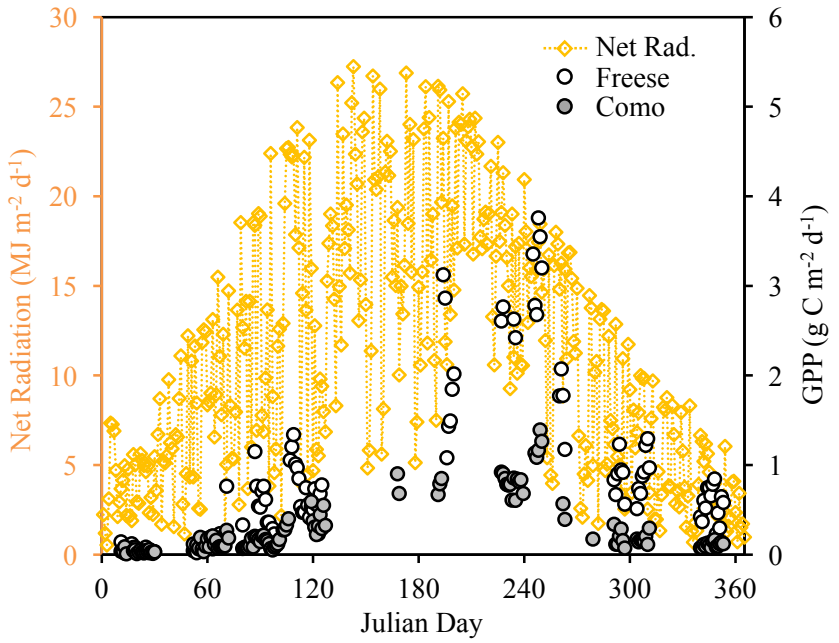

Figure 4.9 Gross primary productivity (GPP) and net incoming solar radiation for Fall Creek, June 2015 – May 2016

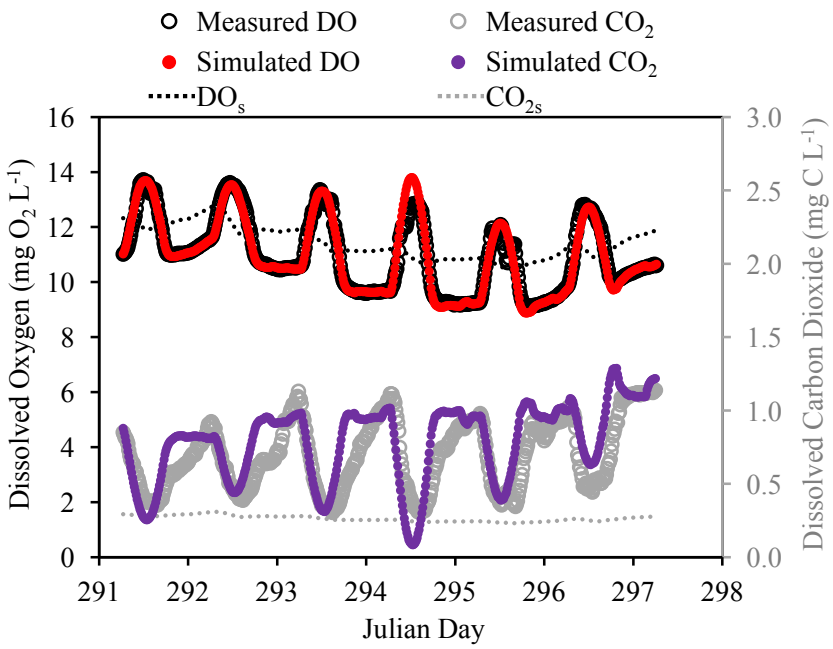

Figure 4.10 Measured and simulated dissolved O_2 and dissolved CO_2 for Freese, 18 – 24 October 2015. Dotted lines indicate DO and CO_2 at saturation.

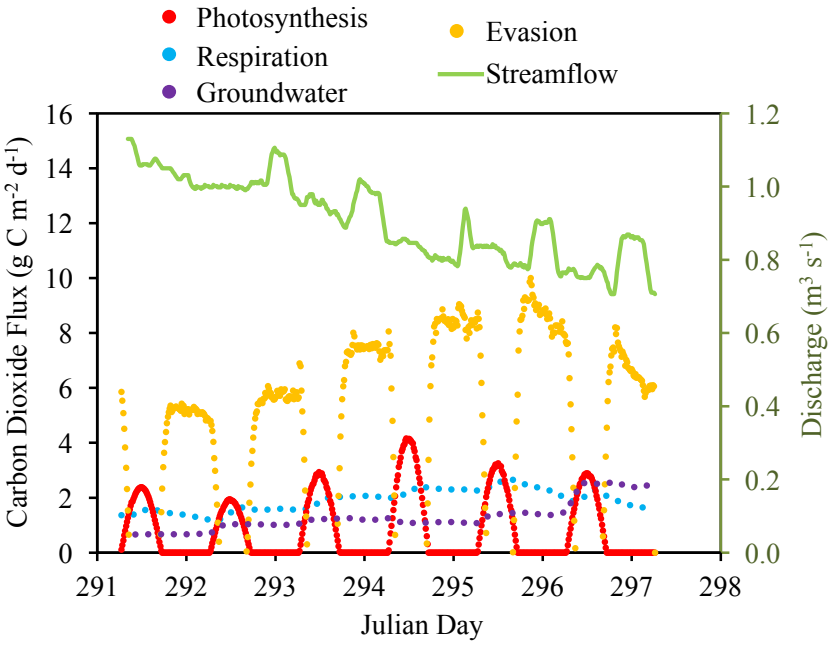

Figure 4.11 Simulated daily carbon fluxes and streamflow for Freese, 18 – 24 October 2015. Blue dots represent autochthonous CO_2 production while the purple dots are allochthonous CO_2 sourced from groundwater.

The parameterizations for RQ, PQ, and allochthonous CO_2 were tested by using $P_{O2,max}$ determined from the EVM (eqn. 4.9), temperature data, and the oxygen and carbon dioxide mass balances (eqns. 4.4 and 4.12) to simulate O_2-CO_2 dynamics at 15-minute time-steps for six days at Freese, 18 – 24 October 2015. Simulation results are provided in Figures 4.10 and 4.11. Figure 4.10 shows the observed DO (black circles) and CO_2 (grey circles) data points along with saturated values for DO and CO_2 based on temperature (eqns. 2.5 and 3.2). The DO simulation (red) matches up well with the observations, while the CO_2 simulation (violet) captures the general trend. Each component of the CO_2 mass balance is illustrated in Figure 4.11 as a daily carbon flux.

4.5 Discussion

4.5.1 Net Daily Metabolism for Fall Creek

Fall Creek is a net heterotrophic system indicating that a subsidy of allochthonous organic carbon inputs are necessary to sustain the observed respiration rates (Cole and Caraco, 2001). Daily rates of photosynthesis (GPP) were tightly linked to stream respiration (Figure 4.2) suggesting that primary production supports respiration during the summer (Beaulieu *et al*., 2013; Hall *et al*., 2015). The relative ratio of GPP:R was consistent (1:1.4) from June 2015 – May 2016 at both Freese and Como on Fall Creek and may represent the proportion of autotrophic respiration to GPP (Hall and Beaulieu, 2013). The fraction of autotrophic (R_{Af}) respiration on Fall Creek may be as high as 0.7 implying that the amount of C available to heterotrophs would be 0.3GPP. R_{Af} for Fall Creek is close to the range of values (0.11-0.69) estimated for 13 streams by Hall and Beaulieu (2013) and closely matched that of a second order

suburban stream in Ohio (Beaulieu *et al*., 2013) and streams receiving wastewater treatment plant (WWTP) effluent in northern Spain (Izagirre *et al*., 2008). While Fall Creek does receive WWTP effluent from the combined Dryden/Freeville outfall, it is neither polluted nor eutrophic like the Spanish streams. Additionally, the GPP:R at Como (upstream of the WWTP outfall) matched that of Freese (downstream of the outfall) suggesting that the WWTP effluent was not the cause of Fall Creek's high R_{Af}.

Figure 4.12 Macrophyte abundance at Como (left) compared to Freese (right), 17 September 2015

Like respiration (chapter 2), GPP also has a strong temperature dependence as indicated by the NDM-temperature curves (Figure 4.8). While the flux attributed to carbon fixation at Freese exceeded that of Como (Figure 4.9), it is important to

recognize that these fluxes are quantified by the total volume of water passing through a monitoring location. Therefore, the productive headwater reaches (e.g. Como) are contributing to the fluxes measured downstream at Freese. The relative productivity of the two sites is qualitatively depicted in Figure 4.12 by the abundant macrophyte biomass at Como compared to the rocky benthos at Freese. GPP also closely tracked with net solar radiation throughout the year (Figure 4.9). Carbon fluxes were greatest for GPP, R, and NDM during summer baseflow.

4.5.2 Allochthonous Sources of CO_2

Autochthonous CO_2 production from aquatic respiration is 1.7 times larger than the estimated terrestrial derived CO_2 from allochthonous loading at Freese and 2.6 times larger at Como (Figure 4.7). This suggests that internal metabolic processes have a stronger influence on pCO_2 in Fall Creek's headwaters and this influence decreases longitudinally downstream matching the theoretical stream-river continuum (Figure 4.13). However, contrary to the theoretical stream-river continuum (Hotchkiss *et al*., 2015), where respiration greatly exceeds GPP upstream and decreases until near-equilibrium is reached between R and GPP downstream, R:GPP remains remarkably consistent with R >> GPP on Fall Creek from Como downstream to Freese, a distance of 43.5 km). While allochthonous organic carbon likely drives aquatic respiration on Fall Creek, as indicated by its heterotrophic status, internally produced CO_2 may be responsible for ~40-60% of Fall Creek's CO_2 emissions (0.45-6.8 g C m^{-2} d^{-1}) as described in chapter 3.

Perhaps due to dilution effects, terrestrial CO_2 generally comprises a more substantial component of in-stream dissolved CO_2 during baseflow than during stormflows (Figures 4.6, for Freese, and 4.13). In Como's case, the influence of allochthonous CO_2 on in-stream CO_2 remains static through all flow regimes (Figure 4.6) with the potential exception of summer storm events (indicated by the two outliers in Figure 4.6), which may contribute pulses of CO_2 supersaturated emergent groundwater (Johnson *et al*., 2006). The daily C fluxes exemplified by the CO_2 simulation (Figure 4.11), show a shift from autochthonous production of CO_2 as the dominant control on in-stream CO_2 to allochthonous CO_2 as stream discharge decreases. CO_2 emissions also increase with decreasing discharge.

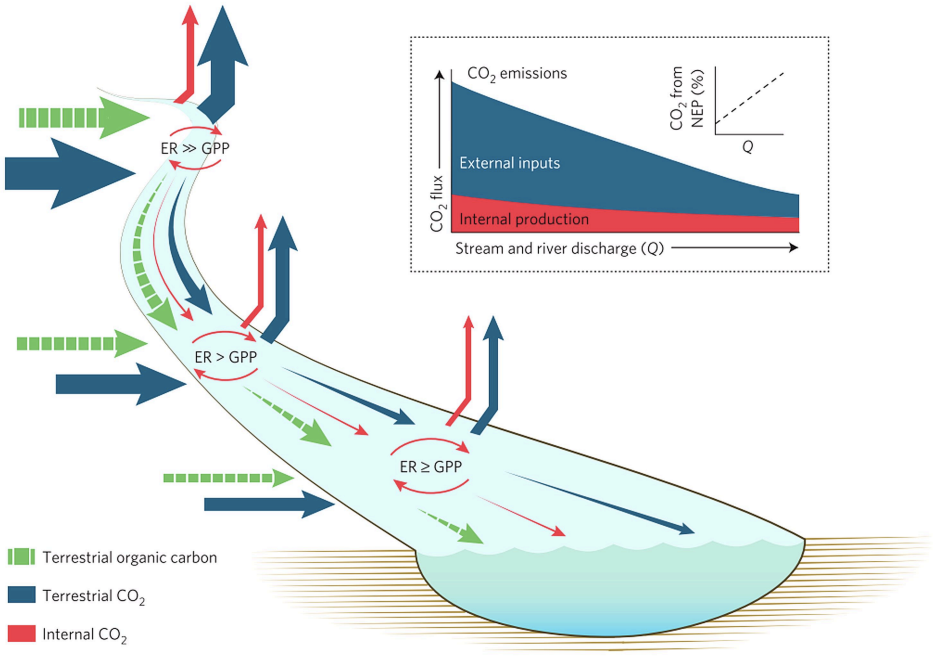

Figure 4.13 Sources and magnitude of net CO_2 emissions along a theoretical stream-river continuum. Reprinted from "Sources of and processes controlling CO_2 emissions change with the size of streams and rivers," by E. R. Hotchkiss *et al*., 2015, *Nature Geoscience, 8,* p. 698. © 2015 Macmillan Publishers Limited.

4.5.3 Biophysical Controls on O_2-CO_2 Dynamics

RQ and PQ varied between the two sites on Fall Creek and may provide insight toward the biophysical controls on O_2-CO_2 dynamics. The RQ for Como (0.95) was within the frequently assumed RQ range of 0.85 – 1.0 (Bott, 2007; Johnson et al., 2012; Perkins *et al*., 2012; Birkel *et al*., 2013; Roley *et al*., 2014). This indicates a nearly 1:1 molar ratio of O_2 consumed to CO_2-C produced during respiration. Freese, however, had a lower than expected RQ of 0.73. This may be indicative of differences in the quality of the carbon pool between the upstream and downstream sites. Suggestive of its RQ~1, organic carbon sources at Como may be more liable than at Freese (Berggren, *et al.*, 2012) which could be a consequence of the high degree of hydrologic connectivity at Como combined with its lush benthos (Figure 4.12). RQ may also be impacted by pH (Hanson *et al*., 2003). The average pH at Como was 7.62 $\pm$ 0.16 and 7.98 $\pm$ 0.24 at Freese for the monitoring period (June 2015 – May 2016). Hanson *et al*. observed a decrease in the RQ for lakes with pH > 8 and postulated that it was caused by interactions of CO_2 with the carbonate system. Freese does have a significantly higher ($p << 0.05$) alkalinity (130 $\pm$ 24.3 mg $CaCO_3$ L^{-1}) than Como (97.1 $\pm$ 17.9 mg $CaCO_3$ L^{-1}, *communityscience.org*).

The PQ values for both Freese (PQ = 2.1) and Como (PQ = 1.6) were higher than the commonly assigned value of 1.2 for most aquatic metabolism studies (Bott, 2007; Johnson *et al*, 2012; Roley *et al*., 2014). Unlike with the RQ, the lower PQ reflects a more efficient conversion between CO_2-C consumption and O_2 production during photosynthesis. Once again, the metabolic O_2-CO_2 conversion was more efficient at Como than at Freese. Smith *et al*. (2012) speculated that PQ could increase from an

increased influx of reactive nitrogen. Due to nutrient inputs from agricultural runoff on Fall Creek, it would be reasonable to expect Freese, with its larger catchment contributing area, to have greater concentrations of reactive nitrogen than Como. Nutrient limitations, photosynthetic capacity, and the tissue-N composition of aquatic macrophytes may also impact PQ (Baattrup-Pedersen *et al*., 2013).

Additionally, differences between heterotrophic and autotrophic communities at Freese and Como could lead to the divergent respiratory and photosynthetic quotients estimated at the two sites. It was surprising that RQ and PQ appeared to remain consistent throughout the year at both sites (Figures 4.4-4.5). However, these results are consistent with the singular reference respiration rates determined for each site throughout the year, which align with Arrhenius kinetics (chapter 2). Finally, both the RQ and PQ values estimated for Freese and Como performed reasonably well in simulating dissolved CO_2 compared to six days of continuous observations for Freese (Figure 4.10).

4.6 Conclusion

Fall Creek is a net heterotrophic stream that requires terrestrially-derived organic carbon inputs to sustain this status. While the allochthonous CO_2 contribution to in-stream pCO_2 was substantial for both sites on Fall Creek, it was not as significant as the autochthonous flux of CO_2 produced during aquatic respiration. NDM is strongly influenced by stream discharge, temperature, net solar radiation. The conversion efficiency of O_2 to carbon equivalents during photosynthesis and respiration is governed by RQ and PQ, which provide below a 1:1 molar ratio. CO_2-C fluxes from metabolic,

groundwater contributions, and gas emissions are greatest during summer baseflow for Fall Creek.

CHAPTER 5

SUMMARY

Diel oxygen and carbon dioxide curves contain a plethora of environmental information. In aquatic ecosystems, dissolved oxygen (DO) increases throughout the morning from photosynthesis until a maximum DO concentration is reached around solar noon. DO continues to decline throughout the afternoon and into the night. Surface-water atmosphere exchange, reaeration, can recharge the water column DO when the concentration is below saturation and may cause a nighttime increase in DO. When the water column is supersaturated in oxygen, during the day, oxygen is released to the atmosphere from reaeration. The partial pressure of free carbon dioxide (pCO_2) follows the opposite diurnal trend as DO decreasing throughout the day from photosynthesis and increasing at night from respiration. Inland waters tend to be supersaturated in CO_2 with respect to the atmosphere. Therefore, it is an infrequent occurrence for the atmosphere to recharge the water column in pCO_2 from carbon dioxide reaeration. Rather, there is a CO_2 efflux from surface waters, these emissions are often referred to as CO_2 evasion.

From the nighttime drop in DO, the rates of oxygen reaeration and respiration can be calculated (e.g. the nighttime slope method, chapter 2). These rates can be characterized for lotic systems during baseflow. For Fall Creek, respiration rates estimated by the nighttime slope method for June 2015 – May 2016 had a strong temperature dependence that could be described by Arrhenius kinetics. Reaeration rates

could be described by streamflow and channel morphology and were impacted by temperature and turbulence.

The oxygen reaeration rate coefficient can be converted to a carbon dioxide rate coefficient by relating physical properties of the two gases (e.g. the Schmidt number, chapter 3). Carbon dioxide evasion is a function of the stream-atmosphere CO_2 gradient and the CO_2 reaeration coefficient. Both dissolved CO_2 and the gas transfer velocity for CO_2 were spatially and temporally variable on Fall Creek with generally higher pCO_2 and lower gas exchange rates (k_{CO2}) at upstream locations compared to downstream. While pCO_2 did control evasion rates on diurnal time scales, variability in k_{CO2} was a stronger influence on CO_2 emissions overall.

Aquatic pCO_2 is the product of internal stream metabolism (autochthonous sources) and external terrestrially derived CO_2 (allochthonous sources). Allochthonous CO_2 sources can be determined for streams where external O_2 mass loadings are minimal by, first, determining net daily metabolism (NDM) from the DO mass balance and, second, converting metabolic rates from moles of oxygen to carbon equivalents (e.g. extreme value method, respiration quotient, and photosynthetic quotient, chapter 4). For Fall Creek, both autochthonous and allochthonous CO_2 were significant contributors to the stream pCO_2 pool. Groundwater CO_2 inputs were generally more substantial during baseflow and contributed to 40-60% of Fall Creek's CO_2 emissions. However, in-stream respiration was the primary source of CO_2 for most of the year.

Inland waters are important components of the terrestrial carbon cycle and contributors to atmospheric CO_2. In this dissertation, a new method for identifying

controls on and quantifying CO_2 gas fluxes from well-aerated and non-polluted rivers and stream was detailed. The recommended procedure can be summarized as follows:

(1) Collect pCO_2, DO, specific conductance, and stream temperature measurements at 15-minute sampling intervals using Odum's (1956) single-station method.

(2) Define baseflow using volumetric stream discharge, specific conductance data, and a conductivity mass balance (Miller *et al*., 2014).

(3) Estimate reaeration and respiration rates during baseflow from the diel oxygen curve using the nighttime slope method (NSM, Hornberger and Kelly, 1975).

(4) Normalize respiration rates calculated from the NSM to a reference temperature (e.g. 15^oC) by plotting the natural log of the oxygen flux consumed during respiration against the standardized temperature using the linearized Arrhenius equation (Perkins *et al*., 2012). Note: Depending on the site, the reference value for respiration may vary seasonally.

(5) Standardize the reaeration rates calculated from the NSM to a reference temperature (e.g. 20^oC) by using a temperature and turbulence coefficient based on Dobbins' film penetration theory (Demars and Manson, 2013).

(6) Estimate reaeration rates during all flow regimes by closing the oxygen mass balance using the extreme value method (EVM) and reference respiration rates calculated from step 4 (Wang *et al*., 2003). Note: Check

the oxygen reaeration rate estimates calculated from the EVM against those determined from the NSM, both normalized to 20^{o}C, to validate the EVM estimates.

(7) Characterize reaeration for all flow regimes by determining hydraulic controls on reaeration for the site with discharge, stream morphology measurements, and empirical reaeration rate equations.

(8) Scale oxygen reaeration rate coefficients to carbon dioxide reaeration rate coefficients from the Schmidt number relation (Jähne *et al*., 1987; Raymond *et al*., 2012).

(9) Convert pCO_2 to dissolved CO_2 using Henry's law solubility coefficient (Weiss *et al*., 1974).

(10) Calculate CO_2 efflux from surface waters from the dissolved CO_2 saturation gradient (difference between water and atmospheric CO2) and the reaeration rate coefficient (i.e. gas transfer coefficient, Wallin *et al*., 2011).

(11) Model oxygen fluxes and calculate NDM using the EVM.

(12) Determine the molar efficiency (i.e. respiratory quotient, RQ) for the conversion of O_2 to CO_2 during respiration by comparing respiration calculated using the oxygen mass balance EVM to respiration calculated from the carbon dioxide mass balance EVM assuming no groundwater inputs for several monitoring dates.

(13) Close the nighttime carbon dioxide mass balance by converting respiration in terms of oxygen to carbon dioxide with the RQ and solve for allochthonous CO_2 sources.

(14) Determine the photosynthetic quotient (PQ) for the conversion of CO_2 to O_2 during photosynthesis by solving the daytime carbon dioxide mass balance.

(15) Assess hydrological, environmental, and biophysical controls on the fluvial CO_2 fluxes, which were determined in steps 13-14.

The previous steps are a guide to quantify and isolate CO_2 fluxes from internal metabolic processes and allochthonous sources (e.g. groundwater). The prerequisite assumptions for each step should be carefully considered before applying this procedure to lotic freshwater systems. This procedure allows for the extraction of CO_2 gas transfer rate coefficients from diurnal DO curves. Direct and continuous, coupled O_2-CO_2 measurements can be used to characterize riverine CO_2 emissions, identify hotspots for CO_2 evasion, and indicate when streams "sigh."

APPENDIX A: HYDRAULIC GEOMETRIES, DISCHARGE, AND SPECIFIC CONDUCTANCE FOR FREESE AND COMO SITES ON FALL CREEK

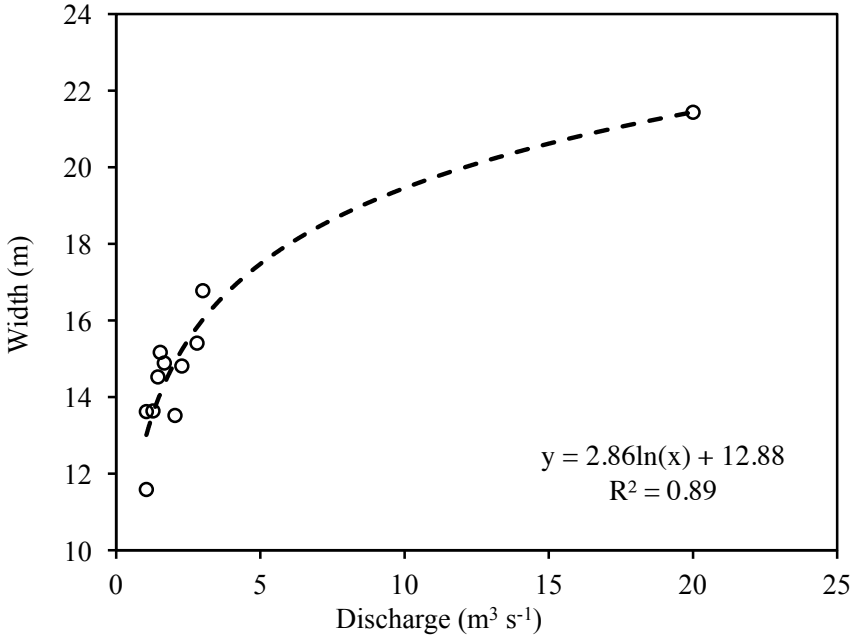

Figure A.1 Regression curve for measured channel width at Freese and streamflow at the USGS gauge on Fall Creek, June-October 2015

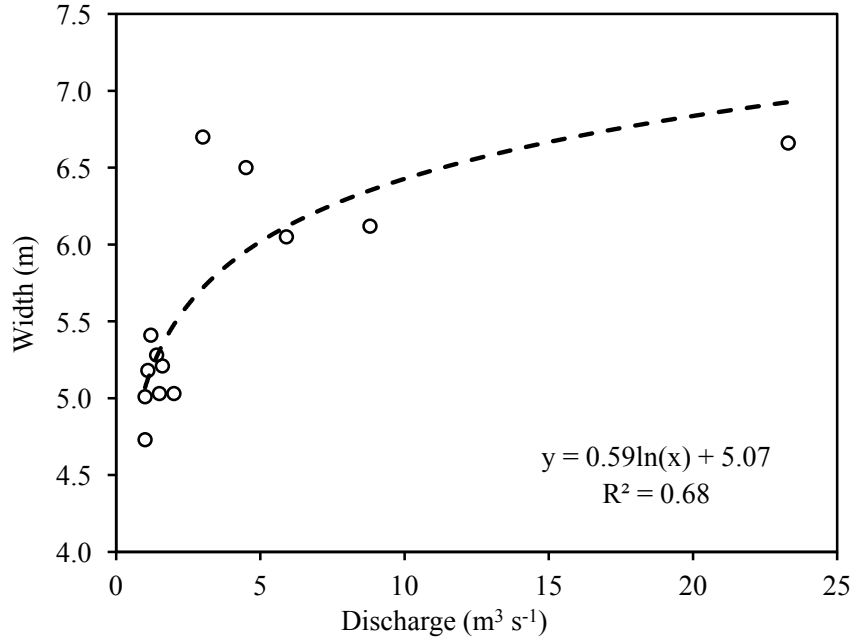

Figure A.2 Regression curve for measured channel width at Como and streamflow at the USGS gauge on Fall Creek, June-October 2015

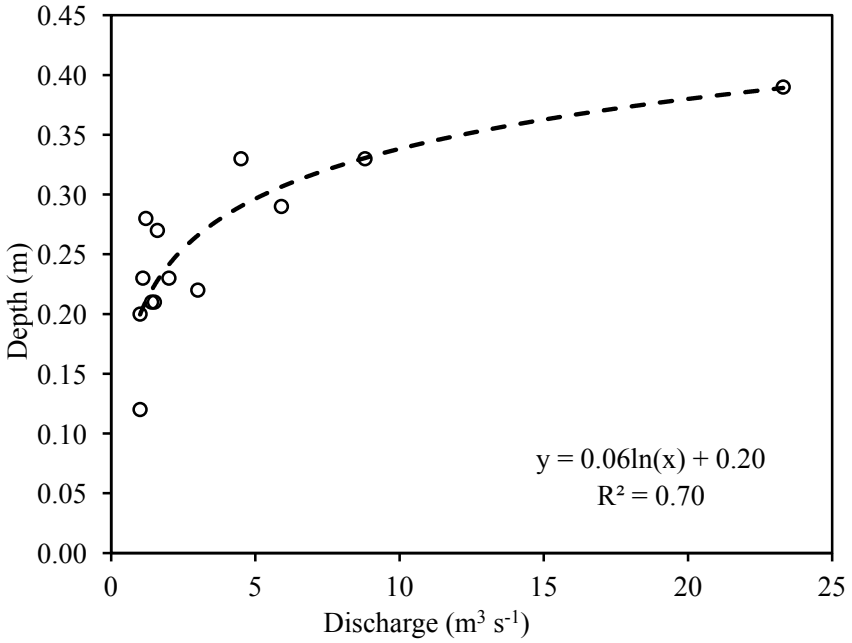

Figure A.3 Regression curve for measured average channel depth at Como and streamflow at the USGS gauge on Fall Creek, June-October 2015

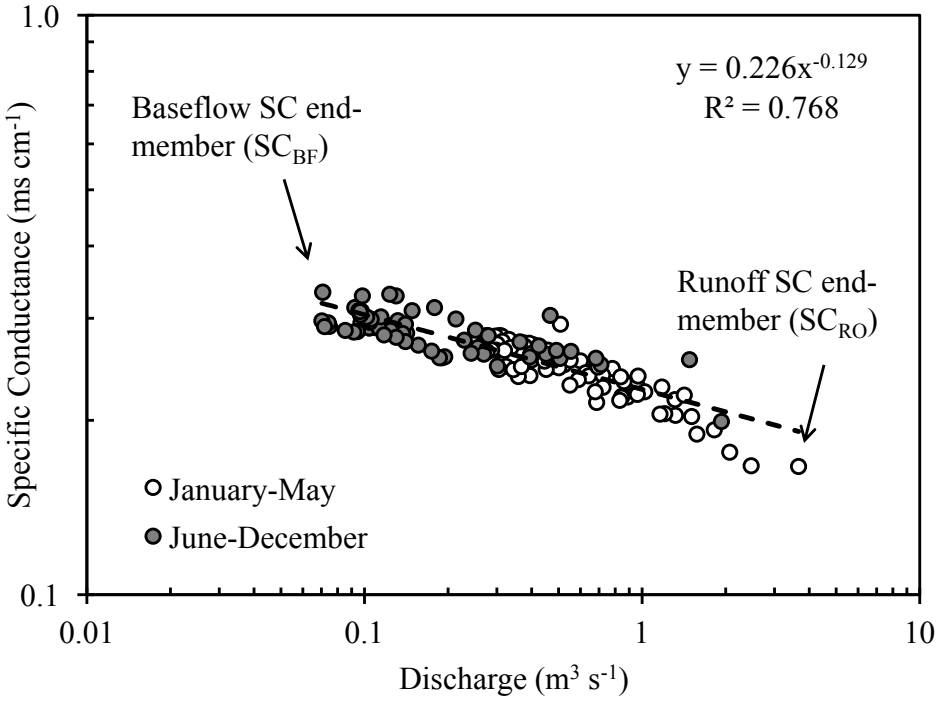

Figure A.4 Baseflow and runoff SC end-member selection for Como

APPENDIX B: NIGHTTIME SLOPE METHOD REGRESSIONS FOR FREESE AND COMO SITES ON FALL CREEK DURING BASEFLOW

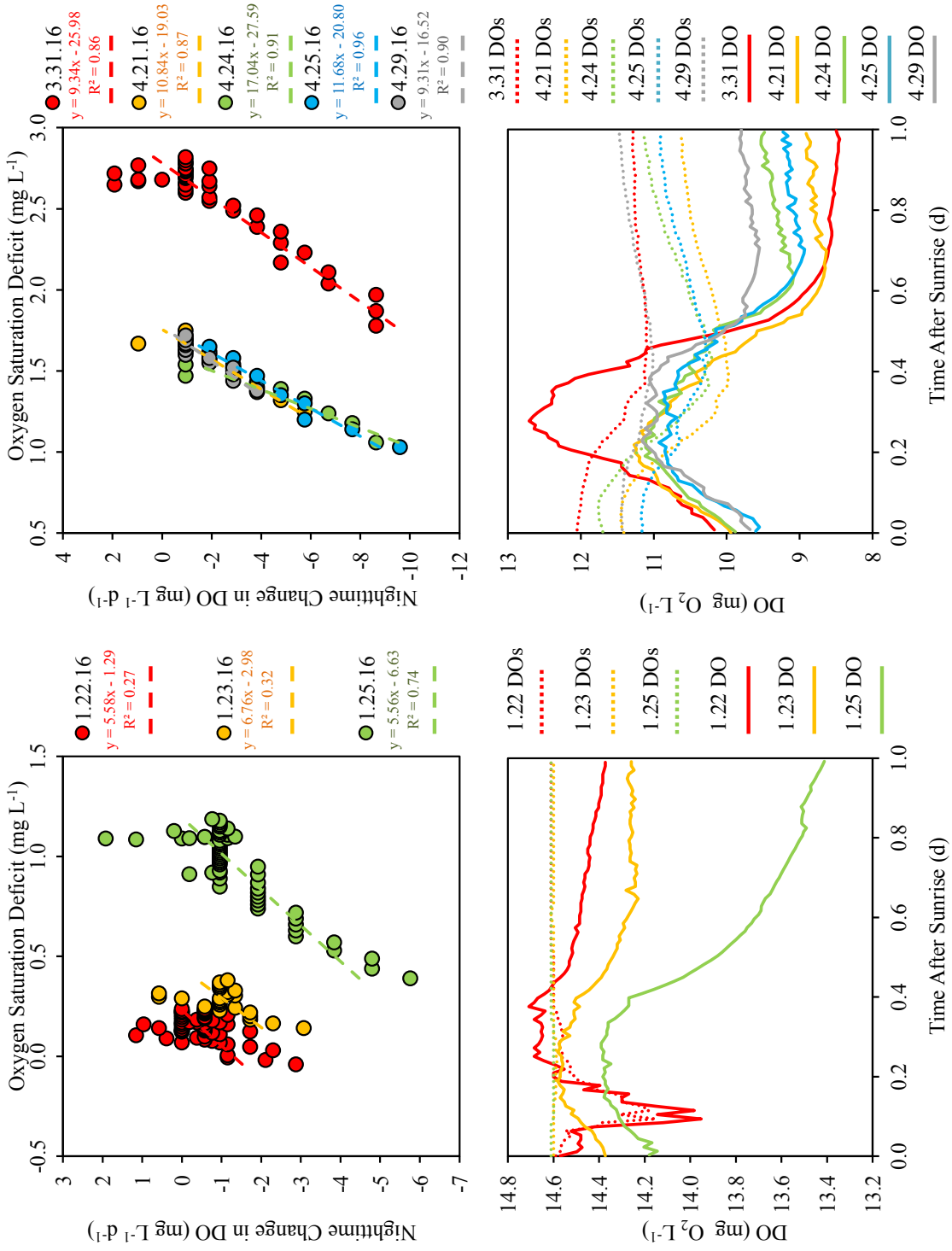

Figure B.1 Diurnal DO at Freese, January – April 2016

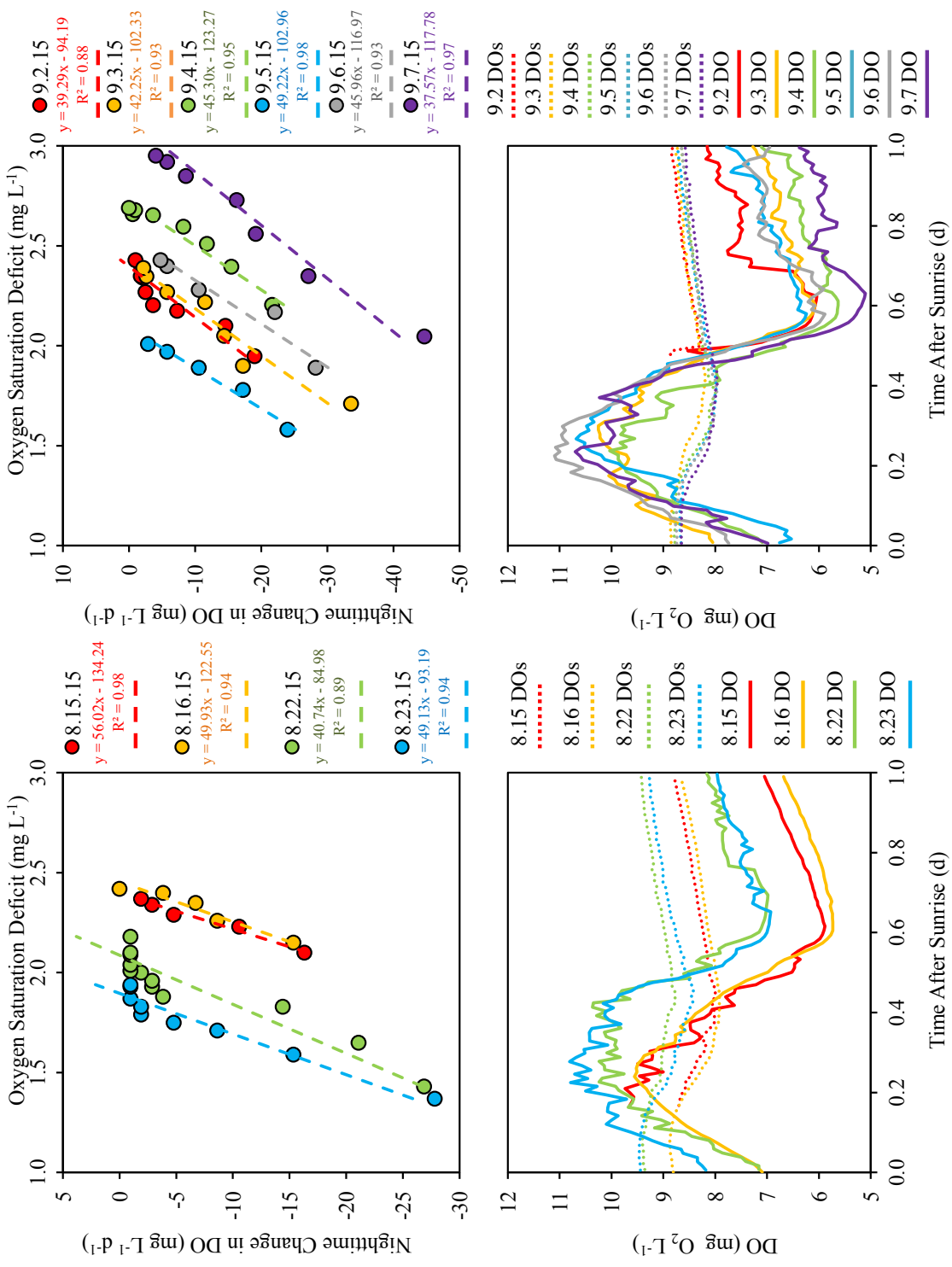

Figure B.2 Diurnal DO at Freese, August – September 2015

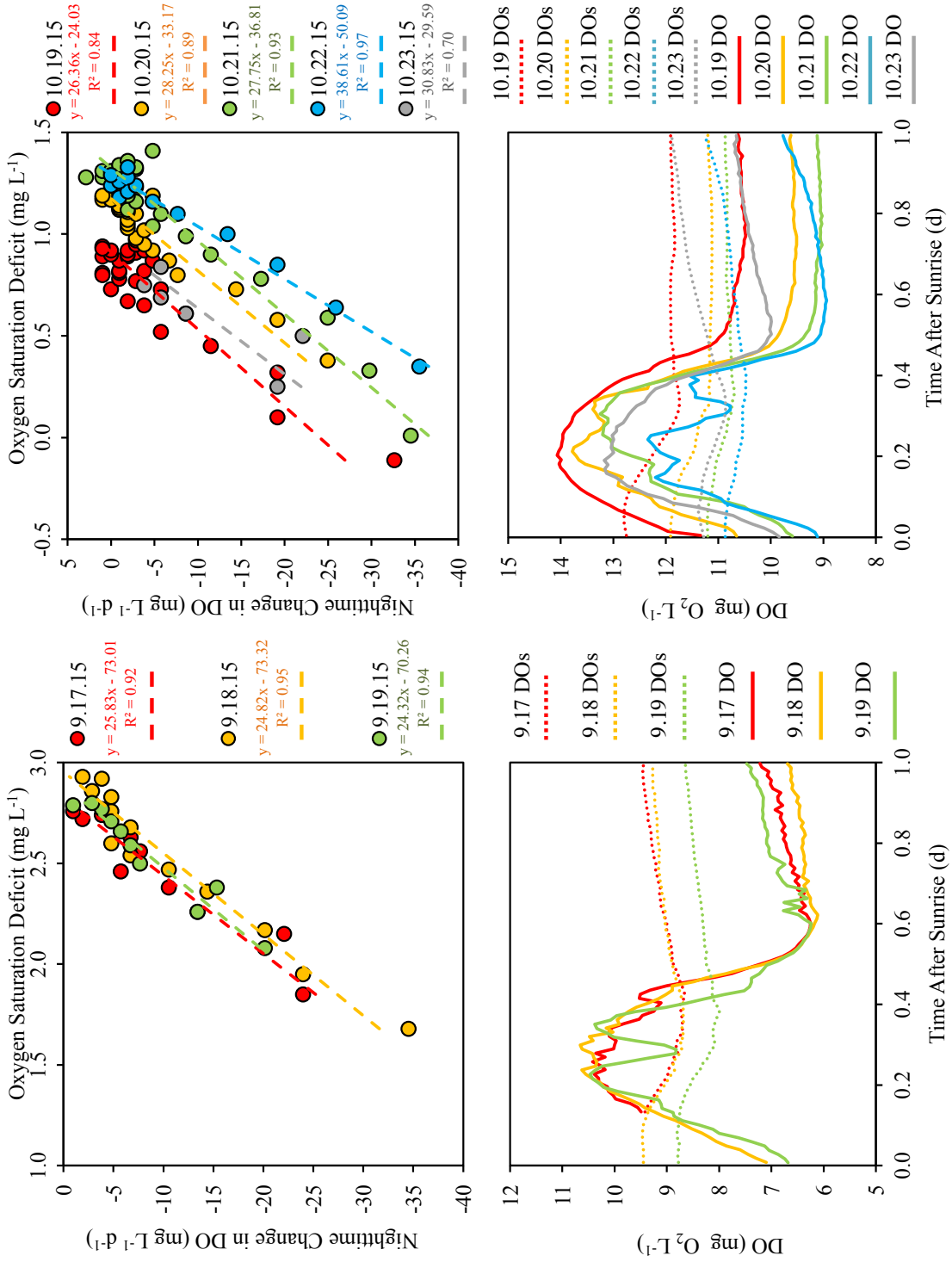

Figure B.3 Diurnal DO at Freese, September – October 2015

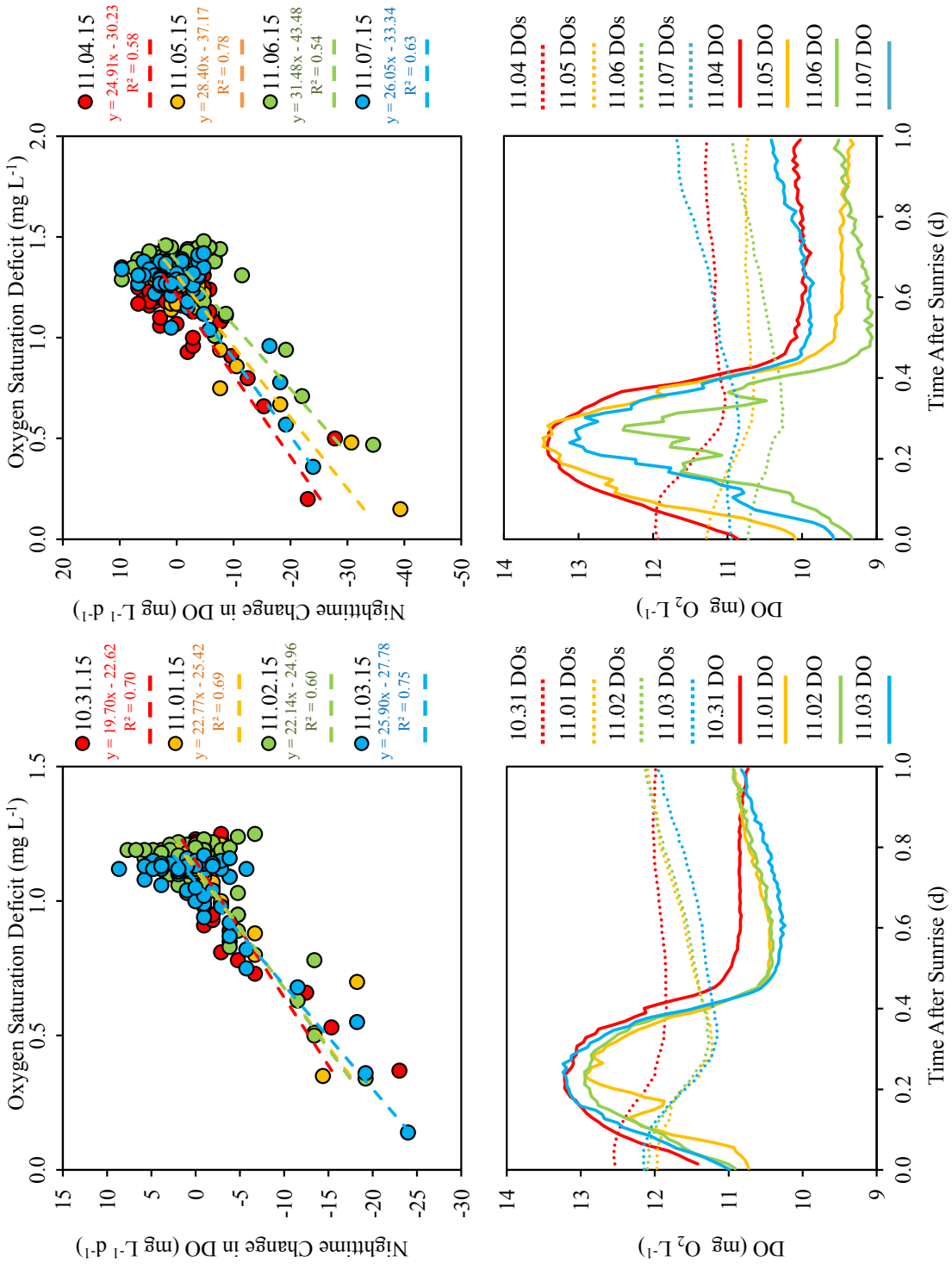

Figure B.4 Diurnal DO at Freese, October – November 2015

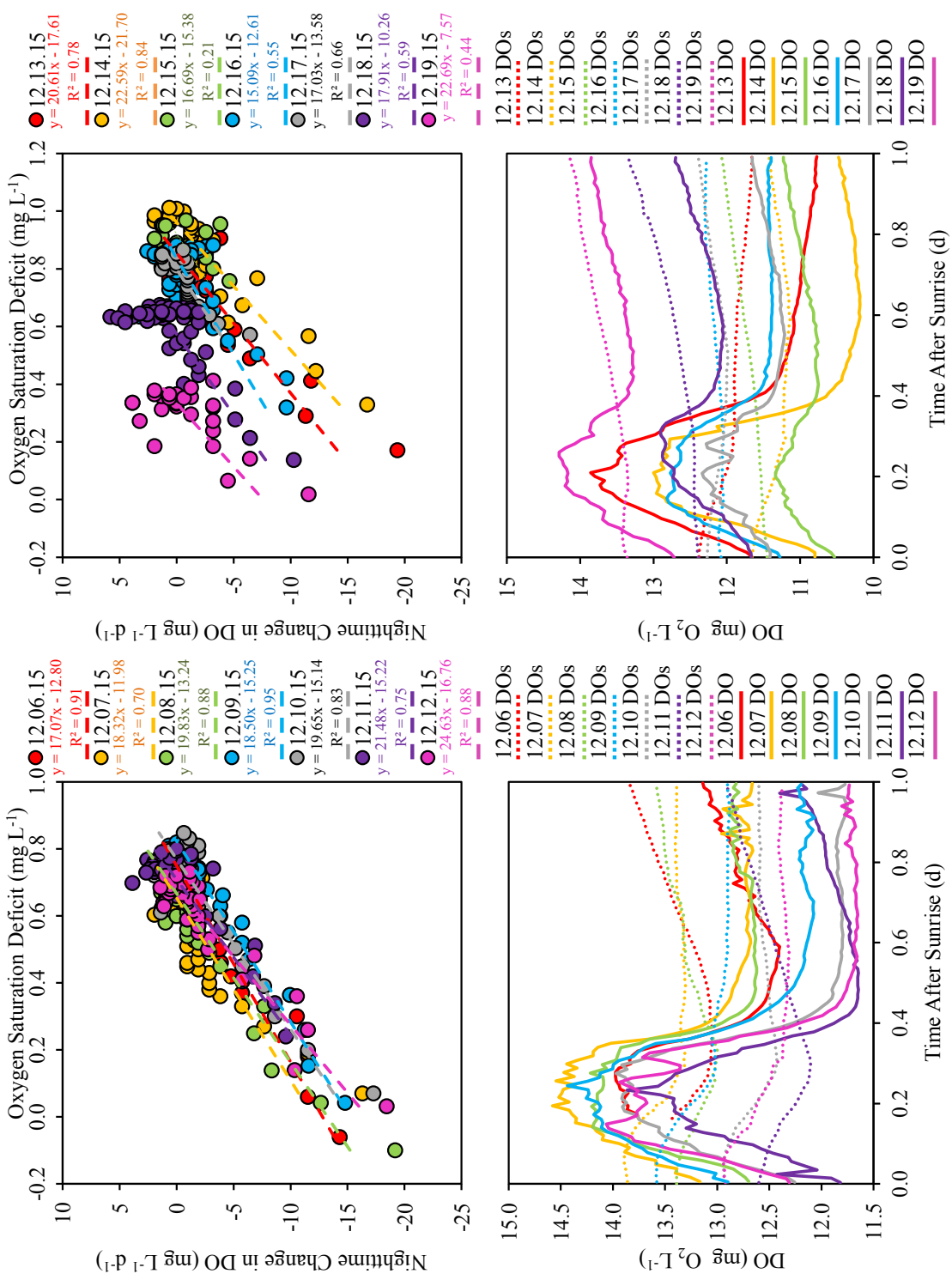

Figure B.5 Diurnal DO at Freese, December 2015

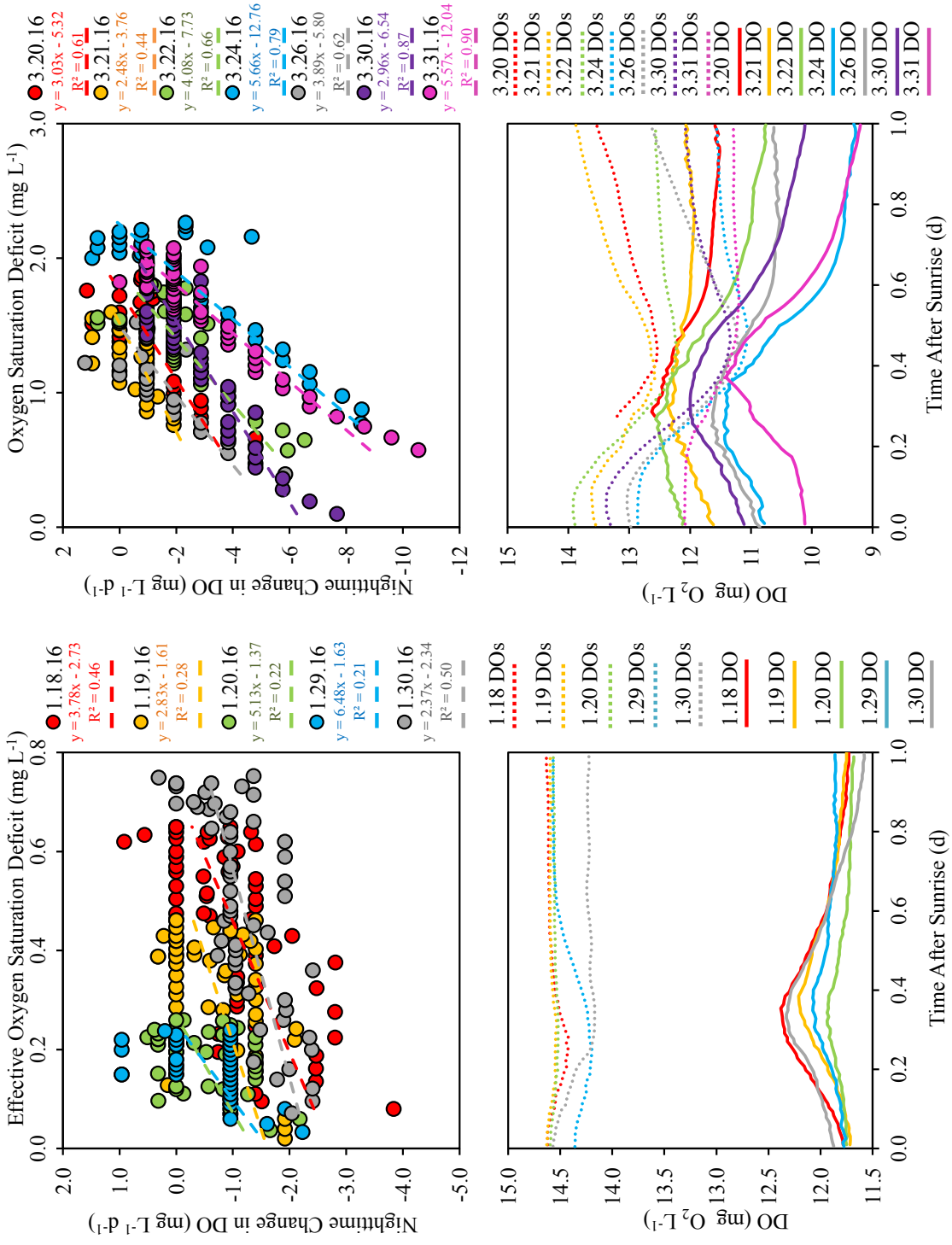

Figure B.6 Diurnal DO at Como, January – March 2016

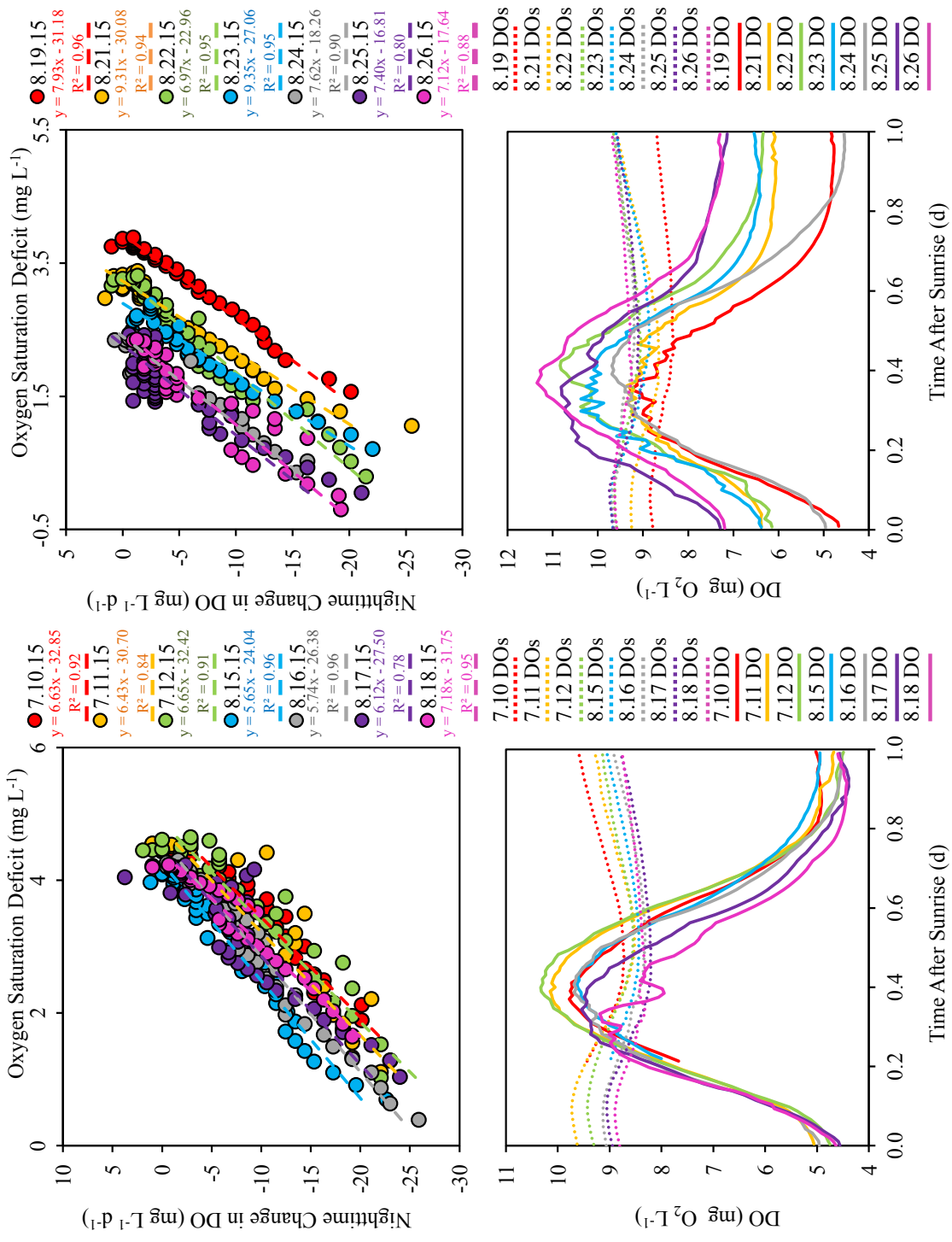

Figure B.7 Diurnal DO at Como, July – August 2015

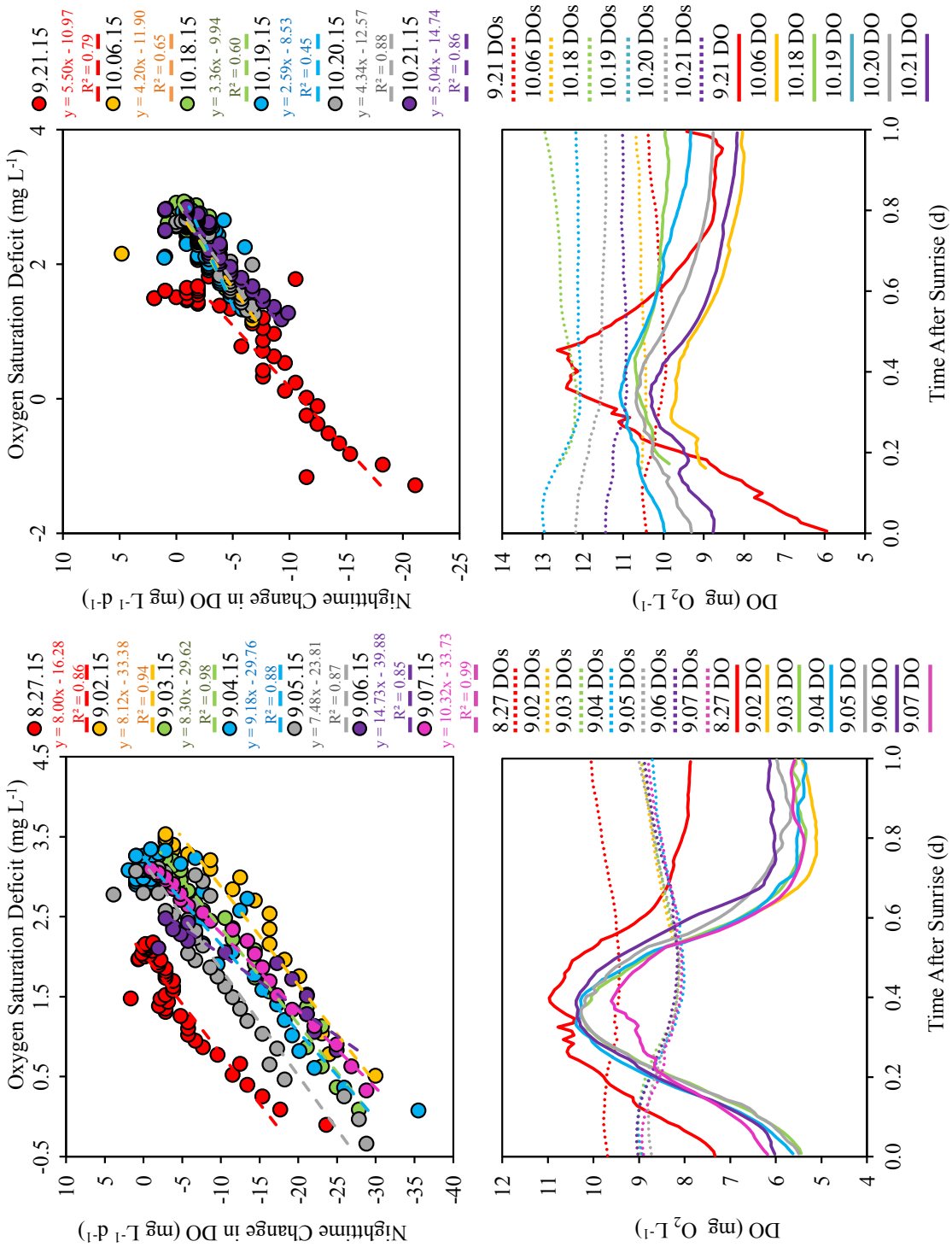

Figure B.8 Diurnal DO at Como, August – October 2015

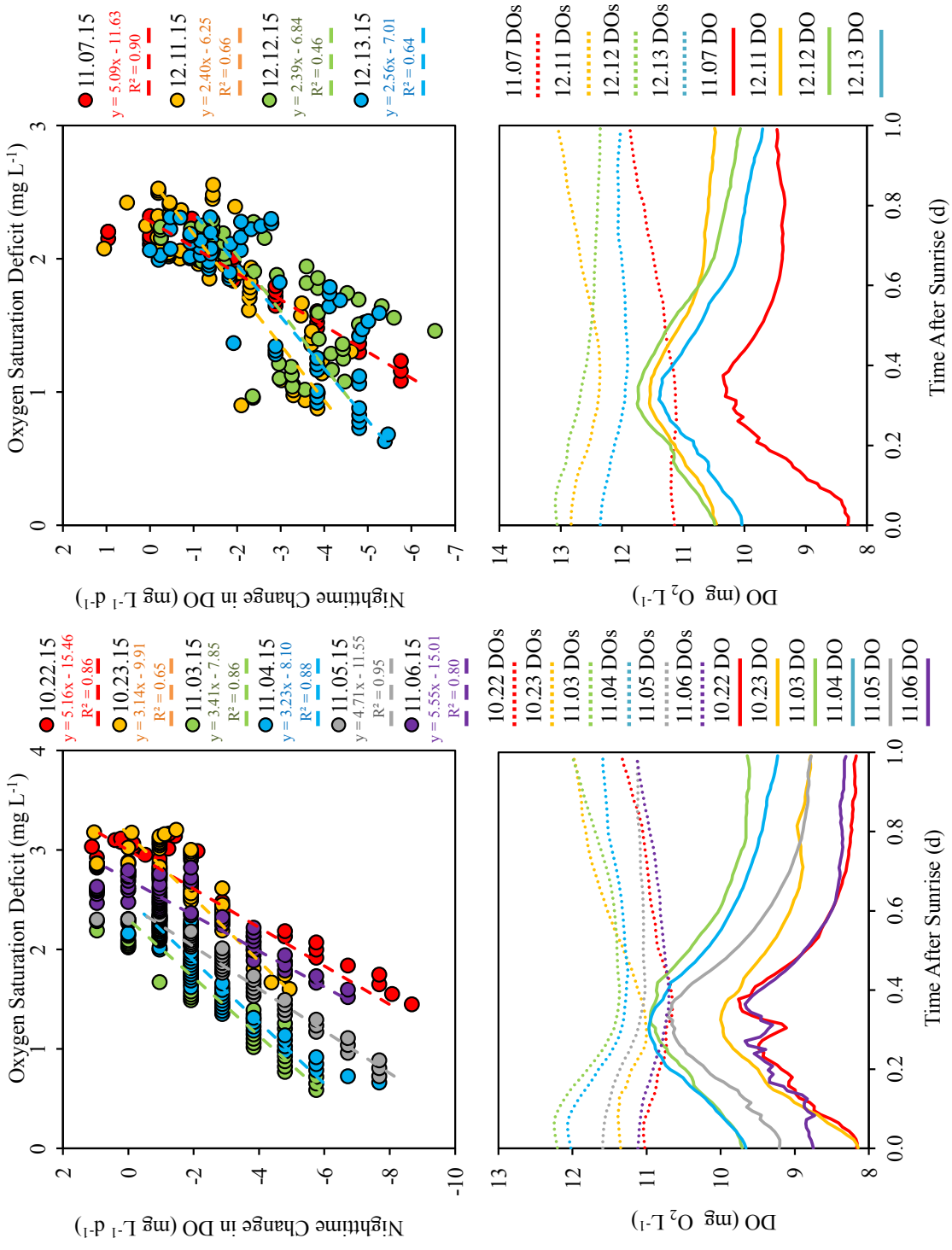

Figure B.9 Diurnal DO at Como, October – December 2015

APPENDIX C: OXYGEN REAERATION RATE COEFFICIENTS CALCULATED FROM SIXTEEN EMPIRICAL EQUATIONS DURING BASEFLOW FOR FREESE AND COMO SITES ON FALL CREEK

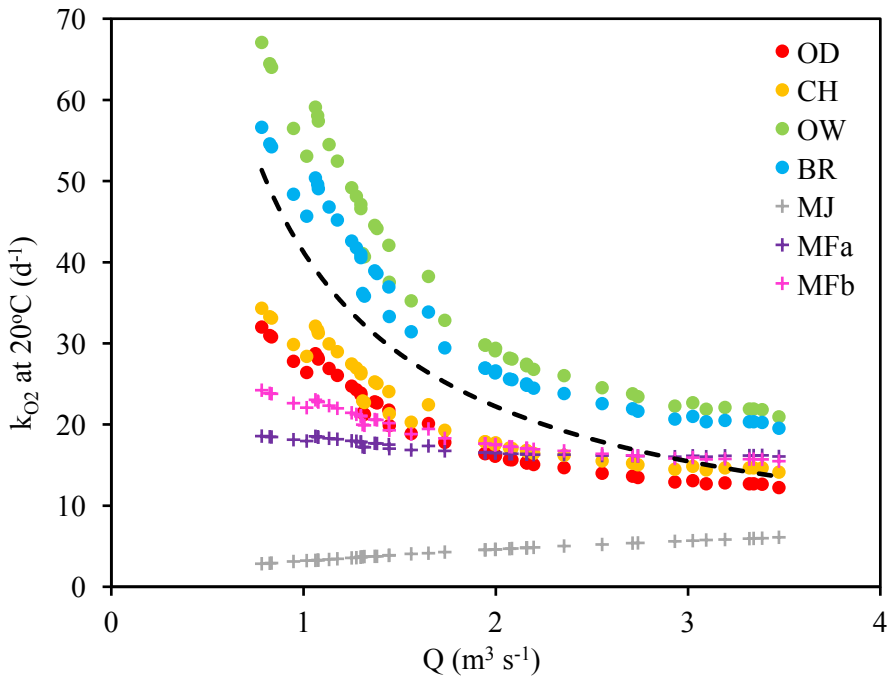

Figure C.1 Reaeration rate coefficients calculated from groups 1-2 empirical equations described in Table 2.1 compared to regression fit (dashed curve) from reaeration rate coefficients calculated by nighttime slope method for Freese.

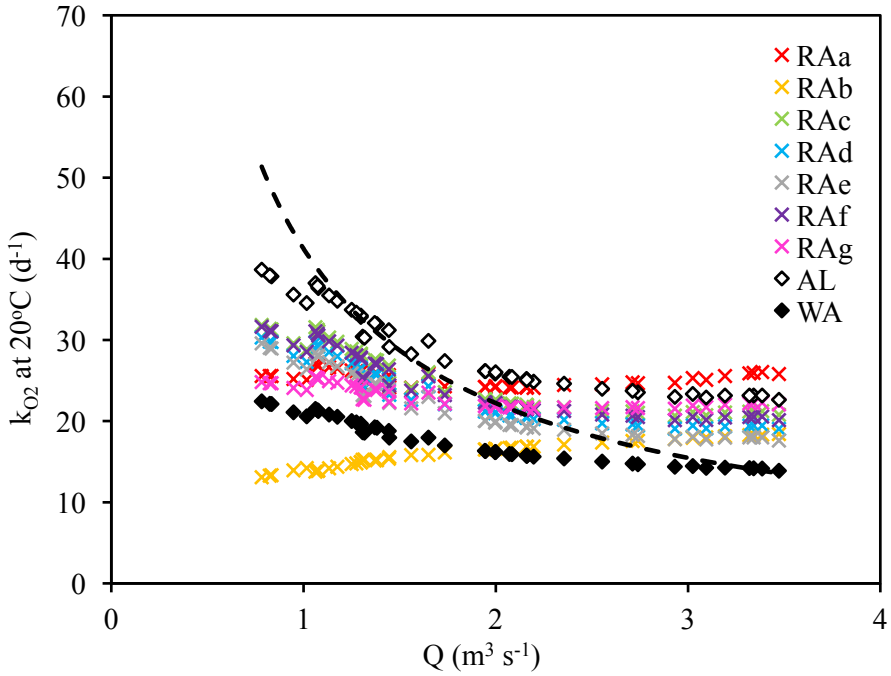

Figure C.2 Reaeration rate coefficients calculated from groups 3-4 empirical equations described in Table 2.1 compared to regression fit (dashed curve) from reaeration rate coefficients calculated by nighttime slope method for Freese.

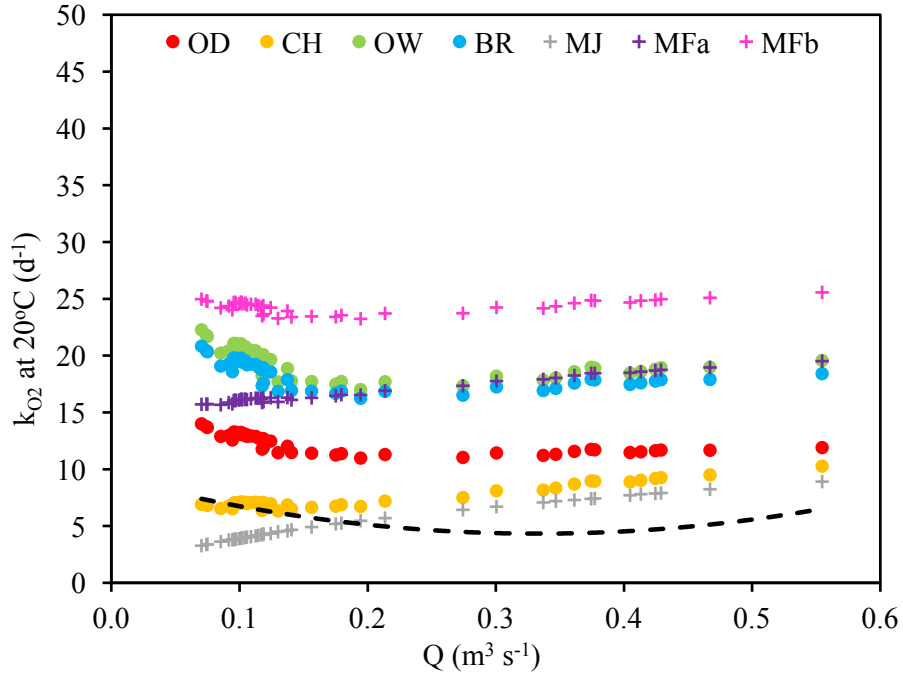

Figure C.3 Reaeration rate coefficients calculated from groups 1-2 empirical equations described in Table 2.1 compared to regression fit (dashed curve) from reaeration rate coefficients calculated by nighttime slope method for Como.

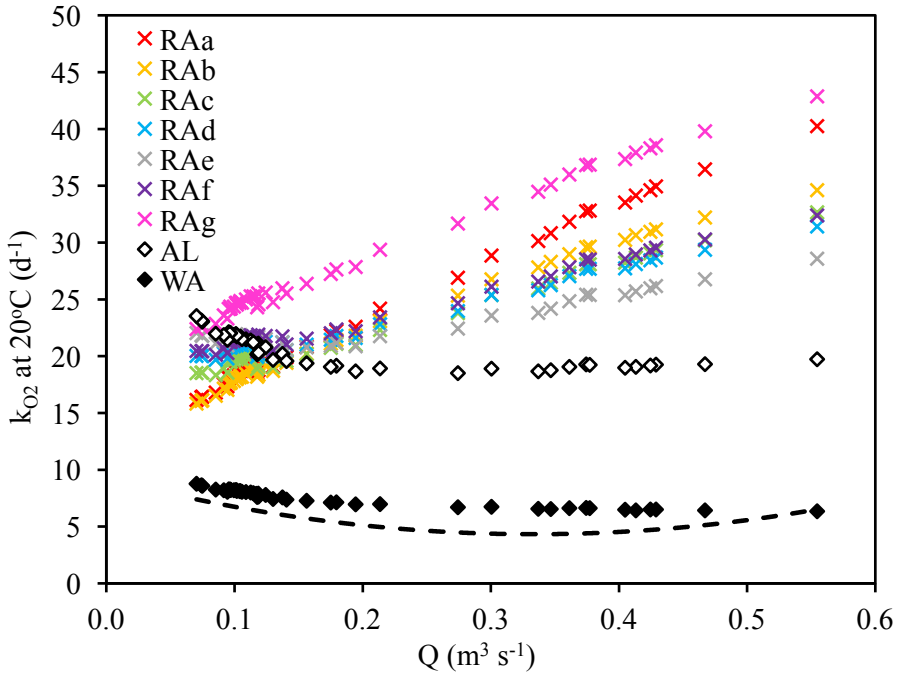

Figure C.4 Reaeration rate coefficients calculated from groups 3-4 empirical equations described in Table 2.1 compared to regression fit (dashed curve) from reaeration rate coefficients calculated by nighttime slope method for Como.

APPENDIX D: OXYGEN REAERATION RATE COEFFICIENTS CALCULATED FROM THE MODIFIED EXTREME VALUE METHOD AT COMO AND FREESE SITES ON FALL CREEK

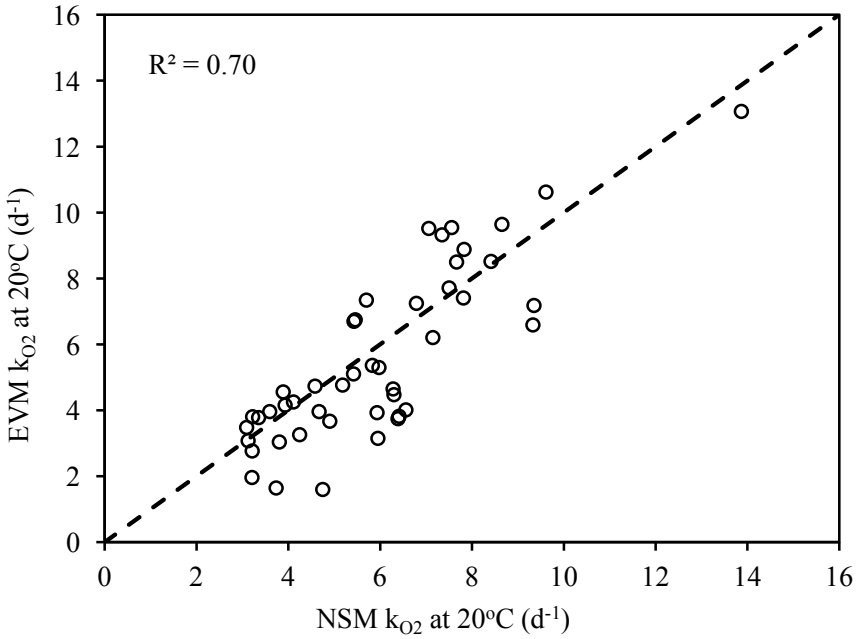

Figure D.1 Comparison of k_{O2} calculated from the nighttime slope method with k_{O2} calculated from the modified extreme value method (eqn. 3.5) for Como baseflow

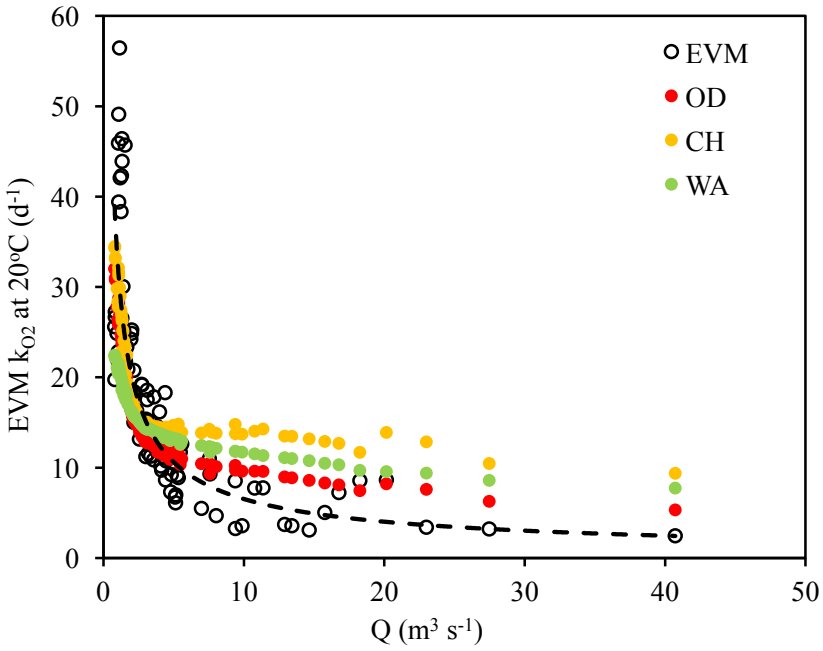

Figure D.2 k_{O2} calculated from modified EVM and empirical equations at Freese

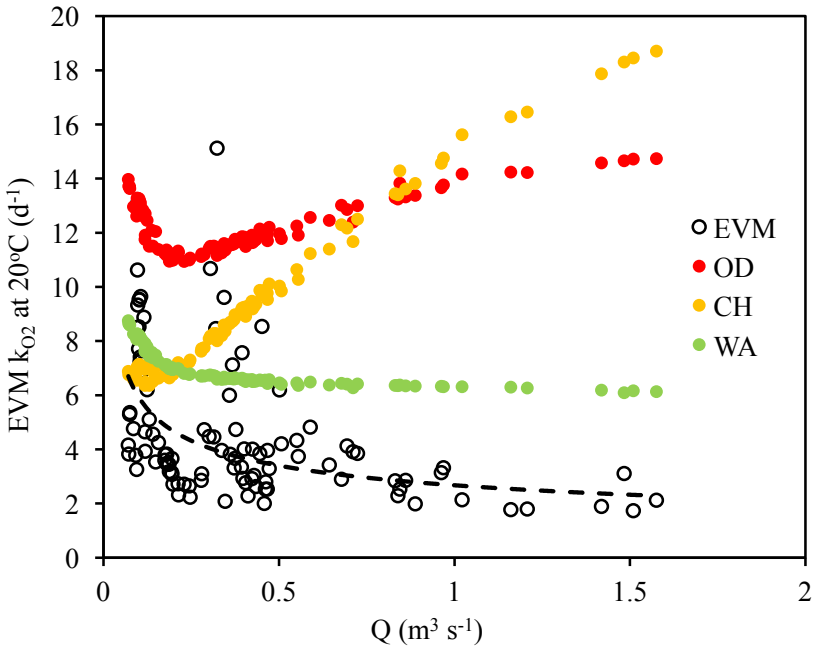

Figure D.3 k_{O2} calculated from modified EVM and empirical equations at Como

APPENDIX E: DIURNAL CHANGES IN CARBON DIOXIDE BEFORE- AND AFTER-NOON FOR FREESE AND COMO

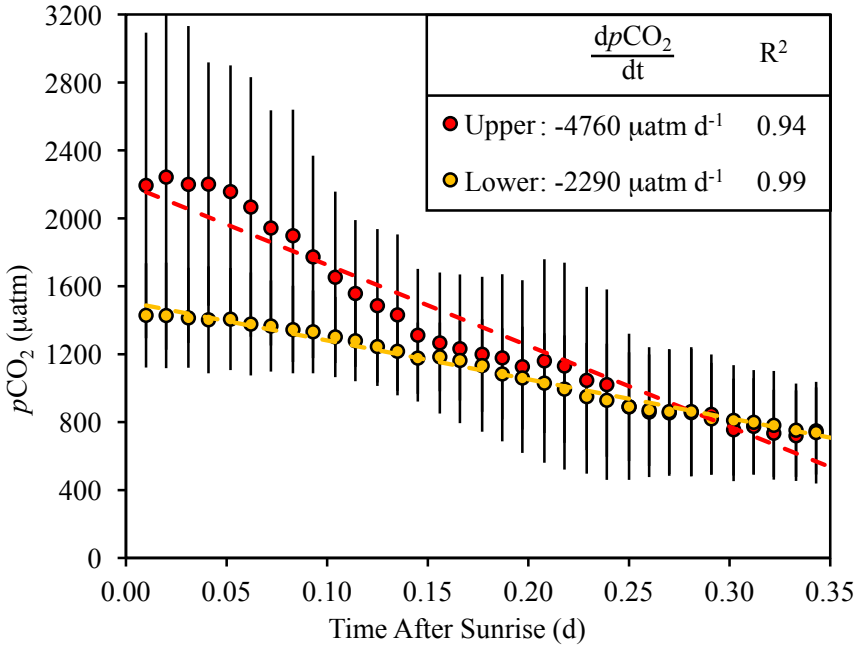

Figure E.1 Freese sunrise to noon average decline in pCO_2 per day for late-spring to early-summer (yellow) and mid-summer to early-autumn (red)

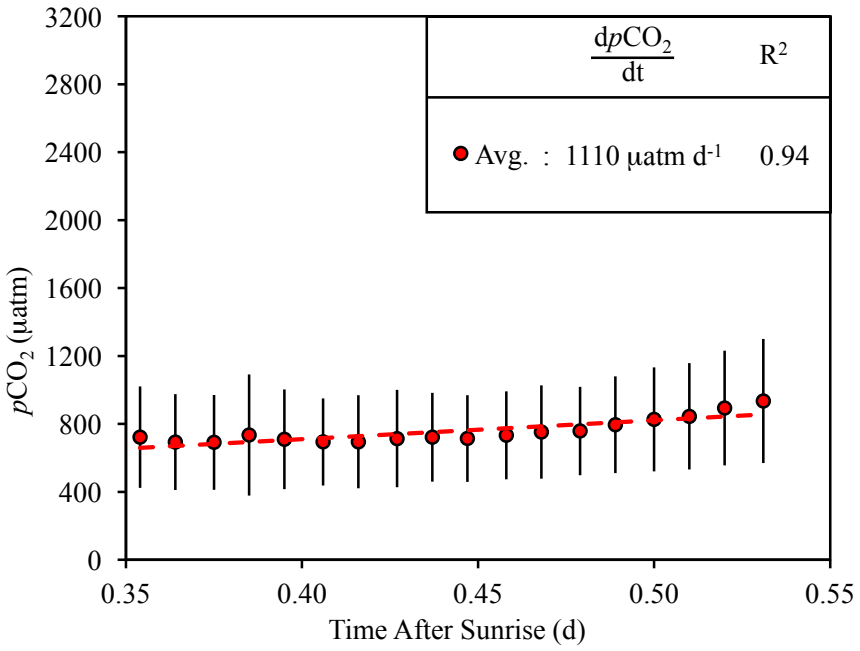

Figure E.2 Freese afternoon increase in pCO_2 per day for late-spring to early-autumn

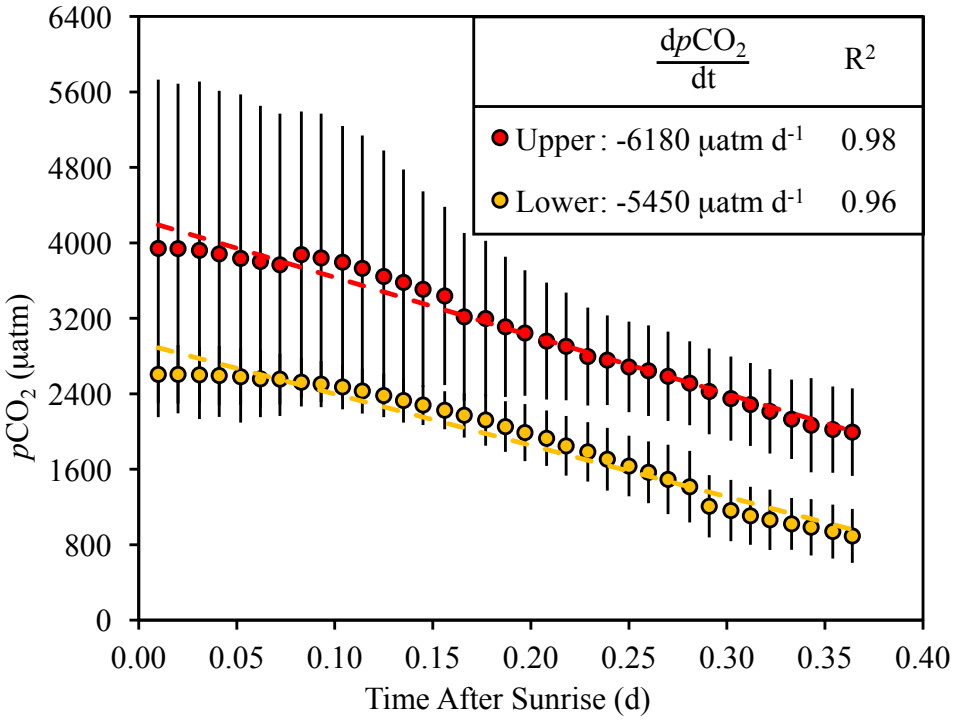

Figure E.3 Como sunrise to noon average decline in pCO_2 per day for late-spring to early-summer (yellow) and mid-summer to early-autumn (red)

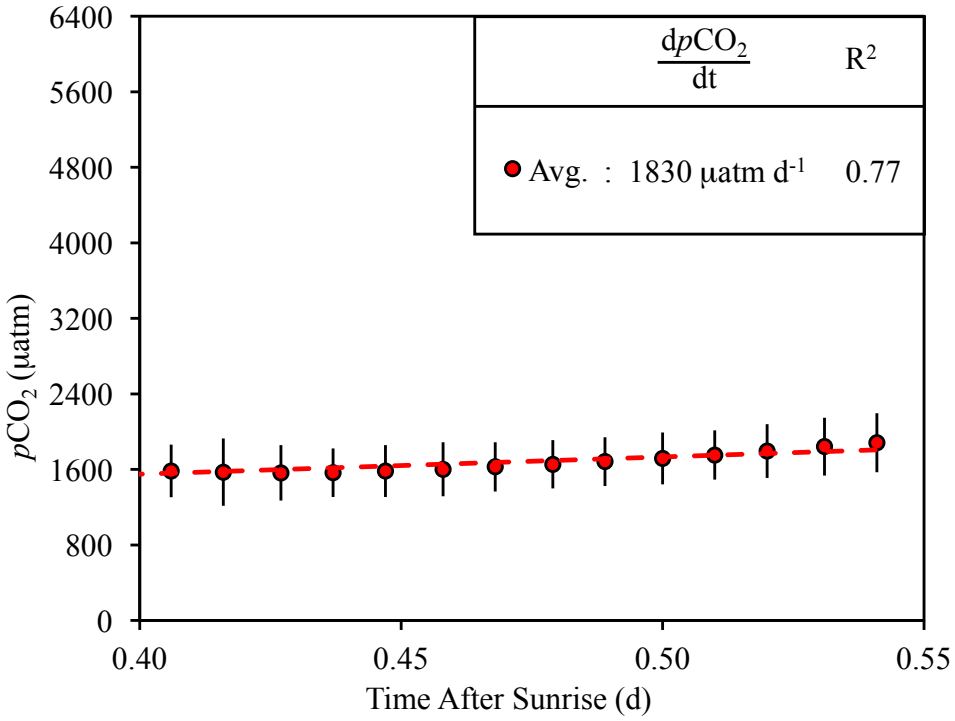

Figure E.4 Como afternoon increase in pCO_2 per day for late-spring to early-autumn

REFERENCES

Alin, S. R., Rasera, M. F. F. L., Salimon, C. I., Richey, J. E., Holtgrieve, G. W., Krusche, A. V., Snidvongs, A. (2011). Physical controls on carbon dioxide transfer velocity and flux in low-gradient river systems and implications for regional carbon budgets. *J. Geophys. Res.* **116**: G01009.

Aristegi, L., Izagirre, O., Elosegi, A. (2009). Comparison of several methods to calculate reaeration in streams, and their effects on estimation of metabolism. *Hydrobiologia* **653**: 113-124.

Asher, W. E., Wanninkhof, R. (1998). The effect of bubble-mediated gas transfer on purposeful dual-gaseous tracer experiments. *J. Geophys. Res.* **103** (C5): 10555-10560.

Atkins, M. L., Santos, I. R., Ruiz-Halpern, S., Maher, D. T. (2013). Carbon dioxide dynamics driven by groundwater discharge in a coastal floodplain creek. *J. Hydrology* **493**: 30-42.

Baattrup-Pedersen, A., Madsen, T. V., Riis, T., Cavalli, G. (2013). Photosynthetic performance of submerged macrophytes from lowland stream and lake habitats with contrasting CO_2 availability. *New Phytologist* **198**: 1135-1142.

Bales, J. D., and Nardi, M. R. (2007). Automated routines for calculating whole-stream metabolism—Theoretical background and user's guide: U.S. Geological Survey Techniques and Methods 4—C2, 33 p. (online at *http://pubs.water.usgs.gov/tm4c2/*)

Battin, T. J., Luyssaert, S., Kaplan, L. A., Aufdenkampe, A. K., Richter, A., Tranvik, L. J. (2009). The boundless carbon cycle. *Nature Geosci.* **2**: 598-600.

Beaulieu, J. J., Arango, C. P., Balz, D. A., Shuster, W. D. (2013). Continuous monitoring reveals multiple controls on ecosystem metabolism in a suburban stream. *Freshwater Bio.* **58**: 918-937.

Belanger, T. V., Korzun, E. A. (1990). Rainfall-reaeration effects. *J. Irrigat. Drain. Engin.* **116** (4): 582-587.

Bennett, J. P. Rathburn, R. E. (1972). Reaeration in open-channel flow: an evaluation of procedures for measuring and predicting the reaeration coefficient of open-channel flows. *Geological Survey Professional Paper 737.* Washington: United States Government Printing Office.

Benson, A., Zane, M., Becker, T. E., Visser, A., Uriostegui, S. H., DeRubeis, E., Moran, J. E., Esser, B. K., Clark, J. F. (2014). Quantifying reaeration rates in alpine streams using deliberate gas tracer experiments. *Water* **6**: 1013-1027.

Berggren, M., Lapierre, J. F., Giorgio, P. A. (2012). Magnitude and regulation of bacterioplankton respiratory quotient across freshwater environmental gradients. *The ISME Journal* **6**: 984-993.

Birkel, C., Soulsby, C., Malcolm, I., Tetzlaff, D. (2013). Modeling the dynamics of metabolism in montane streams using continuous dissolved oxygen measurements. *Water Resour. Res.* **49**: 5260-5275.

Bott, T. L. (2007). Primary productivity and community respiration. In: Hauer, F. R., Lamberti, G.A., [eds.], *Methods in Stream Ecology, 2nd ed.,* 663-690.

Butcher, J. B., Covington, S. (1995). Dissolved-oxygen analysis with temperature dependence. *J. Environ. Engin.* **121** (10): 756-759.

Butman, D., Raymond, P. A. (2011). Significant efflux of carbon dioxide from streams and rivers in the United States. *Nat. Geosci.* **4**: 839-842.

Ciais, P. *et al.* (2013). Carbon and other biogeochemical cycles. In: Stocker, T. F., Qin, D, Plattner, G.-K., Tignor, M, Allen, S. K., Boschung, J., Nauels, A., Xia, Y., Bex, V., Midgley, P. M., [eds.], *Climate Change the Physical Science Basis. Contribution of Working Group I to the Fifth Assessment Report of the Intergovernmental Panel on Climate Change.* Cambridge University Press, Cambridge University Press, Cambridge, U.K. and New York, NY, USA: pp. 465-570.

Chapra, S. C., Di Toro, D. M. (1991). Delta method for estimating primary production, respiration, and reaeration in streams. *J. Environ. Eng.* **117**: 640-655.

Choi, J., Hulseapple, S. M., Conklin, M. H., Harvey, J. W. (1998). Modeling CO_2 degassing and pH in a stream-aquifer system. *J. Hydrology* **209**: 297-310.

Churchill, M. A., Elmore, H. L., Buckingham, R. A. (1962). The prediction of stream reaeration rates. *Int. J. Air Wat. Poll.* **6**: 467-504.

Cole, J., Caraco, N., Kling, G. W., Kratz, T. K. (1994). Carbon dioxide supersaturation in the surface waters of lakes. *Science* **265**: 1568-1570.

Cole, J., Caraco, N. (2001). Carbon in catchments: connecting terrestrial carbon losses with aquatic metabolism. *Mar. Freshwater Res.* **52**: 101-110.

Cole, J., Prairie, Y. T., Caraco, N. F., McDowell, W. H., Tranvik, L. J., Striegl, R. G., Duarte, C. M., Kortelainen, P., Downing, J. A., Middelburg, J. J., Melack, J. (2007). Plumbing the global carbon cycle: integrating inland waters into the terrestrial carbon budget. *Ecosys.* **10**: 172-185.

Correa-González, J. C., Chávez-Parga, M. C., Cortés, Pérez-Munguía, R. M. (2014). Photosynthesis, respiration and reaeration in a stream with complex dissolved oxygen pattern and temperature dependence. *Ecol. Model.* **273**: 220-227.

Crawford, J. T., Striegl, R. G., Wickland, K. P., Dornblaser, M. M., Stanley, E. H. (2013). Emissions of carbon dioxide and methane from a headwater stream network of interior Alaska. *J. Geophys. Res. Biogeosci.* **118**: 482-494.

Crawford, J. T., Lottig, N. R., Stanley, E. H., Walker, J. F., Hanson, P. C., Finlay, J. C., Striegl, R. G. (2014). *Global Biogeochem. Cycles* **28**: 197-210.

Demars, B. O. L., Manson, R. J., Ólafsson, J. S., Gíslason, G. M., Gudmundsdottir, R., Woodward, G., Reiss, J., Pichler, D. E., Rasmussen, J. J., Friberg, N. (2011). Temperature and the metabolic balance of streams. *Freshwater Bio.* **56**: 1106-1121.

Demars, B. O. L., Manson, J. R. (2013). Temperature dependence of stream aeration coefficients and the effect of water turbulence: A critical review. *Water Res.* **47**: 1-15.

Demars, B. O. L., Thompson, J., Manson, R. (2015). Stream metabolism and the open diel oxygen method: principles, practice, and perspectives. *Limn. Oceanog.: Methods* **13** (7): 256-374.

Dingman, S. L. (2002). *Physical Hydrology.* 2nd ed. Long Grove, IL: Waveland Press, Inc., pp. 342-344.

Dinsmore, K. J., Wallin, M. B., Johnson, M. S., Billett, M. F., Bishop, K., Pumpanen, J., Ojala, A. (2013). Contrasting CO_2 concentration discharge dynamics in headwater streams: A multi-catchment comparison. *J. Geophys. Res.: Biogeosci.* **118**: 445-461.

Dobbins, W. E. (1956). The nature of the oxygen transfer coefficient in aeration systems. *Biological Treatment of Sewage and Industrial Waters*. McCabe, J., Eckenfelder, W. W. (eds.). Chapman and Hall, New York, pp. 141-148.

Dobbins, W. E. (1963). B.O.D. and oxygen relationships in streams. Water Resources Conference, *ASCE*, Milwaukee, WI, 13-17 May.

Doctor, D. H., Kendall, C., Sebestyen, S. D., Shanely, J. B., Ohte, N., Boyer, E. W. (2008). Carbon isotope fractionation of dissolved inorganic carbon (DIC) due to outgassing of carbon dioxide from a headwater stream. *Hydrol. Processes* **22**: 2410-2423.

Edward, J. T. (1970). Molecular volumes and the Stokes-Einstein equation. *J. Chem. Educ.* **47**: 261-270.

Elmore, H. L., West, W. F. (1961). Effect of water temperature on stream reaeration. *J. Sanitary Engin. Div. ASCE* **87** (SA6): 59-71.

Finlay, J. (2003). Controls of streamwater dissolved inorganic carbon dynamics in a forested watershed. *Biogeochem.* **62**: 231-252.

Freeman, M. C., Pringle, C. M., Jackson, C. R. (2007). Hydrologic connectivity and the contribution of stream headwaters to the ecological integrity at regional scales. *JAWRA* **43** (1): J06011.

Gillooly, J. F., Brown, J. H, West, G. B., Savage, V. M., Charnov, E. L. (2001). Effects of size and temperature on metabolic rate. *Science* **239**: 2248-2251.

Guasch, H., Armengol, J., Martí, E., Sabater, S. (1998). Diurnal variation in dissolved oxygen and carbon dioxide in two low-order streams. *Water Res.* **32** (4): 1067-1074.

González-Pinzón, R, Peipoch, M., Haggerty, R., Martí, Fleckenstein, J. H. (2016). Nighttime and daytime respiration in a headwater stream. *Ecohydrol.* **9**: 93-100.

Grant, R. S. (1976). *Reaeration-coefficient measurements of 10 small streams in Wisconsin using radioactive tracers: with a section on the energy-dissipation model.* Madison, WI: U.S. Geological Survey.

Haider, H., Ali, W., Haydar, S. (2013). Evaluation of various relationships of reaeration rate coefficient for modeling dissolved oxygen in a river with extreme flow variations in Pakistan. *Hydrol. Process.* **27**: 3949-3963.

Haith, D. A., Hollingshead, N., Bell, M. L., Kreszewski, S. W., Morey, S. J. (2012). Nutrient loads to Cayuga Lake, New York: Watershed modeling on a budget. *J. Water Res. Plan. Mgmt.* Oct., 571-581.

Hall, R. O., Tank, J. L. (2005). Correcting whole-stream estimates of metabolism for groundwater input. *Limnol. Oceanogr.: Methods* **3**: 222-229.

Hall, R. O., Beaulieu, J. J. (2013). Estimating autotrophic respiration in streams using daily metabolism data. *Freshwater Sci.* **32** (2): 507-516.

Hall, R. O., Tank, J. L., Baker, M. A., Rosi-Marshal, E. J., Hotchkiss, E. R. (2016). Metabolism, gas exchange, and carbon spiraling in rivers. *Ecosys.* **19**: 73-86.

Hanson, P. C., Bade, D. L., Carpenter, S. R., Kratz, T. K. (2003). Lake metabolism: Relationships with dissolved organic carbon and phosphorus. *Limnol. Oceanogr.* **48** (3): 1112-1119.

Hope, D., Palmer, S, Billett, M. F., Dawson, J. J. C. (2001). Carbon dioxide and methane evasion from a temperate peatland stream. *Limnol. Oceanogr.* **46**: 847-857.

Hornberger, G. M., Kelly, M. G. (1975). Atmospheric reaeration in a river using productivity analysis. *J. Environ. Eng.* **101**: 729-739.

Hotchkiss, E. R., Hall Jr., R. O., Sponseller, R. A., Butman, D., Klaminder, J., Luadon, H., Rosvall, M., Karlsson, J. (2015). Sources of and processes controlling CO2 emissions change with the size of streams and rivers. *Nat. Geosci.* **8**: 696-699.

Hunt, C. W., Salisbury, J. E., Vandemark, D. (2011). Contribution of non-carbonate anions to total alkalinity and overestimation of pCO_2 in New England and New Brunswick rivers. *Biogeosci.* **8**: 3069-3076.

Izagirre, O., Bermejo, M., Pozo, J., Elosegi, A. (2007). RIVERMET©: An Excel-based tool to calculate river metabolism from diel oxygen-concentration curves. *Environ. Modell. Software* **22**: 24-32.

Izagirre, O., Agirre, U., Bermejo, M., Pozo, J., Elosegi, A. (2008). Environmental controls of whole-stream metabolism identified from continuous monitoring of Basque streams. *J. Am. Benth. Soc.* **27** (2): 252-268.

Jähne, B., Heinz, G., Dietrich, W. (1987). Measurement of the diffusion coefficients of sparingly soluble gases in water. *J. Geophys. Res.* **92** (C10): 10767-10776.

Jankowski, K., Schindler, D. E., Lisi, P. J. (2014). Temperature sensitivity of community respiration rates in streams associated with watershed geomorphic features. *Ecology* **95** (10): 2707-2714.

Jassal, R. S., Black, T. A., Drewitt, G.B., Novack, M. D., Gaumont-Guay, D., Nesic, Z. A model of the production and transport of CO_2 in soil: predicting soil CO2 concentrations and CO_2 efflux from a forest floor. *Agri. Forest. Meteor.* **124**: 219-236.

Jenkins, M. E., Adams, M. A., (2011). Respiratory quotients and Q_{10} of soil respiration in sub-alpine Australia reflect influences of vegetation types. *Soil Bio. & Biochem.* **43**: 1266-1274.

Johnson, L. T., Royer, T. V., Edgerton, J. M., Leff, L. G. (2012). Manipulation of the dissolved organic carbon pool in an agricultural stream: responses in microbial community structure, denitrification, and assimilatory nitrogen uptake. *Ecosys.* **15**: 1027-1038.

Johnson, M. S., Lehmann, J., Couto, E. G., Filho, J. P. N., Riha, S. J. (2006). DOC and DIC in flowpaths of Amazonian headwater catchments with hydrologically contrasting soils. *Biogeochem.* **81**: 45-57.

Johnson, M. S., Lehmann, J., Riha, S., Krusche, A. V., Richey, J. E., Ometto, J. P., and Couto, E. G. (2008). CO_2 efflux from Amazonian headwater streams represent a significant fate for deep soil respiration. *Geophys. Res. Lett.* **35**: L171401.

Johnson, M. S., Billett, M. F., Dinsmore, K. J., Wallin, M., Dyson, K. E., Jassal, R. S. (2010). Direct and continuous measurement of dissolved carbon dioxide in freshwater aquatic systems—method and applications. *Ecohydrol.* **3**: 68-78.

Jones, J. B., Mulholland, P. J. (1998). Carbon dioxide variation in a hardwood forest stream: an integrative measure of whole catchment soil respiration. *Ecosys.* **1**: 183-196.

Jones, J. B., Stanley, E. H., Mulholland, P. J. (2003). Long-term decline in carbon dioxide supersaturation in rivers across the contiguous United States. *Geophys. Res. Lett.* **30** (10): 1495.

Kaushal, S. S., Groffman, P. M., Likens, G. E., Belt, K. T., Stack, W. P., Kelly, V. R., Band, L. E., Fisher, G. T. (2005). Increased salinization of fresh water in the northeastern United States. *PNAS* **102** (102): 13517-13520.

Kent, R., Belitz, K., Burton, C. A. (2006). Algal productivity and nitrate assimilation in an effluent dominated concreate lined stream. *JAWRA* **02074**: 1109-1128.

Khadka, M. B., Martin, J. B., Jin, J. (2014). Transport of dissolved carbon and CO_2 degassing from a river system in a mixed silicate and carbonate catchment. *J. Hydrol.* **513**: 391-402.

Knapp, J. L. A., Osenbrük, K., Cirpka, O. A. (2015). Impact of non-idealities in gas-tracer tests on the estimation of reaeration, respiration, and photosynthesis rates in streams. *Water Res.* **83**: 205-216.

Kokic, J., Wallin, M. B., Chmiel, H. E., Denfield, B. A., Sobek, S. (2015). Carbon dioxide evasion from headwater systems contributes to the total export of carbon from a small boreal lake catchment. *J. Geophys. Res. Biogeosci.* **120**: JG002706.

Leopold, L. B., Maddock, T. (1953). The hydraulic geometry of stream channels and some physiographic implications. U.S. Government Printing Office: Washington.

Leopold, L. B., Wolman, M. G., Miller, J. P. (1964). *Fluvial Processes in Geomorphology*. Freeman and Company, San Francisco.

Lewis, W.K., Whitman, W. G. (1924). Principles of gas absorption. *Indust. Engin. Chem.* **16** (12): 1215-1220.

Li, S, Lu, X. X., He, M., Zhou, Y., Li., L., Ziegler, A. D. (2012). Daily CO_2 partial pressure and CO2 outgassing in the upper Yangtze River basin: A case study of the Longchuan River, China. *J. Hydrol.* **466-467**: 141-150.

Lorke, A., Peeters, F. (2006). Toward a unified scaling relation for interfacial fluxes. *J. Phys. Ocean.* **36** (5): 955-961.

Lynch, J. K., Beatty, C. M., Seidel, M. P., Jungst, L. J., DeGrandpre, M. D. (2010). Controls on riverine CO_2 over an annual cycle determined using direct, high temporal resolution pCO_2 measurements. *J. Geophys. Res.* **115**: G03016.

Macpherson, G. L. (2009). CO_2 distribution in groundwater and the impact of groundwater extraction on the global C cycle. *Chem. Geol.* **264**: 328-336.

Mahecha, M. D., Reichstein, M., Carvalhais, N., Lasslop, G., Lange, H., Seneviratne, S. I., Vargas, R., Ammann, C., Arain, M. A., Cescatti, A., Janssens, I. A., Migliavacca, M., Montagnami, L., Richardson, A. D. (2010). Global convergence in the temperature sensitivity of respiration at ecosystem level. *Science* **329**: 838-840.

McBride, G. B. Chapra, S. C. (2005). Rapid calculation of oxygen in streams: approximate delta method. *J. Environ. Eng.* **131** (3): 336-342.

Meeus, J. H. (1991) *Astronomical Algorithms.* Willmann-Bell, Incorporated.

Melack, J. (2011). Riverine carbon dioxide release. *Nature Geosci.* **4** (12): 821-822.

Melching, C. S., Flores, H. E. (1999). Reaeration equations derived from U.S. Geological Survey Database. *J. Environ. Eng.* **125** (5): 407-414.

Miller, M. P., Susong, D. D., Shope, C. L., Heilweil, V. M., Stolp, B. J. (2014). Continuous estimation of baseflow in snowmelt-dominated streams and rivers in the Upper Colorado River Basin: A chemical hydrograph separation approach. *Water Resour. Res.* **50**: 6986-6999.

Miller, M. P., Johnson, H. M., Susong, D. D., Wolock, D. M. (2015). A new approach for continuous estimation of baseflow using discrete water quality data: Method description and comparison with baseflow estimates from two existing approaches. *J. Hydrol.* **522**: 203-210.

Moog, D. B., Jirka, G. H. (1998). Analysis of reaeration equations using mean multiplicative error. *J. Environ. Eng.* **124** (2): 104-110.

Morse, N., Bowden, W. B., Hackman, A., Pruden, C., Steiner, E., Berger, E. (2007). Using sound pressure to estimate reaeration in streams. *J. N. Am. Benthol. Soc.* **26** (1): 28-37.

Nguyen, M. T, Tan, D. S., Tan, S. K. (2015). Reaeration model for a still-water body. *J. Environ. Eng.* **141** (1): 04014052.

O'Connor, D. J., Dobbins, W. E. (1956). Mechanism of reaeration in natural streams. *J. Sanitary Engin. Div. ASCE* **82** (SA6): 1-30.

O'Connor, D. J. (1958). *The Measurement and Calculation of Stream Re-aeration Ratio*. Seminar on Oxygen Relationships in Streams, Robert A. Taft Sanitary Engineering Center, Tech. Rep. **W58-2**: 35-45.

O'Connor, D. J., Di Toro, D. M. (1970). Photosynthesis and oxygen balance in streams. *J. Sanitary Engin. Div. ASCE* **96** (SA2): 547-571.

Odom, H. T. (1956). Primary production in flowing waters. *Limnol. Oceanogr.* **1** (2): 102-117.

Odom, H. T. (1957). Trophic structure and productivity of Silver Springs, Florida. *Ecol. Monogr.* **27** (1): 55-112.

Öquist, M. G., Wallin, M., Seibert, J., Bishop, S. K., Laudon, H. (2009). Dissolved inorganic carbon export across the soil/stream interface and its fate in a boreal headwater stream. *Environ. Sci. Technol.* **43**: 7364-7369.

Ostrom, N. E., Carrick, H. J., Twiss, M. R., Piwinksi, L. (2005). Evaluation of primary Production in Lake Erie by multiple proxies. *Oecologia* **144**: 115-124.

Owens, M., Edwards, R. W., and Gibbs, J. W. (1964). Some reaeration studies in streams. *Int. J. Air Wat. Poll.* **8**: 469-486.

Palmer, M. A., Febria, C. (2012). The heartbeat of ecosystems. *Science* **336**: 1393-1394.

Parker, G. W., DeSimone, L. A. (1992). Estimating reaeration coefficients for low-slope streams in Massachusetts and New York, 1985-88. *USGS Rep. No. WRI 91-4188*, U.S. Geological Survey.

Perkins, D. M., Yvon-Durocher, G., Demars, B. O. L., Reiss, J., Pichler, D. E., Friberg, N., Trimmer, M., Woodward, G. (2012). Consistent temperature dependence of respiration across ecosystems contrasting in thermal history. *Glob. Change Bio.* **18**: 1300-1311.

Peter, H., Singer, G. A., Preiler, C., Chifflard, P., Steniczka, G., Battin, T. J. (2014). Scales and drivers of temporal pCO_2 dynamics in an Alpine stream. *J. Geophys. Res. Biogeosci.* **119**: 1078-1091.

Pinder, G. F., Jones, J. F. (1969). Determination of the ground-water component of Peak discharge from the chemistry of total runoff. *Water. Resour. Res.* **5**: 438-444.

Prasad, M. B. K., Kaushal, S. S., Murtugudde, R. (2013). Long-term pCO_2 dynamics in rivers in the Chesapeake Bay Watershed. *Appl. Geochem.* **31**: 209-215.

Raymond, P. A., Bauer, J. E., Cole, J. J. (2000). Atmospheric CO_2 evasion, dissolved inorganic carbon production, and net heterotrophy in the York River estuary. *Limnol. Oceanogr.* **45** (8): 1707-1717.

Raymond, P. A., Zappa, C. J., Butman, D., Bott, T. L., Potter, J., Mulholland, P., Larsen A. E., McDowell, W. H., Newbold, D. (2012). Scaling the gas transfer velocity and hydraulic geometry in streams and small rivers. *Limn. Oceanogr.: Fluids and Environments* 2, 41-53.

Raymond, P. A., Hartmann, J., Lauerwald, R., Sobek, S., McDonald, C., Hoover, M., Butman, D., Striegl, R., Mayorga, E., Humborg, C., Kortelainen, P, Dürr, H., Meybeck, M., Ciais, P, Guth, P. (2013). Global carbon dioxide emissions from inland waters. *Nature* **503**: 355-359.

Richey, J. E., Melack, J. M., Aufdenkampe, A. K., Ballester, V. M., Hess, L. L. (2002). Outgassing from Amazonian rivers and wetlands as a large tropical source of atmospheric CO_2. *Nature* **416**: 617-620.

Riley, A. J., Dodds, W. K., (2013). Whole-stream metabolism: strategies for measuring and Modeling diel trends of dissolved oxygen. *Freshwater Sci.* **32** (1): 56-59.

Roley, S. S., Tank, J. L., Griffiths, N. A., Hall, R. O., Davis, R. T. (2014). The influence of floodplain restoration on whole-stream metabolism in an agricultural stream: insights from a 5-year continuous data set. *Freshwater Sci.* **33** (4): 1043-1059.

Rosenberg, G., Littler, D. S., Littler, M. M., Oliveira, E. C. (1995). Primary production and photosynthetic quotients of seaweeds from São Paulo State, Brazil. *Botanica Marina* **38**: 369-377.

Rusjan, S., Mikos, M. (2010). Seasonal variability of diurnal in-stream nitrate concentration oscillations under hydrologically stable conditions. *Biogeochem.* **97**: 123-140.

Sand-Jensen, K., Staehr, P. A. (2012). CO_2 dynamics along Danish lowland streams: Water-air gradients, piston velocities and evasion rates. *Biogeochem.* **111**: 615-628.

Schneiter, R. W., Grenney, W. J. (1983). Temperature corrections to rate coefficients. *J. Environ. Engin.* **109** (3): 661-667.

Shaw, S. B., Marjerison, R. D., Bouldin, D. R., Parlange, J. Y., Walter, M. T. (2012). Simple model of changes in stream chloride levels attributable to road salt applications. *J. Environ. Engin.* **138** (1): 112-118.

Sheridan, C., Petersen, J., Rohwer, J. (2012). On modifying the Arrhenius equation to compensate for temperature changes for reactions within biological systems. *Water SA* **38** (1): 149-151.

Smith, L. M., Silver, C. M., Oviatt, C. A. (2012). Quantifying variation in water column photosynthetic quotient with changing field conditions in Narragansett Bay, RI, USA. *J. Plankton Res.* **34** (5): 437-442.

Sobek, S., Tranvik, L. J., Cole, J. J. (2005). Temperature independence of carbon dioxide supersaturation in global lakes. *Global Biogeochem. Cycl.* **19:** GB2003.

Streeter, H., Phelps, E. (1925). A study of the pollution and natural purification of the Ohio River III. *Public Heath Bulletin* **146**: 1-69.

Thyssen, N., Erlandse, M., Jeppesen, E., Ursin, C. (1987). Reaeration of oxygen in shallow, macrophyte rich streams: I – determination of the reaeration rate coefficient. *Int. Rev. Hydrobiol.* **72** (4): 405-429.

Tsivoglou, E. C., Neal, L. A. (1976). Tracer measurement of reaeration III: Predicting the reaeration capacity of inland streams. *J. Poll. Contr. Fed.* **48**: 2669-2689.

Uehlinger, U., König, C., Reichert, P. (2000). Variability of photosynthesis-irradiance curves and ecosystem respiration in a small river. *Freshwater Bio.* **44**: 493-507.

Wallin, M. B., Öquist, M. G., Buffam, I., Billett, M. F., Nissell, J., and Bishop, K. H. (2011). Spatiotemporal variability of the gas transfer coefficient (K_{CO2}) in boreal streams: implications for large scale estimates of CO_2 evasion. *Global Biogeochem. Cycl.* **25**: GB3025.

Wallin, M. B., Löfgren, S., Erlandsson, M., Bishop, K. (2014). Representative regional sampling of carbon dioxide and methane concentrations in hemiboreal headwater streams reveal underestimates in less systemic approaches. *Global Biogeochem. Cycl.* **28**: GB004715.

Wallis, S. G., Manson, J. R. (2004). Methods for predicting dispersion coefficients in rivers. *Proc. Inst. Civil Eng. Water Mgmt.* **157**: 131-141.

Wang, H., Hondzo, M., Xu, C., Poole, V., Spacie, A. (2003). Dissolved oxygen dynamics of streams draining an urbanized and an agricultural catchment. *Ecol. Model.* **160**: 145-161.

Wanninkhof, R. (1992). Relationship between wind speed and gas exchange over the ocean. *J. Geophys. Res.* **97** (C5): 7373-7382.

Wanninkhof, R. (2014). Relationship between wind speed and gas exchange over the ocean revisited. *Limn. Oceanogr.: Methods* **12**: 351-362.

Weiss, R. F. (1970). The solubility of nitrogen, oxygen, and argon in water and seawater. *Deep-Sea Res.* **17**: 721-735.

Weiss, R. F. (1974). Carbon dioxide in water and seawater: the solubility of a non-ideal gas. *Mar. Chem.* **2**: 203-215.

Worrall, F., Lancaster, A. (2005). The release of CO_2 from river waters—the contribution of excess CO_2 from groundwater. *Biogeochemistry* **76**: 299-317.

Wright, J. C., Mills, J. K. (1967). Productivity studies on the Madison River, Yellowstone National Park. *Limn. Oceanogr.* **12**: 568-577.

Young, R. G., Huryn, A. D. (1999). Effects of land use on stream metabolism and organic matter turnover. *Ecolog. Appl.* **9** (4): 1359.

YSI. (2012). *6-Series multiparameter water quality sondes user manual.* Yellow Springs, OH: YSI International.

Yvon-Durocher, G., Caffrey, J. M., Cescatti, A., Dossena, M., Giorgio, P., Gasol, J. M., Montoya, J. M., Pumpanen, J., Staehr, P. A., Trimmer, M., Woodward, G., Allen, A. P. (2012). Reconciling the temperature dependence of respiration across timescales and ecosystem types. *Nature* **487**: 427-476.

Zappa, C. J., McGillis, W. R., Raymond, P. A., Edson, J. B., Hintsa, E. J., Zemmelink, H. J., Dacey, J. W. H., Ho, D. T. (2007). Environmental turbulent mixing controls on air-water gas exchange in marine and aquatic systems. *Geophys. Res. Lett.* **34**: L10601.